INVESTIGATION OF COMBUSTION CHARACTERISTICS OF INDIGENOUS LIGNITE IN A 150 KWT CIRCULATING FLUIDIZED BED COMBUSTOR

A THESIS SUBMITTED TO
THE GRADUATE SCHOOL OF NATURAL AND APPLIED SCIENCES
OF
THE MIDDLE EAST TECHNICAL UNIVERSITY

BY

AYKAN BATU

IN PARTIAL FULFILLMENT OF THE REQUIREMENTS
FOR
THE DEGREE OF DOCTOR OF PHILOSOPHY
IN
CHEMICAL ENGINEERING

MARCH 2008

Approval of the thesis:

INVESTIGATION OF COMBUSTION CHARACTERISTICS OF INDIGENOUS LIGNITE IN A 150KWT CIRCULATING FLUIDIZED BED COMBUSTOR

submitted by **AYKAN BATU** in partial fulfillment of the requirements for the degree of **Doctor of Philosophy in Chemical Engineering Department, Middle East Technical University** by,

Prof. Dr. Canan Özgen _____
Dean, Graduate School of **Natural and Applied Sciences**

Prof. Dr. Gürkan Karakaş _____
Head of Department, **Chemical Engineering**

Prof. Dr. Nevin Selçuk
Supervisor, **Chemical Engineering Dept., METU** _____

Assist. Prof. Dr. Görkem Külah
Co-Supervisor, **Chemical Engineering Dept., METU** _____

Examining Committee Members:

Prof. Dr. İnci Eroğlu _____
Chemical Engineering Dept., METU

Prof. Dr. Nevin Selçuk _____
Chemical Engineering Dept., METU

Prof. Dr. Yavuz Samim Ünlüsoy _____
Mechanical Engineering Dept., METU

Assoc. Prof. Dr. Murat Köksal _____
Mechanical Engineering Dept., Hacettepe University

Assoc. Prof. Dr. Göknur Bayram _____
Chemical Engineering Dept., METU

Date: **14.03.2008**

I hereby declare that all information in this document has been obtained and presented in accordance with academic rules and ethical conduct. I also declare that, as required by these rules and conduct, I have fully cited and referenced all material and results that are not original to this work.

Name, Last name : Aykan Batu

Signature :

ABSTRACT

INVESTIGATION OF COMBUSTION CHARACTERISTICS OF INDIGENOUS LIGNITE IN A 150 KWT CIRCULATING FLUIDIZED BED COMBUSTOR

Batu, Aykan

Ph.D., Department of Chemical Engineering

Supervisor : Prof. Dr. Nevin Selçuk

Co-Supervisor : Assist. Prof. Dr. Görkem Külah

March 2008, 194 pages

Coal is today the fossil fuel which offers the greatest proven reserves. Due to increasingly stringent environmental legislation, coal fired combustion systems should be based on clean coal combustion technologies. For clean and efficient energy generation from coal reserves, the most suitable technology known to date is the 'Fluidized Bed Combustion' technology. Applications of circulating fluidized bed combustion (CFB) technology have been steadily increasing in both capacity and number over the past decade for the utilization of this resource. Designs of these units have been based on the combustion tests carried out in pilot scale facilities to determine the combustion and desulfurization characteristics of the coals and limestones in CFB conditions. However, utilization of Turkish

lignites with high ash, volatile matter and sulfur contents in CFB boilers necessitates adaptation of CFB combustion technology to these resources. Therefore, it has been the objective of this study to investigate combustion characteristics of an indigenous lignite in a circulating fluidized bed combustor.

In this study, a 150 kWt Circulating Fluidized Bed (CFB) Combustor Test Unit was designed and constructed in Chemical Engineering Department of Middle East Technical University, based on the extensive experience acquired at the existing 0.3 MWt Bubbling Atmospheric Fluidized Bed Combustor (AFBC) Test Rig. Following the commissioning tests, combustion tests were carried out for investigation of combustion characteristics of Çan lignite in CFB conditions and for comparison of the design of the test unit with experimental findings.

The steady state results of the combustion tests reveal that Çan lignite is fired with high combustion efficiency. Temperature profile along the riser is achieved to be almost uniform by good control of cooling system. Pressure drop through the dilute zone is found to be negligible because of low solid hold up in this zone. CO and NO concentrations within the flue gas are fairly lower, whereas N_2O concentration is higher compared to the ones obtained in the bubbling AFBC test rig firing the same lignite. The deviation of particle size distributions of bottom ash and circulating ash among the tests are in line with the deviation of superficial velocity. In order to assess the validity and predictive accuracy of the pressure balance model, it was reapplied to the test unit utilyzing the revised input data based on the results of the combustion tests. Comparison of the model predictions with experimental results revealed that the predictions have acceptable agreement with the measurements. In conclusion, the performance of 150 kW CFBC Test Unit was found to be satisfactory to be utilized for the long term research studies on combustion and desulfurization characteristics of indigenous lignite reserves in circulating fluidized bed combustors.

Keywords: CFBC, Combustion Test Unit, Turkish Lignites

ÖZ

150 KWT DOLAŞIMLI AKIŞKAN YATAKLI YAKICIDA YERLİ LİNYİTİN YANMA ÖZELLİKLERİNİN İNCELENMESİ

Batu, Aykan

Doktora, Kimya Mühendisliği Bölümü

Tez Yöneticisi : Prof. Dr. Nevin Selçuk

Ortak Tez Yöneticisi : Yrd. Doç. Dr. Görkem Külah

Mart 2008, 194 sayfa

Kömür, bugün en yüksek rezervlere sahip fosil yakıttır. Giderek katılaşan çevresel mevzuatlardan dolayı, kömür yakıtlı yakma sistemlerinde temiz kömür yakma teknolojileri kullanılmalıdır. Kömür kaynaklarından temiz ve verimli enerji eldesi için en uygun teknoloji "Akışkan Yataklı Yakma" teknolojisidir. Bu kaynağın değerlendirilmesinde dolaşımlı akışkan yataklı (DAY) yakıcı teknolojisinin uygulamaları son on yılda hem kapasite hem de sayı olarak sürekli artmaktadır. Bu ünitelerin tasarımı, DAY şartlarında yakıt ve kireçtaşının yanma ve desülfürizasyon özelliklerinin belirlenmesi için pilot ölçekli tesislerde gerçekleştirilen yakma testlerine dayandırılmıştır. Ancak, yüksek uçucu madde, kükürt ve kül içeriği ile Türk linyitlerinin DAY kazanlarında değerlendirilmesi, DAY yakma teknolojisinin bu yakıtlara adapte edilmesini gerektirmektedir. Bu

nedenle, bu çalışmanın amacı yerli bir linyit kaynağının dolaşımlı akışkan yataklı yakıcıda yanma özelliklerinin belirlenmesi olmuştur.

Bu çalışmada, mevcut 0,3 MWt Kabarcıklı Atmosferik Akışkan Yataklı Yakıcı (AAYY) Test Ünitesi'nde elde edilen kapsamlı deneyimlere dayanarak bir adet 150 kWt Dolaşımlı Akışkan Yataklı Yakıcı Test Ünitesi tasarlanmış ve Orta Doğu Teknik Üniversitesi Kimya Mühendisliği Bölümü'nde kurulmuştur. Devreye alma testlerini takiben, Çan linyitinin DAY şartlarında yanma özelliklerini incelemek ve test ünitesinin tasarım verilerini deneysel bulgularla karşılaştırmak için yakma testleri gerçekleştirilmiştir.

Yakma testlerinin yatışkın durum sonuçları, Çan linyitinin yüksek yanma verimliliği ile yakıldığını göstermektedir. Soğutma sisteminin iyi idare edilmesi sayesinde yakıcı boyunca sıcaklık profilinin neredeyse sabit olması sağlanmıştır. Seyrek bölgedeki düşük katı derişimi sebebiyle bu bölgedeki basınç düşümünün kayda değer olmadığı bulunmuştur. Kabarcıklı AAYY test ünitesinde aynı linyit yakılırken edinilen tecrübelerle karşılaştırıldığında, baca gazındaki CO ve NO derişimleri oldukça düşük, N_2O derişimi ise yüksektir. Yatak altı külü ve dolaşan külün boyut dağılımlarındaki değişimler, deneyler arasındaki kolon hızı farkıyla iyi bir uyum içindedir. Basınç denkliği modelinin geçerliliği ve öngörü doğruluğunu test etmek amacıyla, test çalışmalarının sonuçlarına dayanan düzeltilmiş girdi verileri kullanılarak model test ünitesine tekrar uygulanmıştır. Model öngörülerinin deneysel sonuçlarla karşılaştırılması, öngörülerin ölçümlerle kabul edilebilir bir uyum içinde olduğunu göstermiştir. Sonuç olarak, 150 kWt DAYY Test Ünitesinin başarımı, yerli linyit kaynaklarının dolaşımlı akışkan yataklı yakıcılardaki yanma ve kükürt giderme özellikleri üzerine yapılacak uzun dönemli araştırma çalışmalarında kullanım için tatmin edici bulunmuştur.

Anahtar Kelimeler: DAYY, Yakma Testi Ünitesi, Türk Linyitleri

To Firuze

ACKNOWLEDGMENTS

I would like to express my deepest gratitude to my supervisor Prof. Dr. Nevin Selçuk for all motivation and guidance she provided during this study and my entire graduate study. I wish to show my appreciation to my co-supervisor, Assist. Prof. Dr. Görkem Külah for her valuable efforts throughout the study. Thanks for her support and patience during the completion of this thesis.

I also would like to thank to my friends in the FBC research team for their support for completion of the study; Yusuf Göğebakan, Zuhal Göğebakan, Işıl Ayrancı, Ahmet Bilge Uygur, Mehmet Moralı and the others that had worked in this research team.

Special thanks to Dr.Olcay Oymak and Ümit Kırmızıgül for their endless support till the end. The support by TÜBİTAK – TEYDEB supplied through R&D project No. 3040029 executed by Mimag-Samko Inc., namely 'Circulating Fluidized Bed Combustor Test Unit', is greatly acknowledged.

I would like to thank especially to my wife Firuze for her patience and support. Finally, sincere thanks to my parents for their great support during all the study and especially for their lifetime effort on me. My brother, Dr. Tuğkan Batu, deserves special thanks for his guidance.

TABLE OF CONTENTS

ABSTRACT iv

ÖZ vi

ACKNOWLEDGMENTS ix

TABLE OF CONTENTS x

LIST OF TABLES xvi

LIST OF FIGURES xix

LIST OF SYMBOLS xxii

CHAPTER

1. INTRODUCTION 1

1.1 Energy Review 2

1.1.1 World Energy Review 2

1.1.1.1 World Energy Demand 2

1.1.1.2 World Energy Resources 3

1.1.2 Turkey Energy Review 4

1.1.2.1 Energy Demand and Generation Projections 4

1.1.2.2 Coal Reserves in Turkey 5

1.1.2.3 Coal Fired Power Plants of Turkey 6

1.1.3 Fluidized Bed Combustion (FBC) Technology 7

1.1.3.1 General Characteristics 7

1.1.3.2 Advantages of FBC Technology 8

1.1.3.3 Types of FBCs 8

1.2 Literature Survey 9

1.2.1 CFB Boiler Design 9
1.2.2 CFB Test Facilities 11
1.3 Scope Of The Thesis 12
2. DESIGN STUDIES 17
2.1 Basic Design Studies 17
2.1.1 Fuel Range Determination 17
2.1.2 Design Basis And Assumptions 19
2.1.3 Mass Balance 25
2.1.3.1 Solid Input 25
2.1.3.2 Combustion Air 25
2.1.3.3 Flue Gas 26
2.1.3.4 Flue Gas Composition 28
2.1.3.5 Ash Content 28
2.1.3.6 Species Balance 28
2.1.3.7 Discussions On Mass Balance 29
2.1.4 Heat Balance 29
2.2 Detailed Design Studies 32
2.2.1 Process And Instrumentation 32
2.2.1.1 Flue Gas System 33
2.2.1.2 Combustion Air System 34
2.2.1.3 CFB Combustor 36
2.2.1.4 Solids Handling and Feeding System 37
2.2.1.5 Gas Analysis System 39
2.2.2 Control System 41
2.2.3 Equipment Design 42
2.2.3.1 Furnace 42
2.2.3.2 Cyclone 42
2.2.3.3 Coal and Limestone Silos 46
2.2.4 Solids Holdup Profile snd Pressure Balance 46
2.2.4.1 Pressure Balance Model 47
2.2.4.2 Pressure Drop Through Riser (ΔP_r) 48

2.2.4.3 Pressure Drop Through Cyclone (ΔP_c) 53
2.2.4.4 Pressure Drop In The Loop Seal (ΔP_{ls}) 53
2.2.4.5 Pressure Balance For Downcomer (ΔP_{dc}) 56
2.2.4.6 Solid Mass In Riser And Loop Seal 57
2.2.4.7 Input Data To The Pressure Balance Model 58
2.2.4.8 Results Of The Pressure Balance Model..... 59
2.2.4.9 Pressure Drop Profile 60
2.2.5 Heat Transfer Analysis 62
2.2.5.1 Modules Without Cooling 63
2.2.5.2 Modules With Cooling 68
2.2.6 Detailed Design of Combustor 70
2.2.6.1 Windbox Module 71
2.2.6.2 Distributor 71
2.2.6.3 Module-1 73
2.2.6.4 Module-2 73
2.2.6.5 Module-3 73
2.2.6.6 Module-4 74
2.2.6.7 Exit Module 74
2.2.6.8 Instrument Ports..... 74
3. PROCUREMENT and INSTALLATION 75
3.1 Procurement Activities..... 75
3.1.1 Steel Structure..... 75
3.1.2 Circulating Fluidized Bed Combustor Riser 75
3.1.2.1 Distributor and Bearing Plates 76
3.1.2.2 Module – 1 77
3.1.2.3 Module – 2 77
3.1.2.4 Module – 3 79
3.1.2.5 Module – 4 79
3.1.2.6 Exit Module 79
3.1.3 Cyclone..... 79
3.1.4 Start-Up Burner..... 80

3.1.5 Piping 83
3.1.6 Combustion Air Fan 83
3.1.7 Solids Handling and Feeding 84
3.1.7.1 Solids Handling 84
3.1.7.2 Solids Feeding 85
3.1.8 Instrumentation 85
3.1.8.1 Pressure Transmitters (PT) 85
3.1.8.2 Delta Pressure Transmitters (DPT) 86
3.1.8.3 Air Flow Rate Transmitters (FT) 86
3.1.8.4 Air Rotameters (RM) 86
3.1.8.5 Water Flowmeters (FT) 86
3.1.8.6 Temperature Transmitters (TT) 86
3.1.8.7 Air Flow Control Valves (FCV) 86
3.1.8.8 Load Cells (WT) 87
3.1.8.9 Load Cell Current Transformers 87
3.1.8.10 Oxygen Analyzer 87
3.1.8.11 Purge System 89
3.1.9 Electrical System 90
3.1.9.1 Motor Control Hardware 90
3.1.9.2 Motor Control and Auxiliary Loads Panel 90
3.1.9.3 Motor Protection and Isolation Reactors 91
3.1.9.4 Cabling 91
3.1.10 Insulation 92
3.2 INSTALLATION ACTIVITIES 93
3.2.1 Combustion Air System 93
3.2.2 Instrumentation 94
3.2.2.1 Temperature Transmitters 94
3.2.2.2 Differential Pressure Transmitters 95
3.2.2.3 Load Cells 95
3.2.2.4 Water Flowmeters 98
3.2.3 Control System 98

3.2.4 Summary of Installation and Commissioning Works 103

4. OPERATION 110

4.1 Refractory Drying 110

4.1.1 Procedure 110

4.1.2 Drying Operation 113

4.2 Coal Fired Combustion Test 116

4.2.1 Commissioning Tests 116

4.2.1.1 Procedure 117

4.2.1.2 Operation 117

4.2.2 Combustion Tests 123

4.2.2.1 Procedure 125

4.2.2.2 Operation 125

4.2.2.3 Coal Properties 129

4.2.2.4 Initial Bed Material 131

4.2.2.5 Operating Conditions 132

5. RESULTS AND DISCUSSION 137

5.1 Temperature Profiles 137

5.2 Pressure Profiles 139

5.3 Flue Gas Emissions 144

5.4 Ash Compositions 146

5.5 Ash Split 148

5.6 Particle Size Distributions 149

5.7 Heat Transfer Analysis 152

5.7.1 Heat Transfer In Cooled Modules 153

5.7.2 Overall Heat Balance 155

5.8 Combustion Efficiency 156

5.9 Pressure Balance Model 157

6.CONCLUSIONS 162

6.1 General 162

6.2 Suggestions For Future Work 163

REFERENCES 165

APPENDICES 170

A. ENERGY FIGURES 170
B. BASIC DESIGN 171
C. DETAILED DESIGN 174
D. PROCUREMENT and INSTALLATION 180
E. RESULTS 189

VITA 194

LIST OF TABLES

Table 1.1 Design Parameters 11
Table 1.2 Specifications of Circulating Fluidized Bed Combustor Test Units 13

Table 2.1 Range of Coal Analysis 18
Table 2.2 Mass Balance Results 29
Table 2.3 Heat Balance Results 31
Table 2.4 Unit Dimensions of Cyclone 43
Table 2.5 Particle Capture Efficiency 45
Table 2.6 Design Basis for Pressure Balance Model 58
Table 2.7 Calculated Input Data for Pressure Balance Model 59
Table 2.8 Results of Pressure Balance Model (Gs = 15 kg/m²s) 59
Table 2.9 Pressure Drop Within the CFBC Loop (Gs = 15 kg/m²s) 61
Table 2.10 Solid Mass Within the CFBC Loop 62
Table 2.11 Input Data for Heat Transfer Analysis of Modules w/o Cooling 67
Table 2.12 Results for Heat Transfer Analysis of Modules w/o Cooling 67

Table 4.1 Time Schedule for Drying 112
Table 4.2 Steps of Coal Fired Complementary Operation for Drying 117
Table 4.3 Coal Analysis for Combustion Test-1 129
Table 4.4 Coal Analysis for Combustion Test-2 130
Table 4.5 Particle Size Distribution of Bed Material 132
Table 4.6 Operating Conditions of the Combustion Tests 133

Table 5.1 Overall Pressure Drop Values Through Main Parts 140
Table 5.2 Flue Gas Emissions for Test-2 (dry basis) 145
Table 5.3 Chemical Analysis of Bottom Ash and Bag Filter Ash 147
Table 5.4 Particle Size Distribution of Loop Seal Ash 149
Table 5.5 Particle Size Distribution of Bottom Ash 150
Table 5.6 Heat Transfer Data for Cooled Modules 154
Table 5.7 Heat Balance Analysis 155

Table 5.8 Combustion Efficiency Analysis.....157
Table 5.9 Deviated Input Parameters of Pressure Balance Model 159
Table 5.10 Solid Holdup Values Predicted by Pressure Balance Model.....160
Table 5.11 Pressure Drops within the CFBC Loop 160

Table A.1 World Total Energy Consumption By Fuel (2001 – 2025) 170
Table A.2 World Energy Consumption For Electricity Generation By Fuel.....170

Table B.1 Analysis of Beypazarı Lignite 171
Table B.2 Coal and Limestone Consumptions 171
Table B.3 Oxygen Demand and Combustion Air Data 171
Table B.4 Flue Gas Data 172
Table B.5 Cross Sectional Area and Dimensions 172
Table B.6 Flue Gas Composition 172
Table B.7 Ash Generation and Contents.....173

Table C.1 Cyclone Inlet Duct Data.....174
Table C.2 Cyclone Dimensions (cm).....174
Table C.3 Physical Properties for Pressure Balance Model.....174
Table C.4 Calculated Parameters of Pressure Balance Model (Gs = 15 kg/m²s)...175
Table C.5 Air Box Module Ports.....175
Table C.6 Module-1 Ports 175
Table C.7 Module-2 Ports 176
Table C.8 Module-3 Ports 176
Table C.9 Module-4 Ports 176
Table C.10 Exit Module Ports 177
Table C.11 Temperature Transmitters 177
Table C.12 Pressure/Delta Pressure Transmitters 178
Table C.13 Gas Probes.....178

Table D.1 Specifications of Screw Conveyors And Air Lock 186
Table D.2 Pressure Transmitters 186

Table D.3 Delta Pressure Transmitters 186
Table D.4 Air Flow Rate Transmitters 187
Table D.5 Air Rotameters 187
Table D.6 Water Flowmeters 187
Table D.7 Temperature Transmitters.....187
Table D.8 Air Flow Control Valves.....188
Table E.1 Steady State Temperature Measurements along the Combustor.....189
Table E.2 Steady State Pressure Measurements along the Combustor.....190
Table E.3 Particle Size Distributions of Bag Filter Ash 191

LIST OF FIGURES

Figure 2.1 Schematic Diagram of METU CFBC Test Rig 19
Figure 2.2 Process Diagram of the Test Unit 32
Figure 2.3 PID of the Flue Gas System 33
Figure 2.4 PID of Combustion Air System 35
Figure 2.5 PID of CFB Combustor 36
Figure 2.6 PID of Solids Handling System and Feeding System 38
Figure 2.7 PID of Gas Analysis System 40
Figure 2.8 Schematic Diagram of Control System 41
Figure 2.9 CFB Cyclone 43
Figure 2.10 Schematic Diagram for Pressure Balance Analysis 47
Figure 2.11 Schematic Diagram of Loop Seal (1.Weir, 2.Vertical aeration) 54
Figure 2.12 Solid Hold Up Profile for Dilute Zone (Gs = 15 kg/m²s) 60
Figure 2.13 Pressure Loop Profile (Gs = 15 kg/m²s) 61
Figure 2.14 Schematic Heat Transfer Diagram for First and Fourth Modules 64
Figure 2.15 Schematic Diagram for Cooled Second and Third Modules 69
Figure 2.16 Detailed Design Drawing for the CFBC 72

Figure 3.1 Main Steel Structure of the Test Unit 76
Figure 3.2 Inner Views of Modules 1 and 2 78
Figure 3.3 Schematic Diagram of Start-up Burner System 80
Figure 3.4 Start-up Natural Gas/LPG Burner 82
Figure 3.5 Trimox ZrO2 Oxygen Analyzer 88
Figure 3.6 Sample Diagram for Purge System 89
Figure 3.7 Load Cell Installation 96
Figure 3.8 Screw Feeders of Fuel and Limestone Silos 97
Figure 3.9 DeltaV Controller and I/O Cards 99
Figure 3.10 Main Display Page of Control Computer 100
Figure 3.11 Test Unit - Elevation: 0 m 105
Figure 3.12 Test Unit - Elevation: 5.5 m 106

Figure 3.13 CFBC and BFBC Test Units.....107
Figure 3.14 Test Unit – Elevation 9.5 m (1) 108
Figure 3.15 Test Unit – Elevation 9.5 m (2) 109

Figure 4.1 Typical Drying Schedule for Castable Refractories 111
Figure 4.2 Average Temperature Profiles during Drying Process 114
Figure 4.3Average Temperature Profiles for Commissioning Run-1.....118
Figure 4.4 Average Temperature Profiles for Commissioning Run-2.....120
Figure 4.5 Maximum Temperature Profiles - Drying and Commissioning Runs ..121
Figure 4.6 Schematic Diagram for Vacuum System in Solids Feeding Leg 123
Figure 4.7 Average Temperature Profiles for Combustion Test-1.....126
Figure 4.8 Average Temperature Profiles for Combustion Test-2.....126
Figure 4.9 Dense Bed Pictures During Operation 128

Figure 5.1 Steady State Temperature Profile for Combustion Test-1 138
Figure 5.2 Steady State Temperature Profile for Combustion Test-2 138
Figure 5.3 Steady State Pressure Profile for Combustion Test-1.....142
Figure 5.4 Steady State Pressure Profile for Combustion Test-2.....142
Figure 5.5 Particle Size Distributions of all Solid Streams.....151
Figure 5.6 Predicted and Measured Pressure Profiles for Combustion Test-1 158
Figure 5.7 Predicted and Measured Pressure Profiles for Combustion Test-2 158

Figure A.1 Distribution of world fossil fuel reserves 170

Figure C.1 Instrument Ports 179

Figure D.1 Distributor Plate 180
Figure D.2 Bearing Plate 180
Figure D.3 Module – 1.....181
Figure D.4 Module – 2.....182
Figure D.5 Modules 3 and 4.....183
Figure D.6 Cyclone.....184
Figure D.7 Windbox after Burner Valve Train is Installed.....184
Figure D.8 Solids Handling and Feeding.....185

LIST OF SYMBOLS

A_{ls} : cross sectional area of the loop seal, m^2

A_r : cross sectional area of riser, m^2

A_c : inlet area of cyclone, m^2

A_{dc} : cross sectional area of downcomer, m^2

a : decay constant in the dilute zone, m^{-1}

a_e : decay constant affected by the exit geometry, m^{-1}

C_{bot} : carbon content of bottom ash, %

C_{cy} : empirical coefficient for velocity head at cyclone

C_e : reflux constant

C_D : Drag coefficient

C_{fly} : carbon content of fly ash, %

C_p : specific heat, kcal/kg °C

D : diameter of particle, µm

D_{cut} : diameter of particle for which the capture efficiency is 50%, µm

D_e : diameter equivalent of the riser exit, m

D_r : diameter of riser, m

D_{ls} : diameter of loop seal, m

d_p : particle diameter, mm

G_s : solid circulation rate, kg/m^2 s

G_{sh} : solid mass flux based on horizontal section area of cyclone duct, kg/m^2 s

G_{sd} : solid mass flux based on loop seal area, kg/m^2 s

H_f : height of the dilute zone, m

H_{dc} : height of the solid bed in the downcomer, m

H_e : projected height of the riser exit, m

h_i : heat transfer coefficient to combustor wall, W/m^2 K

h_o : heat transfer coefficient for external surface, W/m^2 K

ΔH_{rxn} : heat of reaction, kcal/kg

K : velocity head multiplier

k_1 : thermal conductivity for refractory layer, W/m K

L_{va} : length of vertical aeration section, m

L_w : length of weir section, m

L_{ls} : total length of the loop seal ($L_{ls} = L_w + L_{va}$), m

M : solid mass, kg

m : mass flow rate, kg/h

N : number of rotation that the gas stream makes in the cyclone

n : molar flow rate, mol/h

ΔP : pressure drop, mmH_2O

Re_p : Reynolds number for particles

T : temperature, °C

T_w : Temperature of cooling water, °C

T_c : Temperature in the combustor, °C

T_{c-s} : Temperature at inner surface of refractory, °C

T_a : Ambient temperature, °C

T_s : External surface temperature of insulation, °C

T_{r1} : Temperature at outer surface of refractory, °C

U_d : superficial solid velocity (G_s/ρ_s), m/s

U_g : gas velocity, m/s

U_t : terminal velocity of particles, m/s

U_{gh} : average velocity at cyclone duct, m/s

U_o : fluidizing gas velocity at loop seal, m/s

V_c : velocity along the circular path, m/s

z : height in the riser, m

z_d : height of the dense bed, m

z_f : height in the dilute zone, m

Greek Letters

$\Delta\varepsilon_{sr}$: deviation of solid holdup by particle reflux

ε_{se} : solid hold up at the exit

ε_s : solid hold up in the dilute zone

$\varepsilon_{s\infty}$: average solid hold up at dilute zone

ε_{sd} : solid hold up in the dense bed of riser

ε_s^* : solid holdup at uniform flow with the slip velocity = U_t

ε_{dc} : voidage of solid bed in downcomer

ε_{ls} : voidage of the solid bed in the loop seal

ϕ_s : particle sphericity

μ : gas viscosity, kg/m s

ρ_s : particle density, kg/m³

ρ_g : gas density, kg/m³

ρ_{bulk} : bulk density of fly ash, kg/m³

η_{comb} : combustion efficiency, %

Subscripts

c : cyclone

dc : downcomer

dense : dense zone

dilute : dilute zone

h : cyclone duct

ls : loop seal

Abbreviations

AI : analog input

AO : analog output

AT : analyzer with anolog output signal

DCS : distributed control system

DI : digital input

DO : digital output

DPT : pressure difference transmitter

FC : fixed carbon, %

FCV : flow control valve

FID : frequency invertor driver

FT : flow transmitter

HMI : human-machine interface

LHV : lower heating value, kcal/kg

LMTD : log mean temperature difference, K

LS : level switch

PID : process and instrumentation diagram

PT : pressure transmitter

SOV : solenoid valve

TCV : temperature control valve

TT : temperature transmitter

UPS : uninterrupted power supply

VM : volatile matter, %

WT : weight transmitter

ZV : sliding gate valve

CHAPTER 1

INTRODUCTION

Coal is today the fossil fuel which offers the greatest proven reserves. Due to increasingly stringent environmental legislation, coal fired combustion systems should be based on clean coal combustion technologies. For clean and efficient energy generation from coal reserves, the most suitable technology known to date is the 'Fluidized Bed Combustion' technology. Applications of circulating fluidized bed combustion (CFB) technology have been steadily increasing in both capacity and number over the past decade for the utilization of this resource. Designs of these units have been based on the combustion tests carried out in pilot scale facilities to determine the combustion and desulfurization characteristics of the coals and limestones in CFB conditions. However, adaptation of CFB combustion technology to Turkish lignites with high ash, volatile matter and sulfur contents necessitates presence of a local CFBC test facility, where CFB combustion characteristics of indigenous reserves can be determined.

Therefore, the objective of this study have been to design and construct a 150 kWt CFB combustor and perform a combustion test with a typical Turkish lignite. For this purpose, the steps to be covered were defined as; i. Basic design of the 150 kW_t METU CFB combustor test unit, ii. Detailed design of the test unit, iii. Equipment and material purchasing and construction, iv. Combustion test with a typical Turkish lignite and generating data for the design of a commercial unit.

In this chapter, introduction of energy review for Turkey and the world including energy demand, projections, and coal reserves of Turkey, followed by the problems of coal fired power plants of Turkey. Then, the general characteristics,

advantages and types of fluidized bed combustion are summarized. In literature survey section, required data for CFB boiler design, and the specifications of some CFB test facilities around the world are presented.

This study covers basic and detailed design of the CFB combustor test unit, manufacturing and installation activities, combustion test run with a typical Turkish lignite, and by employing the experimental data; validation of design for the test unit, and generation of data that can be used as basis for design of commercial boilers.

1.1 Energy Review

1.1.1 World Energy Review

1.1.1.1 World Energy Demand

World energy demand has been increasing tremendously as a result of population increase, industrialization and technological development. Energy consumption; the most important indicator of the industrial and technological development, is expected to increase in 2020 to 1.5 times of the amount in 1999 [1]. The most significant share in this increase will belong to developing countries. The dominancy of fossil fuels' share for meeting this demand will continue in the future as it is today. Fossil fuels still conserve their total share of more than 85% in world energy consumption at the end of next 25 years period (Table A.1 - App. A). Examining the amounts and shares of resources consumed for world electricity generation (Table A.2 - App. A), share of petroleum products is very low, since this resource is mostly utilized in petrochemical industry and transportation. In the next 20 years, it is expected that the generation capacity of nuclear energy will remain constant, and the coal based generation will keep on being the dominant resource.

1.1.1.2 World Energy Resources

Global distribution of petroleum, natural gas and coal reserves shows that the resources other than coal are concentrated in certain areas [2] (Figure A.1 – App.A). As a result of this, petroleum and natural gas reserves are under control of limited number of countries, and in consequence their strategic importance is maximum.

On petroleum equivalent basis, shares of fossil fuel reserves around the world are 68% for coal, %18 for petroleum and %14 for natural gas [3]. Another important parameter for the energy reserves is the life-span of the resources based on the ratio of proved reserves and annual consumption rates. According to this calculation, the life-span of the recoverable reserves based on 2003 figures is 41 years for petroleum, 67 years for natural gas and 192 years for coal [2].

By the year 2003, the states in the Middle East, having the 63% of the total petroleum reserves, are socially and politically unstable, and dealing with many problems which prevent these countries from developing.

Similarly, natural gas reserves are concentrated in two areas; like the Middle East, the states in the Caspian region are still not reliable in terms of economy and administration. Consequently, the problems that may occur as the natural gas reserves get less in the future is unpredictable. However, the production of coal in more than 100 countries in all continents, and the reserve/production ratio for coal resulting in more than 3 times life-span compared to others, guarantee the cheapest price and continuity of the supply of coal [4].

Coal is not only used for steam generation in industrial processes and heating, but also is the resource in many countries that significant share of the electricity generation is based on. The share of coal fired power plants in electricity generation is 53% in USA, 51% in Germany, 65% in Greece, 77% in China, 52% in Denmark, %78 in Australia, 92% in South Africa and 95% in Poland [5,6].

However, only 25% of the total electricity is generated by the coal fired power plants in Turkey.

1.1.2 Turkey Energy Review

1.1.2.1 Energy Demand and Generation Projections

When the situation in Turkey is examined, energy demand in 2025 is expected to increase to 1.7 times the demand in 2000 [1], and the electricity consumption will be approximately doubled from 114 to 226 billion kWh for the same period [7].

Installed power generation capacity of Turkey is dominantly based on hydroelectricity followed by natural gas and coal fired power plants. The breakdown of the capacity based on fossil fuels shows that the share of natural gas is 52%, and is expected to conserve its share against coal and petroleum for the following 20 years, similar to the trend in the last decade [8-10].

As a result of the contribution of such high amount of natural gas and coal import, dependency of total energy consumption on imported sources is expected to be about 75% in 2020, which is presently 65% [11].

This switch from indigenous energy sources to imported ones is claimed to result in significant imbalance in foreign trade of Turkey. Unless there appears a significant technological development resulting in a fuel switch especially in transportation sector and petrochemical industry, dependency on petroleum import cannot be expected to decrease. Also, because of environment and efficiency concerns, natural gas use in residential heating is an acceptable choice against coal and petroleum products. In power generation, coal utilization is still the dominant application all around the world, on the other hand a switch from coal to natural gas occurred in Turkey in the last decade.

However, considering that it is a preferable energy policy to diversify the type of resources and to employ indigenous reserves, lignite reserves should be utilized to

balance the actual natural gas dominancy for electricity generation in Turkey. For this purpose, lignite and hard coal reserves should be examined.

1.1.2.2 Coal Reserves in Turkey

Lignite

Lignite reserves that are dispersed throughout the country have heating values varying between 1,000–5,000 kcal/kg. Lower calorific values of lignite reserves have a breakdown as follows: 6.9% over 3,000 kcal/kg, 13.2% between 2,500 and 3,000 kcal/kg, and 79.9% below 2,500 kcal/kg [12].

Geographical distribution of lignite reserves with a total amount of 9.3 billion tons can be found elsewhere [12]. It must be noted that regional distribution data in different sources is for the reserves operated by Turkish Coal Enterprises (TKİ), but some significant amount of reserves owned by private companies are known to be present.

Hard Coal

Most of the hard coal reserves of Turkey are in Zonguldak region. Total amount of hard coal reserves discovered in that region is about 1.1 billion tons. Average chemical characteristics of the coal reserves is about 55% fixed carbon (FC), 26% volatile matter (VM), 11% ash, 8% moisture resulting in a calorific value of about 5,500 – 6,000 kcal/kg. Other than Zonguldak region, some other hard coal reserves are present with insignificant amounts of reserves. Considerable utilization of hard coal in power plants other than the one located in Çatalağzı is not expected in the near future due to high costs for mining of this resource.

Turkey has asphaltite reserves about 79 million tons, most of which are located in the southeastern part of the country. This resource is characterized by high calorific value of about 5,500 kcal/kg like hard coal, but also high sulfur content like lignite. There is also significant amount of bituminous shale reserves adding

up to 1.1 billion tons. However, the calorific value of the reserves are in between 800 and 1,100 kcal/kg.

Consequently, lignite seems to be the only indigenous coal reserve in Turkey that plays an important role in power generation considering the amount of reserves, and these reserves have been mainly employed in pulverized coal fired power plants.

1.1.2.3 Coal fired power plants of Turkey

Power plants of Turkey based on pulverized coal (PC) technology have serious problems. This technology was developed by the countries who have high quality coal reserves. However, Turkish lignite reserves have high ash, moisture and sulfur contents and low calorific value. It is worth noting that ash fusion temperature of these lignites are low enough to soften at 1000°C and especially the particles having dimension of microns start to melt in regions close to pulverized coal burners. Whenever one single particle melts and sticks on cooling surfaces (water-wall), many others rapidly follows and a glassy layer is formed on the water-walls within a short time. This formation creates resistance against the heat transfer from combustion side to water in the tubes, which results in less steam production under-design conditions, change in physical behaviour of the system, and finally necessitates additional coal consumption to generate same amount of energy (electricity, heat etc.).

This additional coal consumption causes also an increase in emissions per unit energy generation [4]. That's why, clean coal technologies, formerly developed and continuing their growth in terms of application and capacity, should be introduced to Turkey's energy profile.

For clean and efficient energy generation from indigenous lignite reserves, the most suitable technology known to date is the 'Fluidized Bed Combustion' technology that has been applied at a capacity to generate steam for 300MW

electrical power at one unit [13], where conceptual design for 600MWe units are under progress. In Turkey, a power plant based on this application, Çan Thermal Power Plant with a capacity of 2 x 160 MW, is now under operation [14].

1.1.3 Fluidized Bed Combustion (FBC) Technology

In 1930s and 1940s, after extensive research and development activities, many advantages of fluidized beds were recognized. These reactors were first employed in catalytic cracking processes. Afterwards, they were utilized in many other industries.

At the beginning of 1960s, the necessity to decrease the emissions of sulfur dioxide (SO_2) and nitrogen oxides (NO_x) emitted from coal fired power plants, and the potential of fluidized bed reactor process to decrease these emissions, initiated the research on the coal fired fluidized bed combustors (FBC). As a result of these studies, following the introduction of bubbling fluidized bed boilers in 1970s, the applications moved towards circulating fluidized bed boiler technology in 1980s, and since then increasing number of successful power plant applications have been taken into operation.

1.1.3.1 General Characteristics

FBC systems are attractive because better control over combustion is realized so that peak flame temperatures are avoided. Slagging of the ash is eliminated, corrosion problems and nitrogen oxide emissions are reduced, and sulfur control with limestone addition to the bed is possible. Since in-bed heat transfer coefficients are high, fluidized bed boilers are more compact than PC systems. Mixing rate of particles is significant because of high turbulence, enabling close contact between particles and gas.

Consequently, bed temperature and associated heat fluxes are uniform. Moreover fuel particle residence times are longer about ten times than those of the PC

technology. A wide range of fuels including high-ash, high-moisture fuels can be used. The main disadvantage is that the pressure drop across the bed is greater.

1.1.3.2 Advantages of FBC Technology

FBC technology is characterized by many advantages that are given below:

- High combustion efficiency and high heat transfer coefficient
- Ease of fuel preparation
- High availability
- Fuel flexibility
- Low SO_2 and NO_x emissions
- Ash Utilization

1.1.3.3 Types of FBCs

Depending on the state of fluidization, there are two basic types of FBCs; Bubbling FBC (BFBC) and Circulating FBC (CFBC).

Bubbling Fluidized Bed Combustor (BFBC)

In a BFBC, the combination of larger particle diameter and low gas velocity is such that minimum entrainment and carryover of solids occurs. Gas in excess of that required to provide the minimum for fluidization rises through the bed in the form of bubbles. The bed has a discernable surface. Fuel and sorbent particles that are entrained in the gas flow leaving the bed can be captured in dust collectors downstream the combustor. In BFBCs, small particles such as char near burnout tend to be blown out of the bed before combustion is complete. Furthermore, a feed point is needed for approximately every 1 m^2 for good mixing of the coal, which is a limitation for large systems. Circulating fluidized beds have been developed to overcome the tendency for high carbon carryover of bubbling beds and to facilitate fuel feeding.

Circulating Fluidized Bed Combustor (CFBC)

In CFBCs, velocity is increased beyond the particle entrainment velocity, so that the solids are transported up the full height of the chamber and returned in the downward leg of a cyclone separator. The pressure drop across the system is a function of the velocity and the particle loading. This type of fluidization is characterized by high turbulence, solids back mixing, and the absence of a defined bed level.

A small amount of air is usually introduced near the bottom of the cyclone downcomer to control the return rate of the solids. Mixing of fuel with bed material is rapid due to the high turbulence. Although there is no definite fixed bed depth, the density of the bed varies throughout the system, with the highest density near the grid plate.

Secondary air is used to ensure adequate air for combustion of fines in the upper part of the combustion chamber. The chamber may have waterwalls, although the lower portion near the inlet air grid is usually covered with refractory. The cyclone collectors, located at the outlet of the combustion chamber, are steel vessels lined with hard-faced refractory backed by lightweight insulating refractory. Char and bed particles continue to circulate until they are reduced to 5-10 µm, at which point they escape the cyclone collector. The fuel feed rate and airflow rates are adjusted depending on the steam load so that combustion takes place near 850°C. Turndown of 3:1 can be achieved by reducing the air and fuel flow rates.

1.2 Literature Survey

1.2.1 CFB Boiler Design

The primary function of a CFB boiler is to transform and transfer the chemical energy of a fuel into useful heat using the CFB mode of gas-solid contacting. This

transformation should be efficient and have minimum effect on the environment. For this purpose, the following parameters should be considered in a CFB boiler design [16,18]:

- Heat generation demand defined in terms of thermal power requirement, MWt.

- Fuel analysis:
  - Heating value
  - Elementary Analysis (C, H, N, O)
  - Ash content
  - Water content
  - Volatile matter/fixed carbon content
  - Sulfur content
  - Ash analysis
  - Physical characteristics (Particle size distribution, grindability etc.)

- Limestone Analysis
  - $CaCO_3$ content
  - Reactivity
  - Pore structure

The most of the analyses given above are determined by standard analytical methods and devices. However, the combustion and desulfurization characteristics of the fuel and limestone in CFB conditions can only be determined by a combustion test prior to detailed design of the boiler and its auxiliary systems.

The combustion and desulfurization characteristics acquired from combustion tests lead to the prediction of the following design parameters:

Table 1.1 Design Parameters Obtained from Combustion Tests

Combustion Test Data	**Design Parameter**
Combustion efficiency	Prediction of thermal efficiency
Fly/Bottom ash split	Capacity of fly and bottom ash removal systems
Fly / Bottom ash composition (leads to heat capacity of ash streams)	Ash utilization potential Trace elements content Cooling capacities of ash removal equipment Prediction of thermal efficiency
Fly/Bottom ash particle size distribution	Cyclone design Design of particle removal device Design of ash removal systems
Limestone utilization	Limestone consumption and feeding system Selection of the most suitable limestone Best particle size distribution for limestone
Mechanical attrition	Cyclone design Design of particle removal device
Fly ash resistivity	ESP design
Pollutant gas formation/emission	Secondary air ratio and location for NO_x removal Combustion control Optimum Ca/S ratio

The parameters given above are necessary in the design of CFB boilers in order to have high operation performance. Therefore, any coal reserve should be tested in a CFB combustor test facility prior to boiler design.

1.2.2 CFB Test Facilities

Applications of circulating fluidized bed combustion technology developed for burning coal with high efficiency and within acceptable levels of gaseous pollutant emissions have been steadily increasing in both capacity and number over the past decade. Utilization of different kind of solid fuels and gradual

introduction of increasingly restrictive legislations on emissions from combustion sources has been keeping the topic attractive for further research.

A number of CFB combustor test units have been constructed by research centers, universities and companies manufacturing CFBCs around the world, and these facilities are still being utilized for the investigation of different fuels and further development of the technology. Table 1.2 provides a compilation of relevant test facilities and their main specifications. Specifications of these facilities summarized in the table are utilized as reference for design of CFBC Test Unit.

1.3 Scope Of The Thesis

As summarized above, Turkish lignite reserves are characterized by high moisture, ash and sulfur contents, high VM/FC ratio and low calorific value. Circulating fluidized bed technology is the only available application for the utilization of these low quality resources efficiently and environmentally friendly. For the adaptation of this technology to Turkish lignite reserves, METU 150 kWt CFB combustor is designed and constructed, combustion test with a typical Turkish lignite is performed for the assesment of test unit design, and generation of data that can be used as basis for design of commercial boilers. During the progress of this study, following phases are accomplished:

- Basic design of the system
- Detailed design of the equipment
- Equipment and material purchase/manufacture and installation
- Combustion test with a typical Turkish lignite

The first phase; basic design studies include fuel range determination, stochiometric calculations, heat and mass balance, integration requirements with the auxiliaries of the existing system.

Table 1.2 Specifications of Circulating Fluidized Bed Combustor Test Units

Facility	**Power**	**Furnace Dia.**	**Height**	**Measurements**	**Remarks**
Niederaussem Power Plant of RWE, Rheinbraun, Germany [14]	1,200 kW	Nozzle grid: 0.45 x 0.39 m Upper furnace: 0.81 x 0.54 m	Uncooled: 3.5 m With tubes: 6.0 m	CO, CO_2, SO_2, NO_x, O_2	- Fuel and circulating solids mixed before entering combustion chamber - Velocity in the furnace at operating temperature, 5.8 m/s - Particle size; <15 mm for brown coal, <10 mm for bituminous coal - Cross sectional area heat release, 2.7 MW/m^2 - Combustion air warmed up with a tubular air heater - Combustion air can be diluted by recirculated flue gas - Solids discharged by a water cooled screw conveyor - On-line measurements of gas concentrations at the cyclone exit
Dalhousie University, Nova Scotia, Canada [19]	250 kW	0.23 x 23 m	6.5 m		- Two waterwalls, 1.7 m tall - Distributor plate composed of 9 nozzles with 18 orifices in each - Secondary air port at 1.5 m above distributor - Primary and secondary air supplied by a 6 psi blower - Solids mixture fed by a screw feeder - 28 pressure, 30 temperature measurement

Table 1.2 Specifications of Circulating Fluidized Bed Combustor Test Units (cont.'d)

Facility	**Power**	**Furnace Dia.**	**Height**	**Measurements**	**Remarks**
Canmet Ottawa, Canada [20]	800 kW	0.405 m ID 1.02 m OD	6.7 m	CO, CO_2, SO_2, NO_x, O_2	- Refractory lined steel pipe - Screw conveyor for solids feeding - Secondary air supplied at five elevations - Four retractable water cooled tubes - Feed 0.48 m above air distribution nozzles - Alt. feed port 1.52 m above distributor - Fuel and sorbent feed systems separate - Hot cyclone ID, 0.6 m - Cyclone design; capture 95% of >50µm
Ciemat Spain [21]	300 kW	0.2 m	6.5 m	CO, CO_2, SO_2, NO_x, O_2	- Solids feeding by screw feeder - Distributor plate with bubble caps - Secondary air 1.5 m above distributor plate - Refractory lined in the bottom - Water walls in the upper 2 m - Recycle line, 0.09 m I.D. - Gas composition and temperature measurements at different heights
Tampella Power Williamsport, Pennsylvania, USA [22]	3,000 kW	0.91 m	18.29 m	CO, CO_2, SO_2, NO_x, O_2, HC	- Refractory lined combustion chamber - Refractory lined hot cyclone - Separate bunkers and feed systems for fossil fuel, sorbent, and biomass - High degree of instrumentation and fully automated

Table 1.2 Specifications of Circulating Fluidized Bed Combustor Test Units (cont.'d)

Facility	**Power**	**Furnace Dia.**	**Height**	**Measurements**	**Remarks**
EERC University of North Dakota, Grand Forks, USA [23]	1,000 kW	0.508 m	12.8 m		- Refractory lined combustion chamber - 63.5 cm ID Refractory lined cyclone - 45.7 cm ID secondary stainless steel cyclone for fly ash recycle - 12 heat exchange panels - Fuel and sorbent feed by gravity from a horizontal auger - Combustion air preheated to 315°C - Secondary air feed at 1.8 m or 3.35 m above distributor plate

During detailed design phase, furnace, cyclone, fuel and limestone handling and feeding, ash removal, air and flue gas systems, circulation system (loop seal), distributor plate, automation, electrical system, bearing structure and insulation application are designed.

Following the design activities, equipment and material purchase/manufacture and installation works, including the circulating fluidized bed combustor furnace, air blower, refractory, combustion air and flue gas ducts, coal, limestone and bed ash silos, insulation material, instrumentation, control system, motor control unit, electrical equipment are completed.

Finally, the combustor is taken into operation by carrying out a combustion test with a typical Turkish lignite to determine combustion characteristics, flue gas emissions, bottom/fly ash split, and to validate the design of the system.

CHAPTER 2

DESIGN STUDIES

2.1 Basic Design Studies

Basic design studies of METU 150kWt CFB combustor test unit includes: (i) determination of fuel range; (ii) definition of design basis and assumptions; (iii) the mass balance and heat balance.

2.1.1 Fuel Range Determination

In order to determine the range of fuels for the basic design calculations, different coal resources in Turkey having enough reserves for establishing utility power plants were taken into account. Examining the analysis of these resources [23], the following fourteen lignite reserves from different origins all around Turkey were selected:

- Silopi, Şırnak
- Beypazarı, Ankara
- Saray, Tekirdağ
- Keles, Bursa
- Söke, Aydın
- Göynük, Bolu
- Ilgın, Konya
- Kangal, Sivas
- Gölbaşı, Adıyaman
- Elbistan, Kahramanmaraş
- Tufanbeyli, Adana
- Çomaklı, Çanakkale

- Eynez, Manisa
- Deniş-II, Manisa

In addition to the above mentioned Turkish lignite reserves, an imported hard coal reserve was also included in the fuel range to take into account the possibility of firing low quality lignite and imported hard coal mixture. For the basic design studies, following fuel data were obtained from the database of Turkish lignite reserves [23] and steam coal:

- Lower heating value
- Ultimate Analysis (C, H, N, S, O)
- Proximate Analysis (moisture, volatile matter, fixed carbon, ash)

The ranges of the contents and heating values of the selected coal reserves are given in Table 2.1. As can be seen from the table, the coal reserves selected for basic design studies are representative of a wide range of coal analyses.

Table 2.1 Range of coal analyses

	Range
Lower heating value, kcal/kg	1,273 – 6,000
Carbon, %	17.94 – 63.77
Hydrogen, %	1.55 – 5.07
Nitrogen, %	0.25 – 1.44
Oxygen, %	3.36 – 18.47
Combustible Sulfur, %	0.49 – 5.28
Ash, %	8.31 – 34.60
Moisture, %	0.41 – 52.00
Volatile matter, %	20.24 – 45.00
Fixed carbon, %	10.91 – 45.00

2.1.2 Design Basis and Assumptions

Before starting stoichiometric calculations for each coal reserve to obtain the ranges of input and output streams, the design basis and preliminary assumptions were defined based on the extensive experience and data accumulated during the last decade at the METU 0.3 MWt bubbling atmospheric fluidized bed combustor (AFBC) test rig which was later converted to a hybrid AFBC with the provision of recycle leg.

Physical System

In order to simplify the physical system for which the heat and mass balance analyses were carried out, a schematic diagram for METU 150 kWt CFBC Test Unit given in Figure 2.1 was prepared. As can be seen from the diagram, CFBC combustor is comprised of a furnace with a cooling system and a cyclone.

Mass balance and heat balance analyses were carried out around the combustor system (furnace and cyclone) to determine the input and output flow rates of solid and gas streams and cooling water flow rates, respectively.

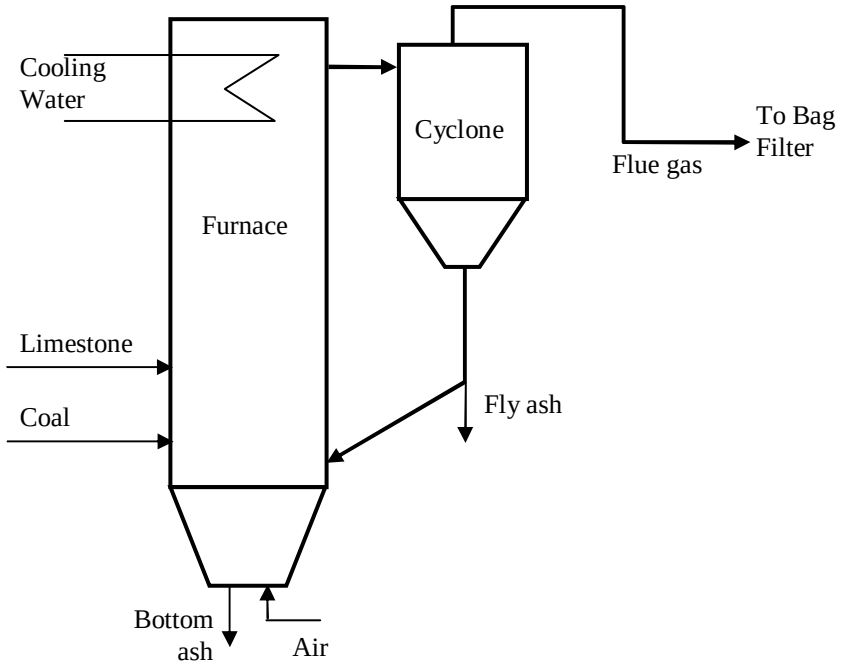

Figure 2.1 Schematic diagram of METU 150 kWt CFBC Test Unit

Basis

Basic design studies were executed on hourly basis for a steady-state operation.

Thermal input of the test unit: 150 kW

For the purpose of combustion tests, capacities of majority of test facilities installed to date are less than 1 MWt [13,18-22]. Based on the experiences gained from the existing 0.3 MWt AFBC Test Rig, 150 kW thermal input capacity was selected for this study as it was considered that this size is large enough to generate reliable data for basic design of industrial CFB boilers and small enough to operate at a lower cost with a few personnel.

However, the design of combustor should be based on one single coal reserve for which thermal load of fuel input is 150 kWt, while this input is needed to be varied for other coals. The reason for this variation of thermal input is the necessity for keeping superfical velocity in the riser – one of the leading design parameters – at 5 m/s, a typical operating parameter for CFBCs [15]. As the velocity in the combustor depends on total gas flow, which is mainly determined by combustion air demand and water content of the fuel, 5 m/s can only be achieved at different thermal fuel inputs for different coals. Therefore, thermal load is variable for different coals to keep hydrodynamic parameters like gas velocity, volume fraction of solids, particle load, pressure distribution etc. at design conditions. In conclusion, thermal input of the test unit; 150 kW, is only valid for design coal, and there is a range for other coals under consideration.

Furnace temperature: 850°C

Typical operating temperature of CFB furnaces is 850°C, which brings in many advantages to this technology. At this temperature, there is no ash fusion, sulfur capture reaction is optimum, alkali metals are not vaporized so that risk of fouling on boiler tubes is reduced, and conversion of nitrogen in the combustion air to NO_x is negligible [15]. Therefore, furnace temperature was considered to be uniform throughout the riser of CFBC and was taken as 850°C in the calculations.

Furnace pressure: 1 atm

Furnace pressure throughout the combustor varies around atmospheric pressure from slightly positive pressure at the distributor plate to a near vacuum condition at the cyclone exit. Therefore, assuming the furnace pressure to be atmospheric is acceptable for basic design calculations, as it is only used in volumetric flow rate conversion between Nm^3 and m^3. Pressure distribution was predicted in the detailed design studies, and it was observed that this asssumption was still acceptable.

Excess air ratio: 20%

Excess air ratio, which is the ratio of air in excess of what is required theoretically for stoichiometric combustion, is typically kept at 20% in CFBC applications [13,15]. Although the design is based on this value for normal operating conditions, design range considers excess air ratios up to 50% for experimental purposes.

Superficial velocity: 5 m/s

The superficial velocity range for the CFB boilers is given as 4 – 8 m/s [14]. Typical operating data for the superficial velocity is generally 5 m/s for CFBCs, because of the general norm for the avoidance of furnace erosion [15]. Moreover, as the test unit can not be as tall as a commercial unit, it is not prefered to enhance entrainment of particles and to decrease residence time by increasing the superficial velocity.

Desulfurization characteristics

One of the most important advantages of fluidized bed combustion technology is the in-situ desulfurization. Sulfur dioxide (SO_2) produced by the oxidation of combustible sulfur reacts with calcium oxide (CaO) particles produced by the calcination of limestone that is fed to the combustor together with coal. As a result of this mechanism, one of the leading pollutant gases emitted from coal fired

power plants is transformed to solid phase ($CaSO_4$) before leaving the combustor. The reactions of this sulfur capture mechanism are given in the mass balance section.

The determining parameter for this in-situ desulfurization mechanism is the temperature within the combustor. The optimum temperature range for the sulfur capture reactions is 800 – 850 °C, as the ractivity is reduced at lower temperatures, whereas $CaSO_4$ is decomposed at higher temperatures [15]. This fact is the leading motivation for the furnace temperature to be 850°C. In addition to this, Ca/S molar ratio and $CaCO_3$ content of the limestone are also effective on sulfur dioxide capture and the design basis for these parameters were determined. The effect of some other parameters like physical structure of limestone particles (size, pore characteristics, etc.), circulation rate, residence time, etc. on sorbent utilization was included in one parameter defined as desulfurization efficiency.

Calcination efficiency: 100%

The first step of sulfur capture mechanism in CFBC conditions is the calcination of $CaCO_3$ (calcium carbonate), which is the major component of limestone fed to the combustor. The calcination reaction is the release of carbon dioxide by an endothermic reaction which produces CaO. Since limestone is easily calcined at operating temperatures of CFBC [15] and the residence time of the particles within the CFB combustors is pretty high, it is assumed that all the $CaCO_3$ reacts to CaO (100% calcination efficiency) which then reacts with sulfur dioxide and oxygen to form $CaSO_4$ that leaves the combustor in solid phase within bottom and fly ash streams.

Ca/S molar ratio: 2.2

Ca/S molar ratio is an indication of operating conditions regarding the desulfurization process. It is the ratio of calcium fed to the combustor to sulfur on molar basis. In this study, Ca/S ratio is based on the calcium coming from the limestone and the combustible sulfur. When this ratio is defined for a system,

limestone consumption is determined by multiplying the ratio with molar sulfur content of the coal and dividing by molar composition of Ca in limestone. Although Ca/S ratios within 1.5 – 2.5 are typical operational ranges for CFBCs [15], a number of physico-chemical parameters like the reactivity of $CaCO_3$ particles at CFBC conditions are the determining factors for desulfurization. Therefore, for basic design calculations, a typical value of 2.2 can be utilized. Although sulfur dioxide capture behavior of each limestone source can be estimated by laboratory reactivity tests, actual performance can only be determined by fluidized bed combustion tests. Considering the experimental requirements, maximum value of Ca/S ratio is taken as 8 for the design basis.

Desulfurization efficiency: 90%

Desulfurization efficiency is the ratio of SO_2 captured by limestone to the SO_2 generated during combustion. It is reported that sulfur capture of 95% and more has been achieved in CFB boilers [13]. Turkish environmental regulations for high capacity utility boilers necessitate at least 90% removal of SO_2 [24]. Therefore, 90% desulfurization efficiency is not only a typical value, but also a low limit for a coal combustor. Although this efficiency can be improved by adding more limestone, this improvement may not be feasible for commercial plants because of thermal efficiency and operational cost concerns. The aim of using this value in the basic design study is to predict SO_2 emissions at a typical desulfurization performance. Actual efficiency values will be observed during the test runs in the future with limestone addition, and will be tested against limestone flow rate, i.e. Ca/S ratio.

$CaCO_3$ content of the limestone: 95%

Similar to the coal reserves, there are many different limestone reserves, with different $CaCO_3$ content, reactivities, etc. However, 95% purity for a limestone has been a typical value in many experiments utilizing limestone from different sources at the existing AFBC test rig [25]. On the other hand, limestone utilization with slightly lower purity does not have a disturbance on the design and operation

of combustor. Therefore, this value was used in the basic design calculations.

Ash Split: Bottom Ash / Total Ash = 40%

The solid streams leaving a CFB combustor are composed of incombustible solids mainly and unburnt combustible particles with a small portion. The incombustible solids include the ash entering within the coal, impurities in limestone and CaO and $CaSO_4$ particles. Ash split is the distribution of total ash between bottom and fly ash streams while leaving the combustor. The output stream composed of fine ash particles that are entrained from the cyclone are named as fly ash, whereas the coarse particles leaving the system from the bottom of riser are named as bottom ash. A significant portion of bottom ash stream is composed of the particles for which the terminal velocity is higher than the superficial velocity. Therefore, these particles stay in the riser and are discharged from the bottom of riser.

The split between bottom and fly ash depends on the nature of the ash and the conditions within the combustor. It is an important parameter in combustor design because of its effect on heat transfer, bed material generation, pressure distribution etc. Ash split at the existing AFBC test rig was generally in the range of 20% – 40% for bottom ash generation [26]. For CFB combustors, 20% of total ash is reported to leave the furnace as bottom ash [15]. In order to have a margin, CFBC test unit design was based on a maximum ash split value of 40% for bottom ash, and minimum value of 60% for fly ash. The design ranges of ash split was defined to be 0 – 40% for bottom ash, and 60 – 100% for fly ash.

Unburnt carbon in bottom and fly ash streams: C_{bot} = 1% , C_{fly} = 2%

In the design study, carbon contents of bottom and fly ash were utilized for the prediction of the combustion efficiency. Tests carried out with lignite on the AFBC test rig operated under bubbling mode revealed that carbon in fly ash varied in the range 1.6% to 4.5% [27]. However, tests carried out with the same lignite on the AFBC test rig operated under circulating mode resulted in lower unburnt carbon contents in both bottom and fly ashes [35]. Based on these data,

design basis for carbon content of bottom ash and fly ash has been defined as 1% and 2%, respectively. However, unburnt carbon contents of bottom and fly ashes are functions of a number of design and operating parameters. Therefore, higher and lower carbon losses and different combustion efficiencies can be observed while firing different coals at different operating conditions.

2.1.3 Mass Balance

Based on the assumptions and design basis given above, stoichiometric calculations were carried out for all of the coal reserves. As the analysis of Beypazarı lignite falls in the middle of the fuel range, this reserve is chosen as the design coal. The analysis and the results of basic design based on Beypazarı lignite are given in Appendix B.

2.1.3.1 Solid input

The starting point of mass balance was the thermal input of the fuel which is 150 kWt. Flow rate of coal was calculated by dividing the heat input by LHV of the coal. Flow rates of components present in coal; ash, water, sulfur, carbon, hydrogen, oxygen and nitrogen, were obtained by multiplying the composition of each ingredient by the flow rate of coal. Limestone consumption was calculated by utilizing the sulfur content of coal, Ca/S ratio and limestone purity.

2.1.3.2 Combustion air

Combustion air requirement was calculated from oxygen demand of the reactions given below:

$$C(s) + O_2(g) \rightarrow CO_2(g) \qquad (rxn.1)$$

$$H_2(g) + \tfrac{1}{2} O_2(g) \rightarrow H_2O(g) \qquad (rxn.2)$$

$$S(g) + O_2(g) \rightarrow SO_2(g) \qquad (rxn.3)$$

$$CaO\,(s) + SO_2\,(g) + \tfrac{1}{2}\,O_2\,(g) \rightarrow CaSO_4\,(s) \qquad (rxn.4)$$

Although the Carbon in coal is not completely converted to CO_2 by reaction#1, stoichiometric air requirement is calculated by assuming complete conversion based on the definition of theoretical air requirement which is the dry air required for complete combustion of a defined weight of coal [15]. In order to obtain combustion air flow rate, oxygen demand is calculated by subtracting the oxygen in the coal from the oxygen demand of the reactions given above. Theoretical air flow rate was calculated by dividing this oxygen demand by oxygen percentage in air (21%). Total combustion air flow was obtained by adding the amount of excess air to the theoretical air flow rate.

2.1.3.3 Flue gas

After obtaining the input terms, flow rates of products within flue gas were calculated. In addition to the products of reactions #1 to #4, there are other sources of gaseous species within the flue gas: (i) calcination of limestone; (ii) reactions of coal nitrogen; (iii) unreacted input streams.

In addition to the combustion reaction, the calcination reaction of limestone given below also produces carbon dioxide.

$$CaCO_3\,(s) \rightarrow CaO\,(s) + CO_2\,(g) \qquad (rxn.5)$$

Regarding the reactions of coal nitrogen, only the reactions for NO and N_2 formation are taken into account to calculate flue gas flow rate and gas composition. The representative reactions for coal-N conversion to NO and N_2 are given below, and the complicated reaction mechanisms of nitrogen species and its oxides can be found elsewhere [25].

$$N + \tfrac{1}{2} O_2(g) \rightarrow NO(g) \qquad (rxn.6)$$

$$2\ N \rightarrow N_2(g) \qquad (rxn.7)$$

Unreacted gaseous species originating from the input streams are; (i) nitrogen in combustion air; (ii) moisture in coal and combustion air; (iii) oxygen that remains after the reactions.

Based on input, generation and consumption rates of nitrogen, water vapor, sulfur dioxide and oxygen, flow rates of these gaseous species within the flue gas were calculated. On the other hand, the exact flow rate of CO_2 could not be calculated at this stage bacause of the fact that the conversion of carbon to CO_2 is not complete. A small portion of unreacted carbon produces carbon monoxide by the following reaction, whereas the rest of the unreacted carbon leaves the combustor within fly ash and bottom ash streams.

$$C(s) + \tfrac{1}{2}O_2(g) \rightarrow CO(g) \qquad (rxn.8)$$

In order to calculate the exact flow rate of CO_2, it was required to calculate the amount of carbon that does not react to CO_2. This deviation from complete conversion is defined as incomplete combustion, and it results in less generation than the theoretical thermal input based on the heating value of the coal. In order to describe the degree of the completeness of combustion, combustion efficiency is defined as ratio of total energy generation by combustion reactions to the theoretical heat input by the fuel. Combustion efficiency (η_{comb}) is calculated from the following equation, which is based on subtracting the ratio of combustion enthalpies of unreacted carbon species in the output streams to the total heat input from unity.

$$\eta_{comb} = 1 - \frac{m(CO)\ x\ \Delta H^{rxn}_{(CO \rightarrow CO2)} + (m(C_{bot}) + m(C_{fly}))\ x\ \Delta H^{rxn}_{(C \rightarrow CO2)}}{m(coal)*LHV} \quad (2.1.a)$$

As the expected combustion efficiency and unburnt carbon loss are defined within design basis, carbon monoxide generation is calculated by rearranging equation (2.1.a):

$$CO,\ kg/h = \frac{m(coal)*LHV*(1 - \eta_{comb}) - (m(C_{bot}) + m(C_{fly}))*\Delta H^{rxn}_{(C \rightarrow CO2)}}{\Delta H^{rxn}_{(CO \rightarrow CO2)}} \quad (2.1.b)$$

After calculating CO flow rate, CO_2 flow rate is determined. Adding up the flow rates of all gaseous species, total flue gas flow rate is obtained.

2.1.3.4 Flue gas composition

Flue gas composition was calculated by dividing the mass flow rates of each component by its molecular weight to obtain their molar flow rates and dividing these molar flow rates by total molar flow rate of flue gas.

2.1.3.5 Ash content

Ash generated within the combustor consists of the ash in the coal, $CaSO_4$ generated by sulfur capture reaction, CaO that did not react with sulfur dioxide, impurities in limestone and unburnt carbon. Based on the ash split taken in the design basis, each component within the ash was calculated.

2.1.3.6 Species balance

Species balance was also carried out by calculating the input and output mass flow rates of each element: C, H, N, O, S, Ca. In these calculations, it was confirmed that the mass balance holds for each element.

2.1.3.7 Discussions on mass balance

The calculations summarized in the mass balance section were carried out for all fifteen coal reserves. In addition to the results obtained for Beypazarı lignite which was taken as the design coal, calculations based on other coal reserves constituted the design range for the test unit as presented in Table 2.2. Another significant outcome of the mass balance was the diamater of combustor which was calculated as 25.37 cm by dividing the flue gas flow rate by the superficial velocity which led to cross sectional area and diameter for cylindrical riser design.

2.1.4 Heat Balance

In order to calculate the cooling capacity required for the combustor, an energy balance around the combustor is carried out. The data for the energy balance, assumptions and design basis are given below:

Combustion air temperature: 40°C

Combustion air is the ambient air which is fed to the combustor via a side channel blower. However, the temperature of the fresh air increases approximately to 40°C leaving the fan where the mechanical work generates heat according to the past experience on 0.3 MWt AFBC.

Table 2.2 Mass Balance Results

	Design Coal	**Minimum**	**Maximum**
Thermal load, kW	150	116	189
Coal consumption, kg/h	48.4	26.2	79.1
Limestone consumption, kg/h	8.7	1.3	19.2
Combustion efficiency, %	97.7	95.3	99.5
Total dry air flow rate, Nm^3/h	195.9	168.4	210.6
Flue gas flow rate, wet, m^3/h	909.2		
Total ash generation, kg/h	22.0	5.5	36.1

Flue gas temperature at the cyclone exit: 850°C

The temperature in the furnace, 850°C, is maintained in the cyclone. Therefore, flue gas temperature at the cyclone exit is taken to be same as the temperature in the cyclone.

Bottom ash temperature: 850°C

It was assumed that the bottom ash leaves the system at furnace temperature.

Overall heat transfer coefficient for surface heat loss: 8.6 kcal/h m² K

This data is based on heat loss from 60°C aluminum cover sheet surface to ambient air. During detailed design, this value was checked for insulation thickness calculations, and it was found that the assumption was valid.

Cooling water inlet and outlet temperatures: 20°C – 60°C

Cooling water inlet temperature was assumed to be maximum 20°C. To prevent evaporation in tubes that can cause water hammer, exit temperature should not be allowed to exceed 60°C. Therefore, cooling load was calculated accordingly.

Defining the assumptions and design basis for heat balance, input, output and generation terms were calculated. Inputs in energy balance are flow enthalpies of coal, limestone, air and cooling water.

Generation term of energy balance consists of the reaction enthalpies of:

- Calcination: CaO formation (n * ΔH_{rxn})

  #5 $CaCO_3(s) \rightarrow CaO(s) + CO_2(g)$ *(41.6 kcal/gmol)*

- Sulfation; $CaSO_4$ formation (n * ΔH_{rxn})

  #4 $CaO(s) + SO_2(g) + \frac{1}{2} O_2(g) \rightarrow CaSO_4(s)$ *(-114.1 kcal/gmol)*

- Combustion (m_{coal} * LHV)

Outputs in energy balance are flow enthalpies of bed ash, fly ash, flue gas, cooling water (hot) and heat loss from the outer surfaces of combustor.

As specific heats of coal and flue gas vary significantly with their water content, water within input and output species was included separately and all other species were included in dry basis during the heat balance.

Mass flow rates of all streams except the cooling water flow rate were calculated during mass balance. Therefore, the heat balance around the combustor was carried out to determine the cooling water flow rate by following the below steps:

- Energy input and output terms (except cooling water) were calculated.
- Generation terms were calculated; calcination(endothermic), sulfation (exothermic), combustion(endothermic)
- All the terms were inserted into the energy balance equation.
- Heat to be removed by cooling water in the furnace was obtained.
- Heat removal requirement was divided by the enthalpy difference of inlet and outlet cooling water streams to obtain cooling water flow rate.

As a result, heat removal requirement and cooling water flow rate for the design coal and the range of these parameters when different coals are fired were obtained and are tabulated in Table 2.3.

Table 2.3 Heat Balance Results

	Design Coal	**Minimum**	**Maximum**
Total generation, kcal/h	126,519	96,708	161,787
Enthalpy difference (Out – In), kcal/h	70,392	66,662	75359
Heat loss to surroundings, kcal/h	8,256		
Heat removal at combustor, kcal/h	47,872	13,094	86,370
Cooling water flow rate, kg/h	1,197	327	2,159

2.2 Detailed Design Studies

Following the completion of basic design, detailed design studies were started which included process and instrumentation design, preliminary equipment design, development of pressure balance model, detailed equipment design and cooling system design.

2.2.1 Process and Instrumentation

150 kWt Circulating Fluidized Bed Combustor Test Unit is comprised of not only the combustor but also the auxiliary systems like air and flue gas systems, solids handling and feeding systems and gas analysis system. Schematic of the process flow diagram of the test unit is given in Figure 2.2. Following this general process diagram, process and instrumentation diagrams (PID) for each system were prepared.

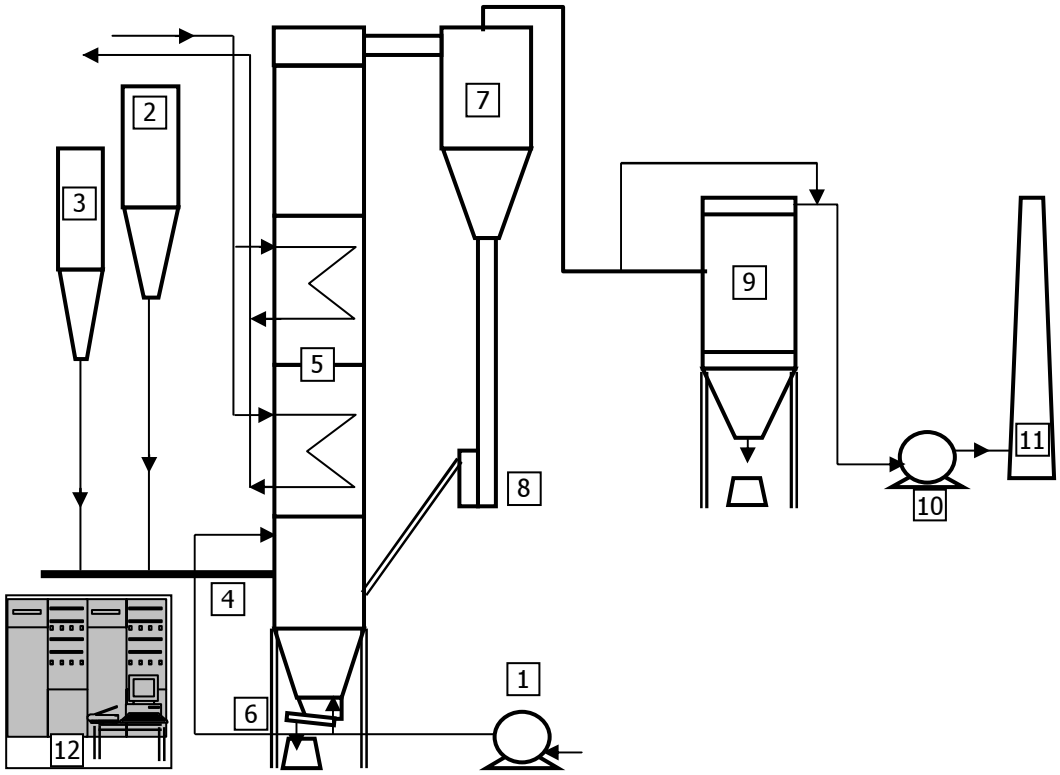

Figure 2.2 Process Diagram of the Test Unit

The components of the test unit given in Figure 2.2 are listed below:

1. Combustion air supply
2. Coal handling
3. Limestone handling
4. Solids feeding
5. CFB combustor
6. Bottom ash withdrawal system
7. Cyclone
8. Loop seal
9. Bag filter
10. Induced draft fan
11. Stack
12. Control room

2.2.1.1 Flue Gas System

Flue gas system is defined to start from the exit of the CFB combustor's cyclone and goes up to the stack. This system is composed of a bag filter, an induced draft fan and flue gas lines. PID of the system is given in Figure 2.3.

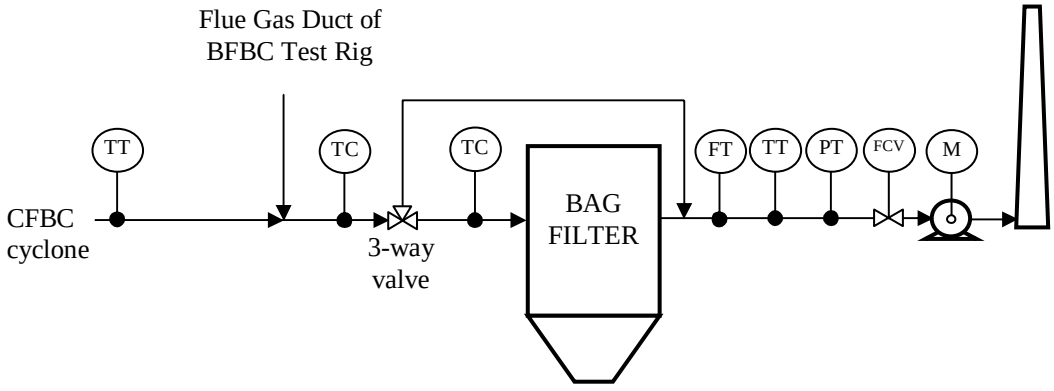

Figure 2.3 PID of the Flue Gas System

Connection to the Existing Flue Gas System of Bubbling AFBC Test Rig

The flue gas line connects the cyclone to the flue gas line of existing test rig where there is a 3-way valve to by-pass the bag filter when the gas temperature is outside the limits of bag filter. Starting from this by-pass valve, the flue gas system of the existing unit is utilized. Therefore, process and instrumentation diagram is the same as the existing installation starting from that point.

Existing Flue Gas System

Through the existing flue gas system, there are thermocouples of bag filter to measure the flue gas temperature to control by-pass valve, and there are pressure, temperature and flow transmitters, flue gas damper control valve and induced draft fan before the stack.

Control Philosophy

Flow control valve before the induced draft fan is utilized to balance the pressure at the exit of combustor together with the blower. For this purpose, the data obtained from the pressure transmitter before the damper valve and the transmitters within the furnace are used as control parameters for the system.

2.2.1.2 Combustion Air System

Combustion air system is the section from the fresh air inlet of blower up to the combustion air inlets of the CFB combustor; windbox (primary air), and secondary air collector. In between, there are blower, combustion air piping, valves, rotameters and instruments for flow measurement. PID of the combustion air system is given in Figure 2.4.

At the exit of blower, the line is divided into two, to primary and secondary air control valves. After the valves, pressure and flow rates are measured. Temperature is only measured on primary air piping, as no deviation is expected between the two streams. Primary air enters the windbox and secondary air is divided into two, to collector feeding the injection tubes and loop seal windbox.

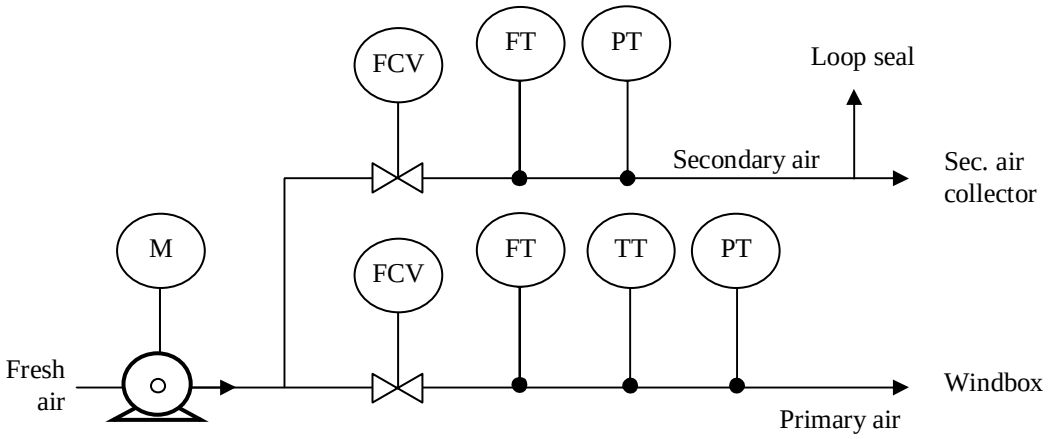

Figure 2.4 PID of Combustion Air System

Control Philosophy

Air flow required by the combustor is a function of coal flow rate and excess air ratio. In order to keep the air flow rate at the required value, control valves are regulated. The control parameter for the valves are the air flow rates that are calculated by using the pressure drop through a flow element and applying temperature and pressure corrections to these data.

Secondary air flow control is based on the 'Primary air / Secondary air' ratio that is defined by the operator. The control system calculates the secondary air flow rate requirement by multiplying this ratio with total combustion air flow rate and regulates the valve accordingly to obtain this calculated flow rate

Similar to the control philosophy of total air flow rate, the control system regulates secondary air control valve based on the data obtained from the flow transmitter.

As the secondary air ratio is defined as the control parameter, the control system keeps the ratio at the required value, regardless of the variations in the total air flow rate.

2.2.1.3 CFB Combustor

CFB combustor is composed of the furnace, cyclone and circulation system. Furnace is divided into modules for ease of manufacturing, installation, future revisions and temperature control during operation. At the return leg of cyclone, there is a J-valve for sealing the return leg and maintaining the circulation.

If the return leg can not isolate the furnace from cyclone by the weight of particles, combustion air by-passes the furnace and flows through the cyclone and leaves the combustor. PID of the system is given in Figure 2.5.

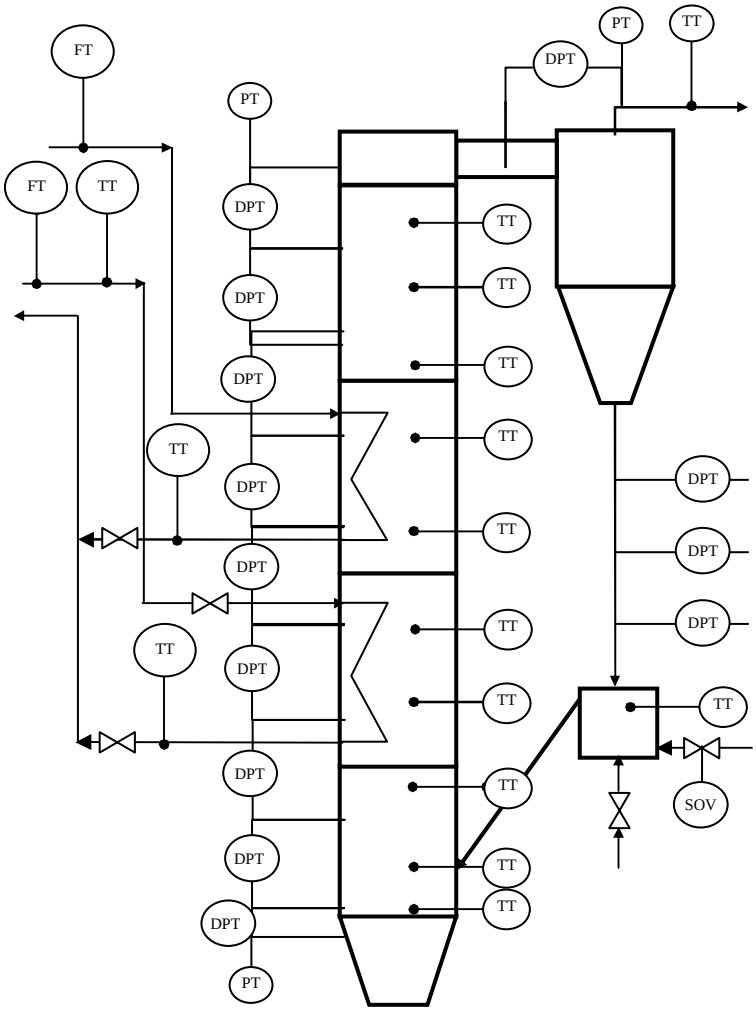

Figure 2.5 PID of CFB combustor

Control Philosophy

There are temperature, pressure and pressure difference transmitters along the combustor. All the signals received from these transmitters are logged into the control system's computer not only for process control but also for evaluation of the combustion test results.

The measurements collected from pressure and differential pressure transmitters are used in determining particle load distribution along the combustor. The pressure data serve as control parameters for control valves of blower and induced draft fan.

Control parameters for combustion chamber temperature control are temperature along the combustor (850°C), and cooling water outlet temperatures (to be max. 60°C). The operator checks both temperature data and regulates the manual valves of cooling water accordingly. Cooling water inlet temperature and flow rate data shall be logged to be utilized in heat transfer studies after test runs.

For particle recirculation in the J-valve, when the particles can not flow into the furnace because of the pressure inside the combustor, the solenoid valve (SOV) of compressed air shall be opened to convey the particles into the furnace. This valve shall be activated manually by the operator when the particle level in the downcomer leg is high.

2.2.1.4 Solids Handling and Feeding System

Solids handling and feeding system is composed of coal, limestone and bed material handling, solids feeding, solids circulation and ash removal systems. Solids in the silos flow through screw feeders that are connected to a main bunker for mixing. At the bottom of this bunker, there is an air lock type main feeder which feeds the solids to an inclined leg that is connected to the furnace. This main feeder is selected as air lock to isolate the furnace from solids feeding system. PID for the system is given in Figure 2.6.

At the bottom of the combustor, there is a discharge line for bed ash removal. The bed ash system is designed to discharge the particles by the help of compressed air conveying system.

The J-valve has an outlet pipe for particle discharge in case it is necessary to decrease the particle load in the system. This outlet line also helps draining of the system after test run is finalized.

Control Philosophy

Coal and limestone silos are equipped with load cells. Weight signals received from load cells are utilized to calculate the solid streams' flow rates. The difference in silo weight within a specific time interval is converted to flow rate of each species.

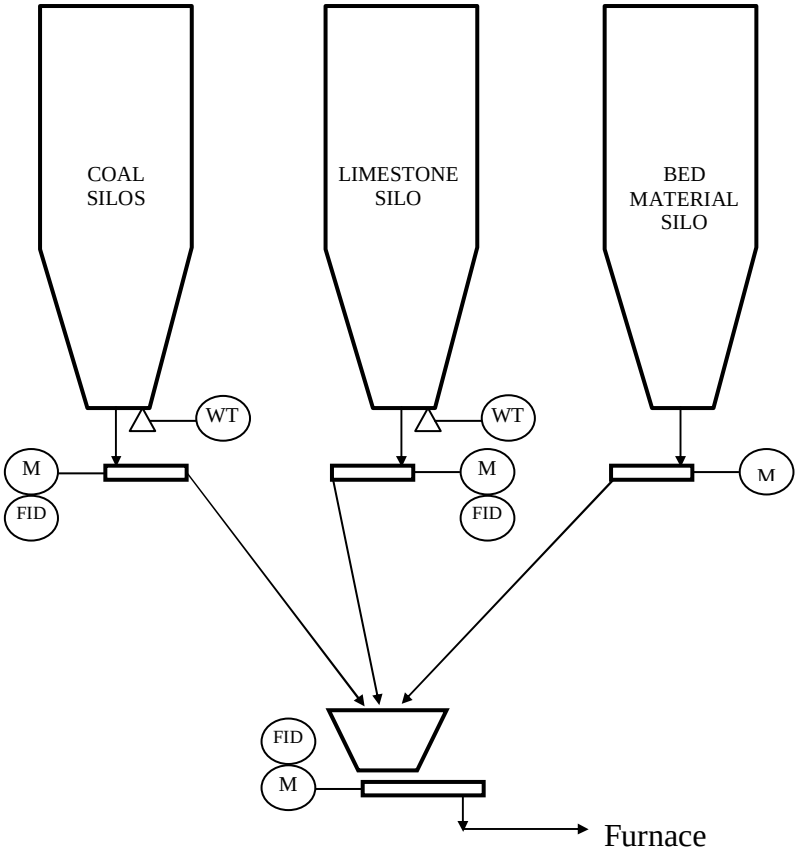

Figure 2.6 PID of Solids Handling System and Feeding System

At the same time, operator can regulate the flow rate of coal according to the variations in many parameters like furnace temperature, pressure (particle load), CO and O_2 concentrations etc. The limestone flow rate should also be changed to control sulfur dioxide emissions. The operator regulates frequencies of the screw feeder motors at the bottom of each silo to feed the solids at required flow rates.

Operation of bed drain discharge system is based on the differential pressure data within the dense zone combustor. The system is turned on when the particle load in the furnace increases.

If the particle accumulation in the downcomer is higher than required, fly ash particles have to be drained from the system. For this purpose, the J-valve discharge system is utilized.

2.2.1.5 Gas Analysis System

The system is designed to have 6 ports for sampling combustion gas along the furnace. All sampling ports are connected to a line heading to the analyzers for CO, NO_x, SO_2 and O_2 concentration measurements via the existing gas conditioning system. There should also be another analyzer for O_2 measurement on wet basis at the exit of furnace for combustion control. PID of this system is given in Figure 2.7.

Control Philosophy

Gas concentration data continuously received from the analyzer at the furnace exit should be utilized for combustion control. Oxygen concentration measured at the exit of cyclone is an indicator for excess air ratio in the furnace. This data helps regulating coal and air flow rates throughout the test runs.

The procedure for sampling flue gas along the combustor is as follows: Operator shall first select the port to sample the combustion gas. Then, all the valves other than the one at the selected port shall be closed. Flue gas is sampled from that port

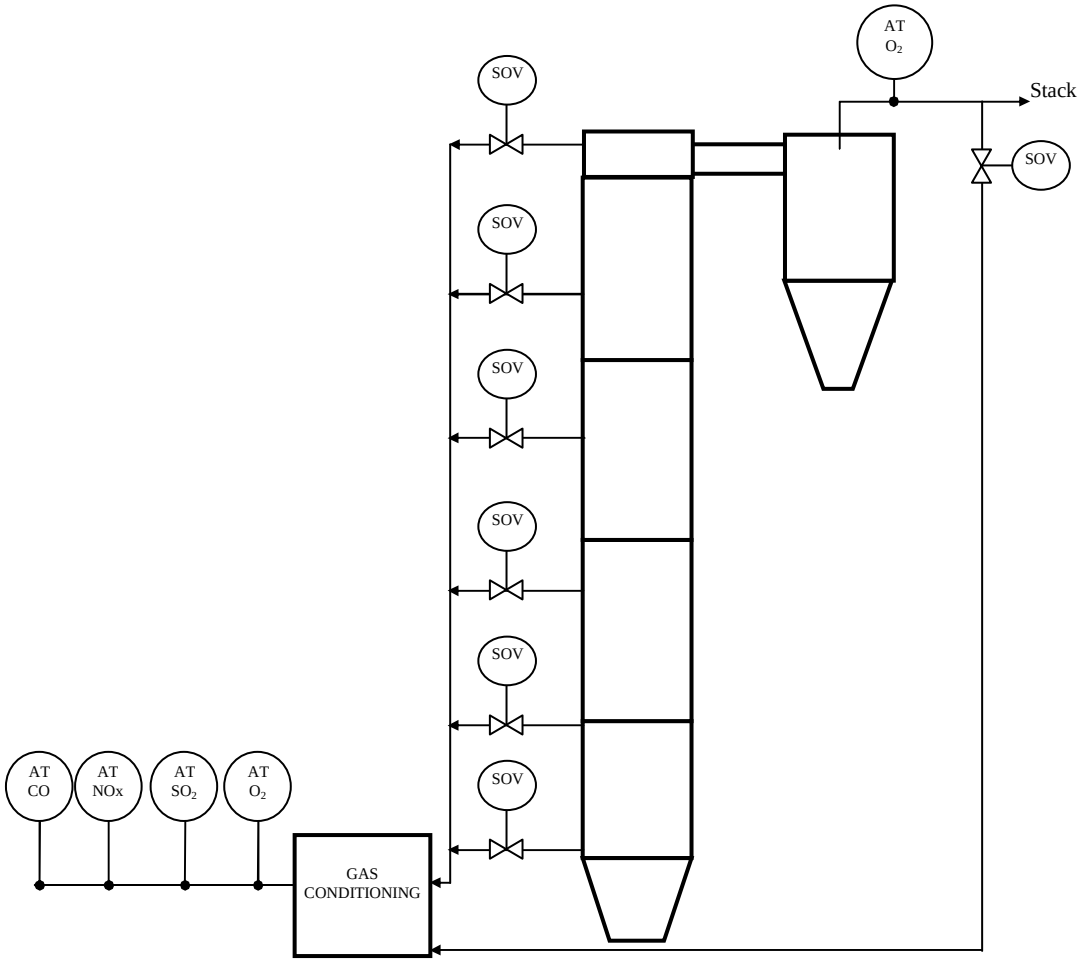

Figure 2.7 PID of Gas Analysis System

and flows through gas conditioning system and analyzers. After the operator decides to pass to another sampling port, sampling valves are regulated again as described above. Gas concentrations shall be logged to the computer and displayed on the monitor for the operator to take actions when necessary.

2.2.2 Control System

Control system is composed of DCS (distributed control system) based process control hardware, a computer (PC) and a UPS. Control hardware panel is comprised of a termination panel for signal cables, input and output cards,

controller, power and PC communication modules. Schematic diagram for control system hardware is given in Figure 2.8.

Based on the instrumentation study summarized above, number of input and output signals of the control hardware was determined, including at least 30% spare I/O for each type of signal.

After installation works for the instruments and cabling were completed, the control system hardware was programmed based on the control philosophy summarized in the previous sections.

2.2.3 Equipment Design

2.2.3.1 Furnace

Although the commercial combustors have rectangular cross-section, because of its size and ease of manufacture, the combustor of the test unit was designed to have cylindirical structure, with an internal diameter of 25 cm, which was obtained in the basic design studies.

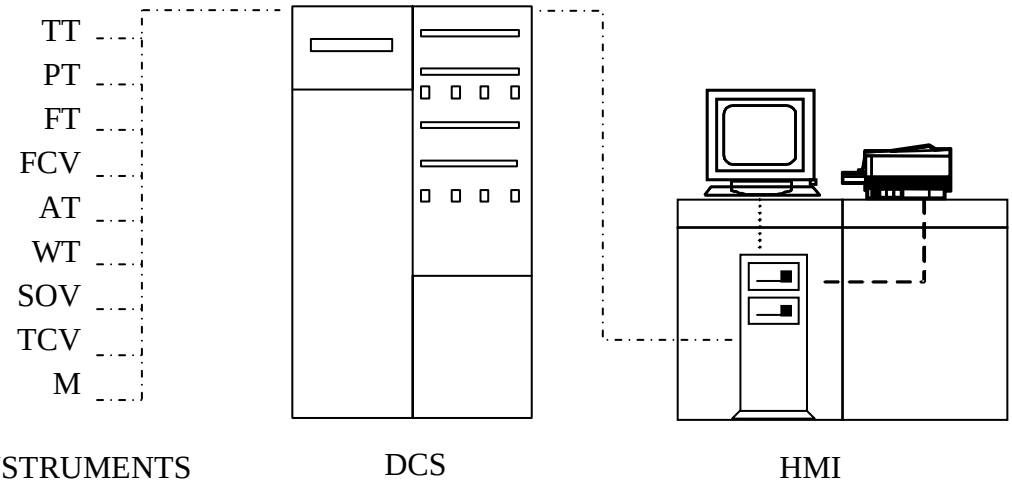

Figure 2.8 Schematic Diagram of Control System

Test units at similar capacity have been reported to have furnace heights up to 6.5 m [18-22, 28-30]. As this test unit was designed to fire mainly low quality lignite, furnace height in this study was chosen as 8 m to be able to use less reactive limestone and yet obtain high sulfur capture by providing more residence time.

Furnace is comprised of 5 modules. Design details of the modules are given in section 2.2.6. Combustion takes place and flue gas flows at the inner part of the modules (D=25 cm). Surrounding this combustion chamber, there is a refractory layer which is integrated with a cylindrical shell (pipe) outside. For two of the modules, there is a water channel system at the outside of this shell.

Detailed design of furnace, including the windbox, distributor plate, air and solids feeding points, bottom ash discharge line, exact locations of instrument and sampling ports, external insulation, and manufacturing details for all these items are given in related sections.

2.2.3.2 Cyclone

For the design of the cyclone, design procedure proposed for a general purpose cyclone is followed [15,31]. According to this procedure, if one of the dimensions of the cyclone was determined, the others can be calculated from Table 2.4 given next to the schematic diagram in Figure 2.9. Proportions given in the table are the dimensions when D_o (cyclone diameter) is taken as 1 unit.

The diagram given in Figure 2.9 was prepared in conformity with these proportions, however, the streamlines in the drawing showing the rotation of gas flow are representative. Following the design procedure, it was assumed that the actual number of rotations that the gas stream makes within the cyclone is 5 [31].

In order to follow the design procedure, one of the dimensions had to be specified. For this purpose, inlet cross-section, which sets the value of W and H_i, was selected as it can be determined from flue gas volumetric flow rate which was

calculated during basic design studies. In this calculation, inlet velocity of the gas was chosen to be 20 m/s, typical design parameter for general purpose cyclones [15,31]. Deciding on the inlet velocity, inlet cross section was calculated from the following formula:

$$\textit{Inlet cross section} = \textit{Flue gas vol. flow rate} \,/\, \textit{Inlet velocity} \qquad (2.2)$$

Effect of inlet velocity was also studied in terms of pressure drop and particle capture efficiency, and this initial assumption was found to be optimum. As the cyclone inlet has a rectangular cross section, with one side being two times the other side ($H/W_i = 2$), cross sectional area is defined as 'a x 2a = $2a^2$' where a is the dimension of W_i. Equalizing this value to the value found from eqn. (2.2),

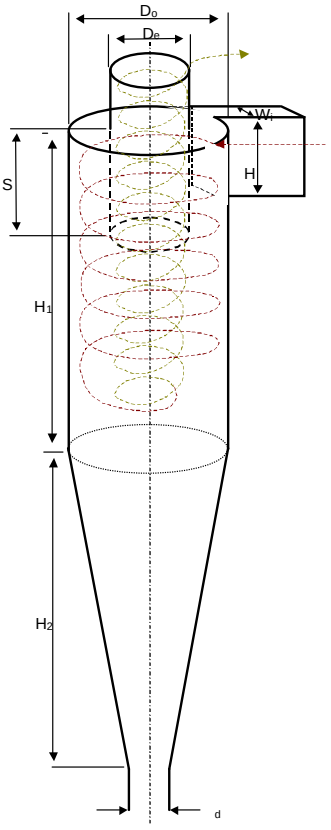

Figure 2.9 CFB cyclone

Table 2.4 Unit Dimensions of Cyclone [31]

Dimension	**Proportion**
Do	1
W_i	0.25
H	0.5
H_1	2
H_2	2
D_e	0.5
S	0.625
D_d	0.25

dimensions of the inlet duct of cyclone were calculated as 7.95 cm x 15.90 cm (H x W_i) for 20 m/s inlet velocity.

Once the inlet dimensions are calculated, rest of the cyclone dimensions can be calculated by utilizing the unit dimensions given in Table 2.4. According to this procedure, the cyclone of CFBC was designed to have a diameter of 31.8 cm and a total height of 127.2 cm. The other dimensions of the cyclone are given in Appendix C. Once the dimensions were determined, particle capture efficiency and pressure drop throughout the cyclone were calculated.

Particle capture efficiency

Fraction of particles that will be captured at the cyclone is predicted by the following equations [31];

for block flow assumption,
$$\eta = \frac{\pi \; N V_c \; D^2 \; \rho_{part}}{9 \; W_i \; \mu} \qquad (2.3)$$

for mixed flow assumption,
$$\eta = 1 - exp - \left(\frac{\pi \; N V_c \; D^2 \; \rho_{part}}{9 \; W_i \; \mu} \right) \qquad (2.4)$$

where N is the number of rotations that the gas makes, V_c is the velocity along the circular path, D is the diameter of particle under consideration, ρ_{part} is the density of particle, W_i is the width of the inlet cross-section, and μ is the viscosity of gas.

Block flow and mixed flow assumptions are the limits of cyclone separators, and the real case is in between. For this purpose, the efficiency is defined by an alternative totally emprical data-fitting equation where the experimental data is represented with satisfactory accuracy:

$$\eta = \frac{(D / D_{cut})^2}{1 + (D / D_{cut})^2} \qquad (2.5)$$

The three efficiency definitions given above are utilized for various particle diameters and the results are given in Table 2.5.

Cut diameter

It is the diameter of the particle for which the capture efficiency has the value of 0.50 (50%). Putting D_{cut} instead of D and 0.50 instead of capture efficiency into the equation for block flow, D_{cut} is calculated from the equation given below.

$$D_{cut} = \left(\frac{9 W_i \mu}{2 \pi N V_c \rho_{part}} \right)^{1/2} \quad (2.6)$$

From this equation, cut diameter for the cyclone was calculated to be 7.0 µm. For a typical cyclone size and the most common cyclone velocity and gas viscosity, the cut diameter is about 5 µm. [31]

Pressure drop

The pressure drop can be calculated by an equation of the form [31],

$$\Delta P = K \frac{V_i^2 \rho_g}{2} \quad (2.7)$$

Table 2.5 Particle Capture Efficiency

Particle Diameter, µ	η_{block}	η_{mixed}	$\eta_{emprical}$
0.1	1.02E-04	1.02E-04	2.05E-04
1	0.010	0.010	0.020
2	0.041	0.040	0.076
5	0.256	0.226	0.339
8	0.656	0.481	0.567
10	1.025	0.641	0.672
12	1.475	0.771	0.747
15	2.305	0.900	0.822

where '$Vi^2\rho_g$ / 2' is referred as the velocity head. Most cyclones have pressure drops of about 10 velocity heads (K = 10). Using this equation, pressure drop throughout the cyclone was calculated to be 59.6 mm H_2O.

A parametric study on the inlet velocity of flue gas showed that if the inlet velocity is increased to 30 m/s to obtain a cut diameter of 5 µm, the pressure drop becomes 116.2 mm H_2O. In addition to the other resistances within the system, this creates further pressure drop for the fans to overcome. The improvement in D_{cut} was not found to be significant against this increase in pressure drop. Therefore, the design inlet velocity of the cyclone was decided to be 20 m/s.

2.2.3.3 Coal and Limestone Silos

The solids handling system of the test unit was designed to handle 24 hours of maximum coal and limestone consumptions. For the ease of manufacture and installation, the system is designed to be composed of three identical silos with rectangular cross section; two for fuel, one for limestone.

In order to avoid any blockage within the silo or at the outlet at the bottom of silo, bunker angle of the silo was chosen to be 70°. Dimensions of the silos were calculated on this basis. Each silo was designed to have an inlet of 30 cm x 100 cm at the top and a discharge outlet of 20 cm x 20 cm at the bottom with a total volume of almost 0.65 m^3 and a total height of 2.7 m.

2.2.4 Solids Holdup Profile and Pressure Balance

In a circulating fluidized bed combustor, solids distribution and flow behavior are the key parameters in successful design and scale-up. The solids distribution governs the pressure drop along the CFB riser. In this study, the flow dynamics around the CFBC Test Unit was determined by utilizing the pressure balance model proposed by Kim et al.[32], of which the application procedure is given below.

2.2.4.1 Pressure balance model

The pressure in the CFB loop should be balanced for stable operation. The schematic diagram and equations for the application of pressure balance model around the CFBC test unit are given in Figure 2.10.

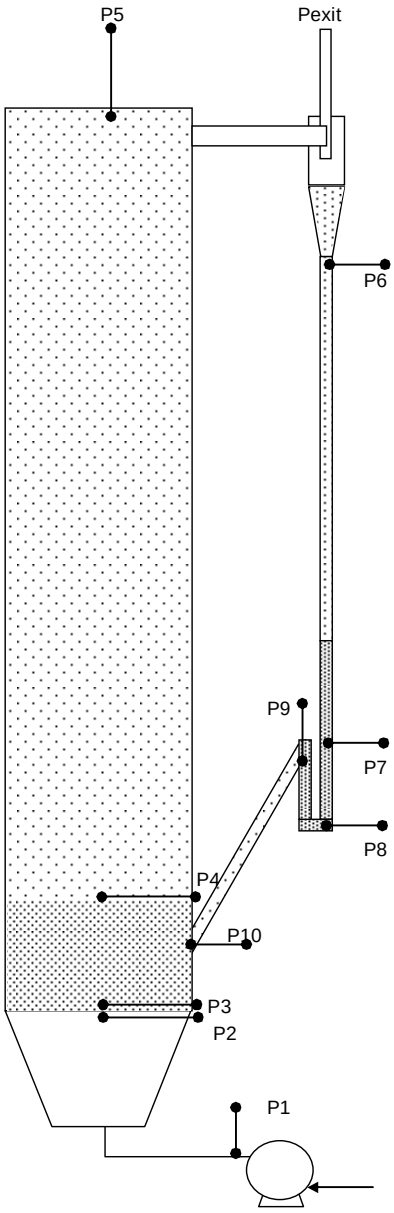

Pressure balance

$\Delta P_{dc} = \Delta P_{ls} + \Delta P_r + \Delta P_c$

$\Delta P_{dc} = P_7 - P_6$

$\Delta P_{ls} = P_7 - P_{10}$

$\Delta P_r = P_{10} - P_5$

$\Delta P_c = P_5 - P_6$

Then the balance is

$P_7 - P_6 = P_7 - \cancel{P_{10}} + \cancel{P_{10}} - \cancel{P_5} + \cancel{P_5} - P_6$

To find the pressure drop through downcomer for the conditions that the pressure balance holds, pressure drop items at the RHS of the balance equation shall calculated:

ΔP_{ls} : Pressure drop through;
- vertical aeration section $P_7 - P_8$
- weir section $P_8 - P_9$
- return leg $P_9 - P_{10}$

ΔP_r = Pressure drop through riser;
- dense zone* $P_3 - P_4$
- dilute zone $P_4 - P_5$

** For the model application, dense zone is taken from the entrance point of return leg, not from distributor.*

ΔP_c = Pressure drop through cyclone; $P_5 - P_6$
- furnace connection
- cyclone

Figure 2.10 Schematic Diagram for Pressure Balance Analysis

2.2.4.2 Pressure drop through riser (ΔP_r)

The pressure balance around the CFB loop is directly related with the voidage profile. For calculation of pressure drop through riser, pressure drops through dense zone and dilute zone are separately analyzed. For this analysis, particle holdup profile within the riser is required.

Solid hold up in the dense bed of riser (ε_{sd})

Particle hold up is assumed to be constant within the dense zone [33]. Then, solid hold up for the dense bed is determined by the following equation:

$$\frac{\varepsilon_{sd}}{\varepsilon_s^*} = 1 + 0.103 \left(\frac{U_g}{U_d}\right)^{1.13} \left(\frac{\rho_{s\text{-}dense} - \rho_g}{\rho_g}\right)^{-0.013} \qquad (2.8)$$

where,

$\varepsilon_s^* = G_s/(\rho_s(U_g - U_t))$: solid holdup at uniform flow with slip velocity = U_t (2.9.a)

$U_d = G_s/\rho_s$: superficial solid velocity (2.9.b)

and,

U_g : gas velocity in the dense zone

$\rho_{s\text{-dense}}$: dense zone particle density

ρ_g : gas density

G_s : solid circulation rate

U_t : terminal velocity of particles

Solid hold up at uniform flow, ε_s^*, which is defined by (2.9.a) is related with the hold up in the dilute zone. Therefore, the variables in (2.9.a) are based on dilute zone, that is mainly composed of circulating fly ash particles. Then, to be employed in (2.9.a), the terminal velocity for circulating fly ash is calculated from: [34]

$$U_t = \left(\frac{4\, d_{p\text{-}dilute}\,(\rho_{s\text{-}dilute} - \rho_g)\, g}{3\, \rho_g\, C_D}\right)^{1/2} \qquad (2.10.a)$$

where,

$$C_D = \frac{24}{Re_p}\left(1 + (8.1716e^{-4.0655\phi_s})Re_p^{\,0.0964+0.5565\phi_s}\right) + \frac{73.69(e^{-5.0748\phi_s})Re_p}{Re_p + 5.378e^{-6.2122\phi_s}} \quad (2.10.b)$$

$$Re_p = \frac{d_p\, u_g\, \rho_g}{\mu} \quad (2.10.c)$$

and,

ϕ_s : sphericity for circulating fly ash

u_g : superficial velocity at dilute zone

$\rho_{s\text{-dilute}}$: dilute zone particle density

$d_{p\text{-dilute}}$: dilute zone particle size

μ : gas viscosity

Putting U_t into (2.9.a) with the input data given previously, solid hold up at uniform flow, ε_s^*, is obtained. Then using (2.8), solid hold up within dense zone is obtained.

Solid hold up in the dilute zone of riser (ε_s)

Following equation is used for calculating the solid holdup at any height (z) in the dilute zone:

$$\frac{\varepsilon_s - \varepsilon_{s\infty}}{\varepsilon_{sd} - \varepsilon_{s\infty}} = exp(-a\,(z - z_d)) \quad (2.11)$$

where,

z : height in the riser (variable)

z_d : height of the dense bed

ε_{sd} : solid hold up at dense zone (2.8)

a : decay constant in the riser

$\varepsilon_{s\infty}$: average solid hold up at dilute zone

To find the solid hold up profile in the dilute zone, first, the decay constant, then the average solid hold up in the dilute zone is calculated.

Decay constant in the riser (a)

For the axial profile of solid fraction in a CFB riser, decay factor (a) is determined from:

$$a\,D_r = 0.019\left(\frac{U_g}{(g\,D_r)^{1/2}}\right)^{-0.32}\left(\frac{G_s}{\rho_g\,U_g}\right)^{-0.22}\left(\frac{\rho_s-\rho_g}{\rho_g}\right)^{0.41} \tag{2.12}$$

where,

U_g : gas velocity in the dilute zone

G_s : solid circulation rate

$\rho_{s\text{-dilute}}$: dilute zone particle density

ρ_g : gas density

D_r : diameter of riser

Average solid hold up at dilute zone ($\varepsilon_{s\infty}$):

Following equation is used for average solid hold up at dilute zone:

$$\varepsilon_{s\infty} = 4.04\,\varepsilon_s^{*\,1.214} \tag{2.13}$$

Putting the parameters obtained from (2.12) and (2.13) into (2.11), solid hold up profile through the dilute zone is obtained. However, (2.11) gives the solid hold up profile for the CFBs with smooth exit. There is the reflux of particles at the exit, back into the riser when there is a sharp exit. This effect is called exit effect.

Dilute zone solid hold up taking the exit effect into account

As the exit of the CFBC Test Unit has a sharp right angle to the vertical upflowing suspension, top of the riser acts as a crude gas-solid seperator. This results in a deviation from dilute zone solid hold up profile calculated from (2.13).

Deviation of solid holdup by particle reflux ($\Delta\varepsilon_{sr}$)

The deviation of solid hold up as a result of exit effect is defined by the following equation:

$$\Delta\varepsilon_{sr} = C_e\ \varepsilon_{se}\ exp(-a_e(H_f - z_f)) \tag{2.14}$$

where,

C_e : reflux constant

ε_{se} : solid hold up at the exit (obtained from (2.6) @z = 8 m)

a_e : decay constant affected by the exit geometry of the riser

H_f : height of the dilute zone

z_f : height in the dilute zone (variable)

Reflux constant (C_e)

Reflux constant is obtained from,

$$C_e = 0.046\left(\frac{(U_g - U_t)^2}{g\ D_r}\right)^{1/2}\left(\frac{G_s}{\rho_s (U_g - U_t)}\right)^{-1/3}\left(\frac{H_e}{d_p}\right)^{1/3}\left(\frac{D_e}{D_r}\right)^{-3/4} \tag{2.15}$$

where,

U_g : gas velocity in the dilute zone

U_t : terminal velocity of the dilute zone particles

G_s : solid circulation rate

ρ_s : dilute zone particle density

ρ_g : gas density

D_r : diameter of riser

D_e : diameter equivalent of the riser exit

d_p : dilute zone particle diameter

H_e : projected height of the riser exit

Decay constant affected by the exit geometry of the riser (a_e)

Decay constant affected by the exit geometry of the riser is defined by the following equation:

$$a_e D_r = 1.27\left(\frac{(U_g - U_t)^2}{g\,D_r}\right)^{1/2}\left(\frac{G_s}{\rho_s (U_g - U_t)}\right)^{-1/2}\left(\frac{D_e}{D_r}\right)^{-1/2}\left(\frac{\rho_s - \rho_g}{\rho_g}\right)^{-1} \tag{2.16}$$

Then, the deviation of solid holdup within the dilute zone is calculated from (2.14) taking the z_f values in the range of 0 m to dilute zone height. Then, solid holdup profile within the dilute zone including exit effect is calculated by the equation below:

$$(\varepsilon_s^{\,i})_{corrected} = \varepsilon_s^{\,i} + \Delta\varepsilon_{sr}^{\,i} \tag{2.17}$$

where the superscript i stands for any point along the height of dilute zone.

Pressure drop through riser (ΔP_r)

Pressure drop through the riser is calculated from the equation given below by using solid holdup in the dense zone and by integrating corrected solid holdup profile in dilute zone:

$$\Delta P_r = \rho_s\, g\, (\varepsilon_{sd}\, z_d + \int \varepsilon_s\, dz) \tag{2.18}$$

However, as there are two type of particles within the system under consideration, the equation is rewritten as follows:

$$\Delta P_r = \rho_{s\text{-}dense}\, g\, \varepsilon_{sd}\, z_d \;+\; \rho_{s\text{-}dilute}\, g \int \varepsilon_s\, dz \tag{2.18.a}$$

Then, for the input data and parameters calculated above, and by integrating the corrected profile of dilute zone solid hold up given by (2.17), riser pressure drop is calculated.

2.2.4.3 Pressure drop through Cyclone (ΔP_c)

In this analysis, the connection between riser and cyclone is also included in the pressure drop term for the cyclone.

Pressure drop in the horizontal section between Riser and Cyclone (ΔP_h)

Pressure drop through the connecting duct between riser and cyclone is calculated by the following equation:

$$\Delta P_h = G_{sh} (2.84 + 0.0108 U_{gh}^2) \quad (2.19)$$

where,

G_{sh} : solid mass flux based on horizontal section area of cyclone connection

U_{gh} : average velocity at cyclone connection

Pressure drop through the Cyclone (ΔP_c)

Although it was calculated during cyclone design, pressure drop through the cyclone is calculated again as a part of this model from the following equation: [31,32]

$$\Delta P_c = C_{cy} (A_r/A_c)^2 \rho_g U_g^2 / 2 \quad (2.20)$$

where,

C_{cy} : velocity head coefficient

A_r : cross sectional area of riser

A_c : inlet area of cyclone

U_g : superficial velocity at riser

2.2.4.4 Pressure drop in the Loop seal (ΔP_{ls})

For pressure balance analysis, the loop seal is divided into two sections: Vertical aeration and weir sections:

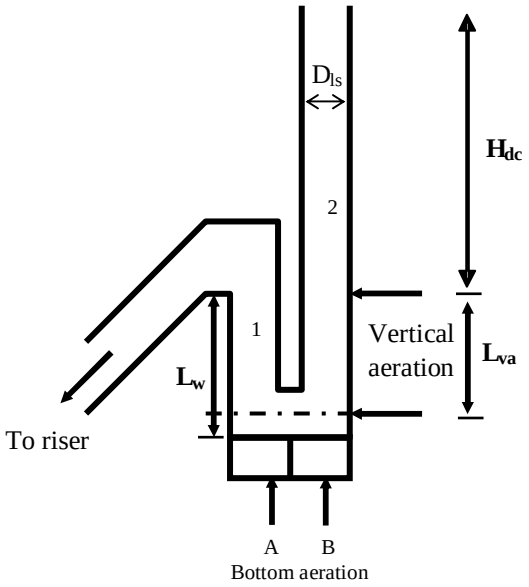

Figure 2.11 Schematic diagram of loop seal (1.Weir, 2.Vertical aeration)

Pressure drop through the loop seal is simply obtained from the addition of pressure drop values at weir and vertical aeration sections:

$$\Delta P_{ls} = \Delta P_w + \Delta P_{va} \tag{2.21}$$

In the weir section, solid flow is in a fluidizing state so that the pressure drop is defined as:

$$(\Delta P/L)_w = \rho_{s\text{-}ls} (1 - \varepsilon) g \tag{2.22}$$

where,

L_w : length of weir section - design basis (see Figure 2.11)

ε : voidage in loop seal and downcomer

$\rho_{s\text{-}ls}$: particle density in the loop seal

To obtain voidage of fluidized bed in weir section, following correlation is adopted: [32]

$$\varepsilon = \frac{1}{2.1}\left(0.4+\left(4\left(\frac{\mu \rho_g U_o}{d_p^2 (\rho_g (\rho_s - \rho_g))\phi_s^2 g}\right)^{0.43}\right)^{1/3}\right) \qquad (2.23)$$

where,

U_o : fluidizing gas velocity at loop seal

$\rho_{s\text{-}ls}$: particle density in the loop seal

ρ_g : gas density in the loop seal

μ : gas viscosity in the loop seal

ϕ_s : particle sphericity

Then voidage of weir section is obtained from (2.23) and put into (2.22) to obtain pressure drop.

For the pressure drop in the vertical aeration section, following equation is used: [32]

$$(\Delta P/L)_{va} = 0.0056 G_{sd}^{0.51} \rho_{bulk}^{2.01} d_p^{-0.97} D_{ls}^{-0.76} \qquad (2.24)$$

where,

D_{ls} : diameter of loop seal

L_{va} : length of vertical aeration section (see Figure 2.11)

ρ_{bulk} : bulk density of dilute zone particles

G_{sd} : solid mass flux based on loop seal area

Obtaining the pressure drops through vertical aeration and weir sections, pressure drop through loop seal is calculated from (2.21).

2.2.4.5 Pressure balance for downcomer (ΔP_{dc})

Pressure drop through downcomer, thus the solid mass and height is obtained from pressure balance. This procedure gives the height of accumulated fly ash at the downcomer leg to keep the system in balance.

Pressure drop through downcomer

Pressure drop through downcomer is obtained from the following balance equation:

$$\Delta P_{dc} = \Delta P_{ls} + \Delta P_r + \Delta P_c \tag{2.25}$$

As the entrance of loop seal leg into the riser is almost at the middle of the dense zone, pressure drop through dense zone is multiplied by 0.5 and then the pressure drop through riser is recalculated to be used in (2.25).

$$\Delta P_r = \Delta P_{dense} / 2 + \Delta P_{dilute} \tag{2.26}$$

Then from (2.25), pressure drop through downcomer is obtained.

Solid mass in downcomer

Having found the pressure drop through downcomer, solid mass is calculated:

$$M_{dc} = \Delta P_{dc} A_{dc} / g \tag{2.27}$$

where,

A_{dc} : cross sectional area of downcomer ($D_{dc} = D_{ls}$ in Figure 2.11)

Solid height in downcomer

Solid height in downcomer is obtained from the following equation given for solid mass in downcomer:

$$M_{dc} = \rho_{s\text{-}dc} (1 - \varepsilon_{dc}) H_{dc} A_{dc} \quad (2.28)$$

where,

$\rho_{s\text{-}dc}$: particle density in the downcomer

ε_{dc} : voidage of solid bed in downcomer (same as loop seal)

H_{dc} : height of the solid bed in the downcomer (see Figure 2.11)

As M_{dc} is found from (2.27) and the other parameters in (2.28) are known, only unknown, H_{dc}, is obtained by rearranging the equation.

2.2.4.6 Solid mass in riser and loop seal

Similar to the calculation of solid mass in downcomer, solid mass in riser and loop seal are obtained.

Solid mass in riser

Solid mass in riser is calculated from:

$$M_r = \Delta P_r A_r / g \quad (2.29)$$

Putting the pressure drop values for dense and dilute zones instead of ΔP_r, solid mass in dense and dilute zones are also obtained.

Solid mass in loop seal

Solid mass in loop seal is calculated from:

$$M_{ls} = \rho_{s\text{-}ls} (1 - \varepsilon_{ls}) L_{ls} A_{ls} \quad (2.30)$$

where,

$\rho_{s\text{-}ls}$: particle density in the loopseal

ε_{ls} : voidage of the solid bed in the loop seal (2.23)

L_{ls} : total length of the loop seal ($L_{ls} = L_w + L_{va}$) (see Figure 2.11)

A_{ls} : cross sectional area of the loop seal (downcomer)

2.2.4.7 Input Data to the Pressure Balance Model

The input data for the application of pressure balance model is composed of design basis, physical properties and some parameters calculated from these data. Operating conditions and dimensions of the system are defined as design basis in Table 2.6. Particle properties are obtained from the experimental studies previously carried out on the 0.3 MWt bubbling fluidized bed combustor test rig firing the design coal for the CFBC test unit under consideration [35-37]. Physical properties of air and combustion gas are based on the data from reference literature [38, 39]. Physical properties for pressure balance model are given in App. C. Based on the design basis and physical properties, input data given in Table 2.7 is obtained. Although the pressure balance model is applied for various solid circulation rates within the range of 5 – 25 kg/m²s, for illustration purpose, the results of the pressure balance model is presented here for G_s = 15 kg/m²s. Some of the input parameters and results varies for different G_s values.

Table 2.6 Design Basis for Pressure Balance Model

Superficial velocity in the riser	U_g	5	m/s
Superficial velocity in dense zone	u_g	3	m/s
Diameter of the riser	D_r	0.25	m
Height of the riser	z	8	m
Height of the dilute zone	H_f	7	m
Cross sectional area of riser	A_r	0.0491	m²
Length of weir section	L_w	0.5	m
Diameter of loop seal	D_{ls}	0.1	m
Length of vertical aeration section	L_{va}	0.5	m
Cross sectional area of downcomer	A_{dc}	0.0079	m²

Table 2.7 Calculated Input Data for Pressure Balance Model

Solid circulation rate (variable parameter)	G_s	15	kg/m²s
Solid mass flux at cyclone connection	G_{sh}	39.95	kg/m² s
Solid mass flux at loop seal	G_{sd}	93.75	kg/m² s
Diameter equivalent of the riser exit	D_e	0.18	m
Projected height of the riser exit	H_e	0.2	m
Gas velocity at loop seal	U_o	0.01	m/s
Average velocity at cyclone connection	U_{gh}	15	m/s
Empirical coefficient for velocity head at cyclone	C_{cy}	10	
Inlet area of cyclone	A_c	0.0126	m²

2.2.4.8 Results of the Pressure Balance Model

Using the input data given above, the pressure balance model is applied to the 150 kWt CFBC Test Unit Design. During the progress of pressure balance model application, it is also required to calculate some parameters given in App. C. The pressure balance model resulted in the operating parameters given in Table 2.8.

Solid hold up profile in the dilute zone (ε_s)

Solid hold up profile through dilute zone is obtained from (2.11) without considering the effect of sharp turn at riser exit. The deviation of dilute zone solid hold up profile by particle reflux as a result of exit effect is obtained from (2.14).

Table 2.8 Results of Pressure Balance Model (G_s = 15 kg/m²s)

Results for G_s = 15 kg/m²s		
Solid hold up in the dense bed of riser	ε_{sd}	0.25487
Average solid hold up at the dilute zone	$\varepsilon_{s\infty}$	0.004106
Voidage of solid bed in downcomer	ε_{dc}	0.20
Voidage in loop seal	ε_{ls}	0.20
Solid height in downcomer, m	H_{dc}	2.10

The array of the results of both equations are added to each other and the solid hold up profile through the dilute zone, including exit effect is given in Figure 2.12.

2.2.4.9 Pressure drop profile

Following the solid holdup profile through the riser, the pressure drop values for riser, cyclone, downcomer and loop seal are obtained. The results are given in Table 2.9. Starting from the outlet of air blower, pressure loop profile for the solid circulation rate of 15 kg/m²s is obtained and shown in Figure 2.13.

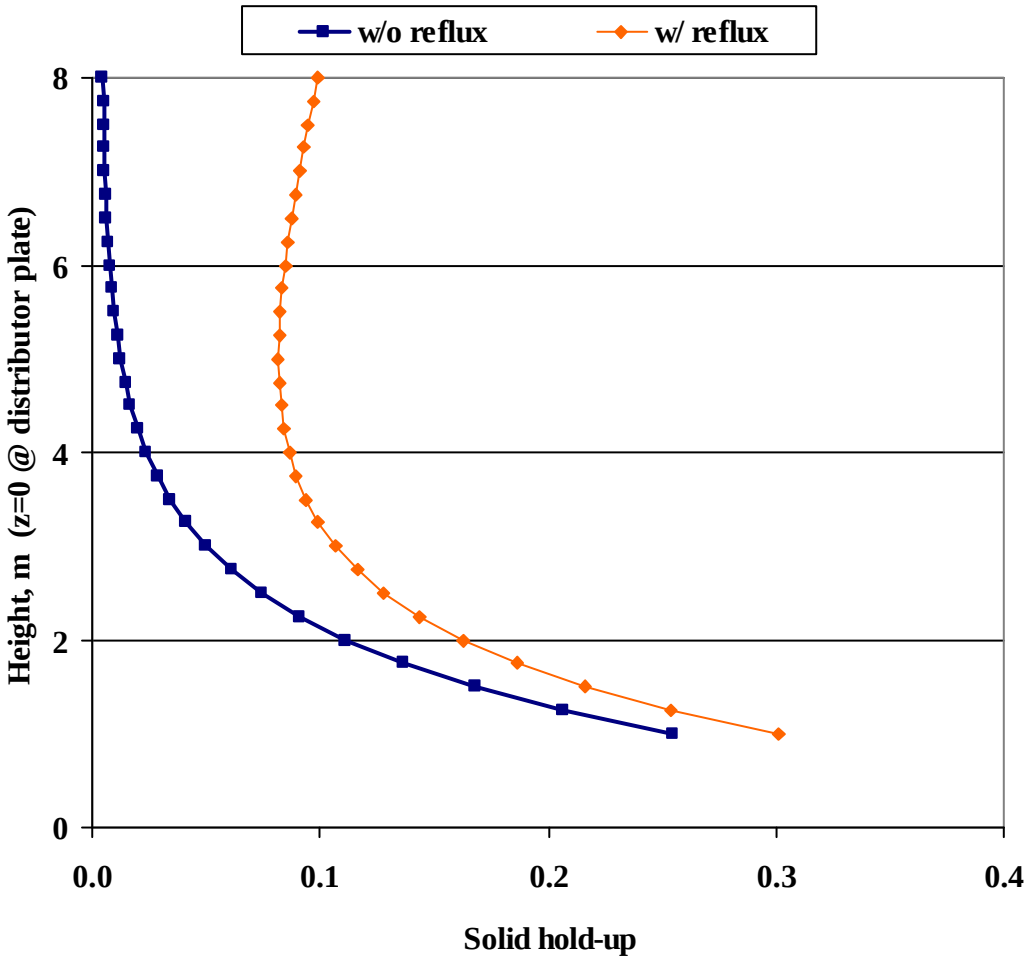

Figure 2.12 Solid Holdup Profile Prediction for Dilute Zone (G_s = 15 kg/m²s)

Table 2.9 Pressure Drops within the CFBC Loop (G_s = 15 kg/m²s)

Dense zone	ΔP_{dense}	471.8	mmH2O
Dilute zone	ΔP_{dilute}	740.4	mmH2O
Cyclone duct	ΔP_h	21.5	mmH2O
Cyclone	ΔP_c	59.6	mmH2O
Loop seal	ΔP_{ls}	508.4	mmH2O
Downcomer	ΔP_{dc}	1565.8	mmH2O

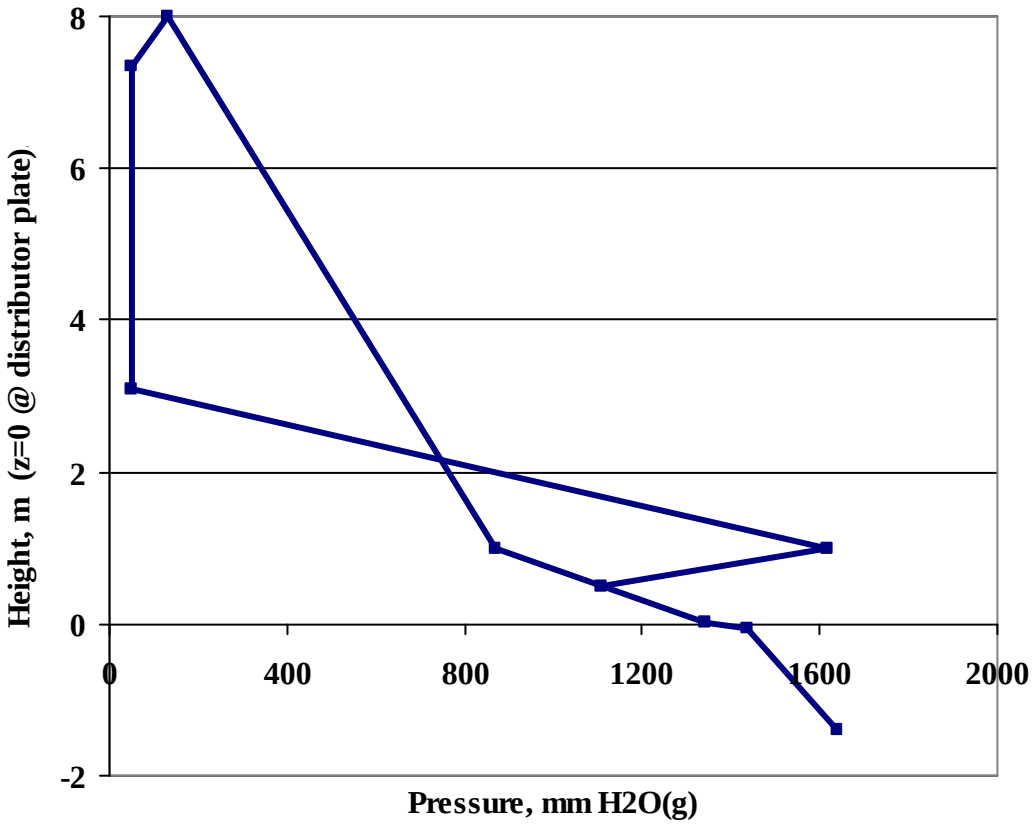

Figure 2.13 Pressure Loop Profile (G_s = 15 kg/m²s)

As can be seen from the figure, combustion air at the outlet of the blower is at a pressure of 1590 mmWG. Calculation procedure of this value is based on the design criteria that the pressure at the cyclone exit is approximately balanced or is slightly negative. To be on the safe side, design basis for the pressure at the

cyclone exit is taken as 0 mmWG. Then, adding up the pressure resistances from cyclone back to the blower outlet – dilute zone, dense zone, distributor, air piping – leads to pressure requirement at the blower exit. The pressure values displayed in Figure 2.13 stands for the points given in Figure 2.10 as explained below:

The data point at the bottom of the profile given in Figure 2.13 is the pressure value at the blower exit (P_1=1590mmWG). From the blower to the air box of the combustor, ΔP through the piping is approximately 200 mmWC (P_2 = 1390 mmWG). Then, air passes through the distributor plate designed to have a ΔP of 0.2 times that of dense zone [15, 34], 94.2 mmWC, and it enters the combustor (P_3=1345mmWG). As given in Table 2.9, with ΔP values of 471.8 mmWC and 740.4 mmWC through the riser, pressure decreases first to 823 mmWG (P_4) after dense zone and then to 81 mmWG (P_5) at the riser exit. Passing through the cyclone duct and the cyclone, pressure at the cyclone exit drops to 0 mmWG (P_6), where pressure is balanced as it is the design basis. As a result of the particle hold up within the downcomer having a height of 2.1 m, the pressure at the entrance of loop seal increases to 1615 mmWG (P_7). At the exit of loop seal, where the particles enter the combustor, pressure is 1107 mmWG (P_9), balanced with the pressure of dense zone at the height of recycle leg. Pressure drop through CFBC loop leads to the amount of solids in the system as given below:

Table 2.10 Solid mass within the CFBC loop

Dense zone	M_{dense}	23.14	kg
Dilute zone	M_{dilute}	36.32	kg
Downcomer	M_{dc}	12.29	kg
Loop seal	M_{ls}	5.85	kg

2.2.5 Heat Transfer Analysis

As given in 'detailed design of combustor', the combustor is composed of five (5) modules, each having 47.5 mm refractory lining at the inner surface. Second and third modules along the combustor are cooled, and the others are only insulated from outside.

2.2.5.1 Modules without Cooling

First, fourth and fifth modules of the combustor, designed without cooling system, are insulated with ceramic fiber blanket from outside to have an external surface temperature of 60°C, and these modules only have heat loss from the external surface to the surroundings. The schematic diagram, summarizing the heat transfer analysis for this design is given in Figure 2.14. As can be seen from the figure, heat transfer through the pipe material is not taken into account. It is assumed that the resistance of carbon steel pipe to heat transfer is negligible compared to other layers.

As 60% of the combustion air is fed from the bottom as primary air, combustion reaction will not be complete within the dense zone. Based on the heat transfer analysis over the dense zone module (module-1), even 60% of the combustion reaction takes place within module-1, temperature within the module does not exceed 850°C, typical operating temperature of CFBCs. As a result of this, there need not be any cooling along this module as the dense zone will be cooled by the primary air entering the combustor from the bottom. Considering the cooling duty in second and third modules, it is not required to design the fourth and fifth modules with cooling systems, either. Therefore, for the modules without cooling, following heat transfer analysis is carried out based on Figure 2.14.

Heat balance for combustor inner surface leads to the equation for module surface temperature at R_1, following the procedure below:

$$Q_{conv\text{-}in} = Q_{cond1} \tag{2.31}$$

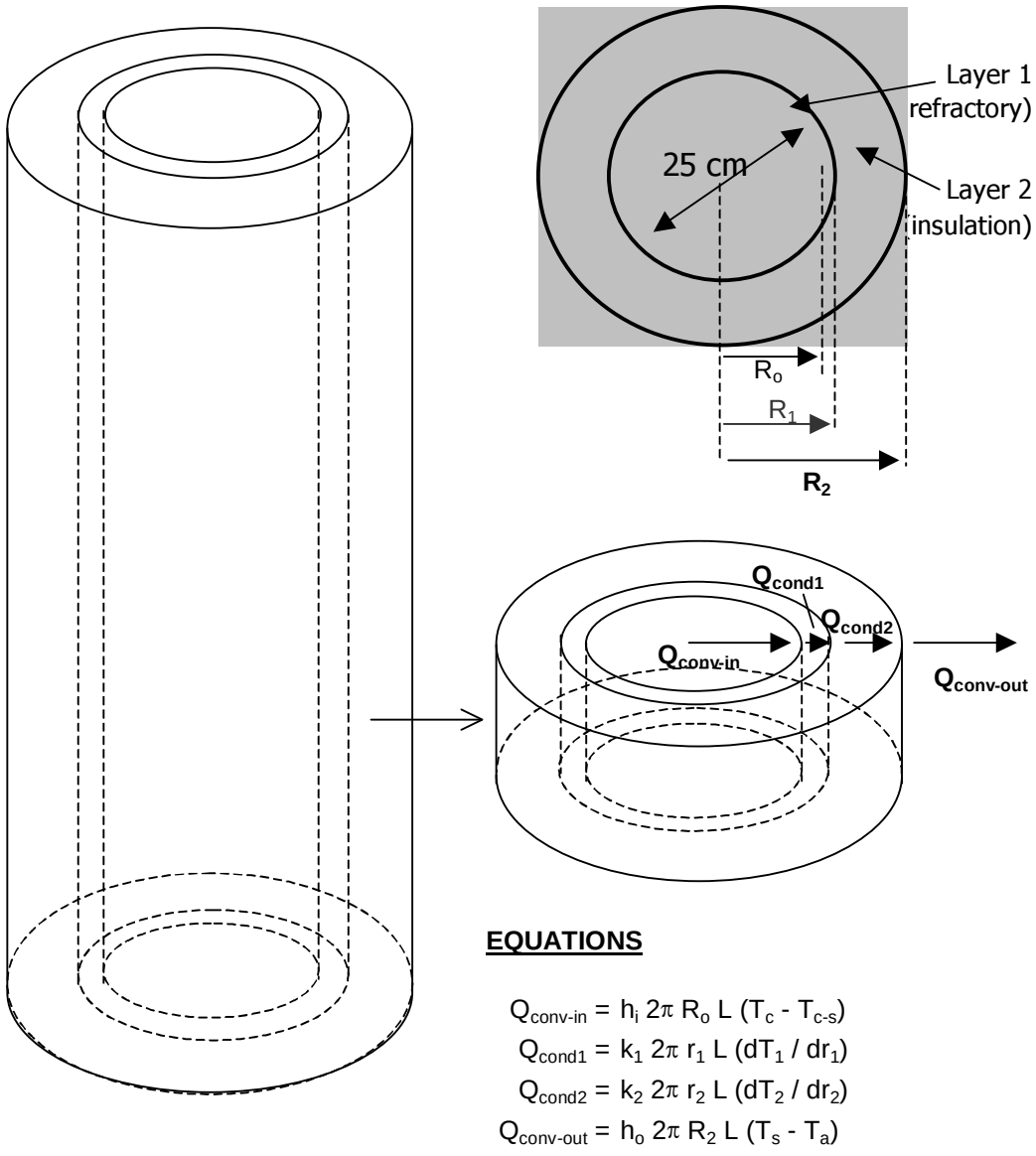

Figure 2.14 Schematic Heat Transfer Diagram for First and Fourth Modules

Inserting the equations given in Figure 2.14 into (2.31):

$$h_i R_o (T_c - T_{c-s}) = - k_1 r_1 (dT_1 / dr_1) \qquad (2.32)$$

Rearranging (2.32):

$$\int_{T_{c-s}}^{T_{r1}} dT_1 = \frac{h_i R_o (T_c - T_{c-s})}{-k_1} \int_{R_o}^{R_1} \frac{dr_1}{r_1} \qquad (2.33)$$

Then the equation for T_{r1}, temperature at R_1, in terms of temperatures within combustor and at inner wall of combustor is obtained by integrating (2.33):

$$T_{r1} = T_{c-s} - \frac{h_i R_o (T_c - T_{c-s})}{k_1} \ln (R_1 / R_o) \qquad (2.34)$$

On the other hand, heat balance for outer surface of the insulation leads to the second equation for T_{r1}, but in terms of ambient air temperature at the laboratory and temperature of outer surface of insulation:

$$Q_{conv\text{-}out} = Q_{cond2} \qquad (2.35)$$

Inserting the equations given in Figure 2.14 into (2.35):

$$h_o R_2 (T_s - T_a) = - k_2 r_2 (dT_2 / dr_2) \qquad (2.36)$$

Rearranging (2.36):

$$\int_{T_{r1}}^{T_s} dT_2 = \frac{h_o R_2 (T_s - T_a)}{-k_2} \int_{R_1}^{R_2} \frac{dr_2}{r_2} \qquad (2.37)$$

Then the second equation for T_{r1} is obtained by integrating (2.37):

$$T_{r1} = T_s + \frac{h_o R_2 (T_s - T_a)}{k_2} \ln (R_2 / R_1) \quad (2.38)$$

Heat balance over the whole system of refractory, pipe and insulation, leads to the equation for inner surface of refractory:

$$Q_{conv\text{-}out} = Q_{conv\text{-}in} \quad (2.39)$$

Inserting the equations given in Figure 2.14 into (2.39):

$$h_o R_2 (T_s - T_a) = h_i R_o (T_c - T_{c\text{-}s}) \quad (2.40)$$

Then the equation for $T_{c\text{-}s}$ is obtained by rearranging (2.40):

$$T_{c\text{-}s} = T_c - \frac{h_o R_2 (T_s - T_a)}{h_i R_o} \quad (2.41)$$

Employing (2.34), (2.38) and (2.41) with the following procedure, temperutare values at the boundaries and insulation thickness is obtained:

1. Guess a value for the thickness of insulation.
2. Calculate the inner surface temperature of combustor from (2.41).
3. Calculate temperature at R_1 (carbon steel surface) from (2.34) and (2.38).
4. Check if the results of (2.34) and (2.38) are equal to eachother.
5. Calculate error between two values.
6. Guess a new insulation thickness with respect to error calculated at step 5 and restart the procedure from step 2.

Input data for the application of this procedure is given in Table 2.11.

Table 2.11 Input Data for Heat Transfer Analysis of Modules w/o Cooling

Temperature in the combustor, T_c	850	°C
External surface temperature of insulation, T_s	60	°C
Ambient temperature, T_a	15	°C
Heat transfer coefficient to combustor wall, h_i	80	W/m²K
Heat transfer coefficient for external surface, h_o	15	W/m²K
Thermal conductivity for layer 1 (refractory), k_1	1	W/mK
Thermal conductivity for layer 2 (ceramic fiber), k_2	0.06	W/mK
Radius of combustion chamber, R_o	0.125	m
Thickness of refractory, δ_1	0.0475	m
Radius of module excl. insulation, R_1	0.1725	m

Inserting the input data into equations, results given in Table 2.12 are obtained. As can be seen from the table, modules without cooling should be insulated with a 5.6 cm thick ceramic fiber, resulting in a total diameter of 45.7 cm. However, as it is also explained in insulation section at Chapter III, standard ceramic blanket thickness starts from 25 mm and increases by factors of this value. As a result of this, application thickness is revised to 5.0 cm that also reduced total diameter of modules approximately to 45 cm. This 6 mm decrease in insulation thickness is expected to be covered by the natural insulation effect of air cavities between combustor, ceramic blanket and aluminum cover sheet. These cavities generally arise from wrapping practice that is not perfect at small diameter applications.

Table 2.12 Results for Heat Transfer Analysis of Modules w/o Cooling

Temperature at inner surface of refractory, $T_{c\text{-}s}$	834.6	°C
Temperature at outer surface of refractory, T_{r1}	784.9	°C
Thickness of layer 2 (insulation), δ_2	5.6	cm
Diameter of insulated module, D_2	45.7	cm

2.2.5.2 Modules with Cooling

Second and third modules of the combustor with cooling system, are designed to have a number of cooling water channels vertically welded to the external surface of module. Then the surrounding of the cooling channels and module surface should be insulated with ceramic fiber blanket from outside to have an external surface temperature of 60°C. These modules are cooled by water with an inlet temperature of 15°C, and the design criteria for the maximum outlet temperature of cooling water is 60°C, not to have evaporation and water hammer in the pipes. The schematic diagram, summarizing the heat transfer analysis for this design is given in Figure 2.15. Heat transfer resistance of pipe is neglected also for these modules, and the combination of pipe surface and cooling water channels is treated as an equivalent annular cooling water layer.

As the design basis for the combustor is to feed 40% of the combustion air from the top of first module as secondary air, combustion reaction is expected to continue within the second module and the third module. However, energy generation is reduced as there is less combustible material going up the riser. This results in different cooling duties for module-2 and module-3. In order to have different amounts heat transfer area in these modules, and based on the heat transfer analysis over dilute zone modules (module-2 and module-3), the modules are designed to supply 70% of total cooling duty in module-2, and 30% in module-3. For this purpose, cooling water surface areas of modules should differ from eachother. Heat transfer analysis to calculate these surface areas of cooled modules is carried out based on the schematic diagram and heat balance equations given in Figure 2.15.

Similar to the approach for uncooled modules, heat balance for combustor inner surface leads to the equation for module surface temperature:

$$T_{r1} = T_{c\text{-}s} - \frac{h_i R_o (T_c - T_{c\text{-}s})}{k_1} \ln (R_1 / R_o) \qquad (2.42)$$

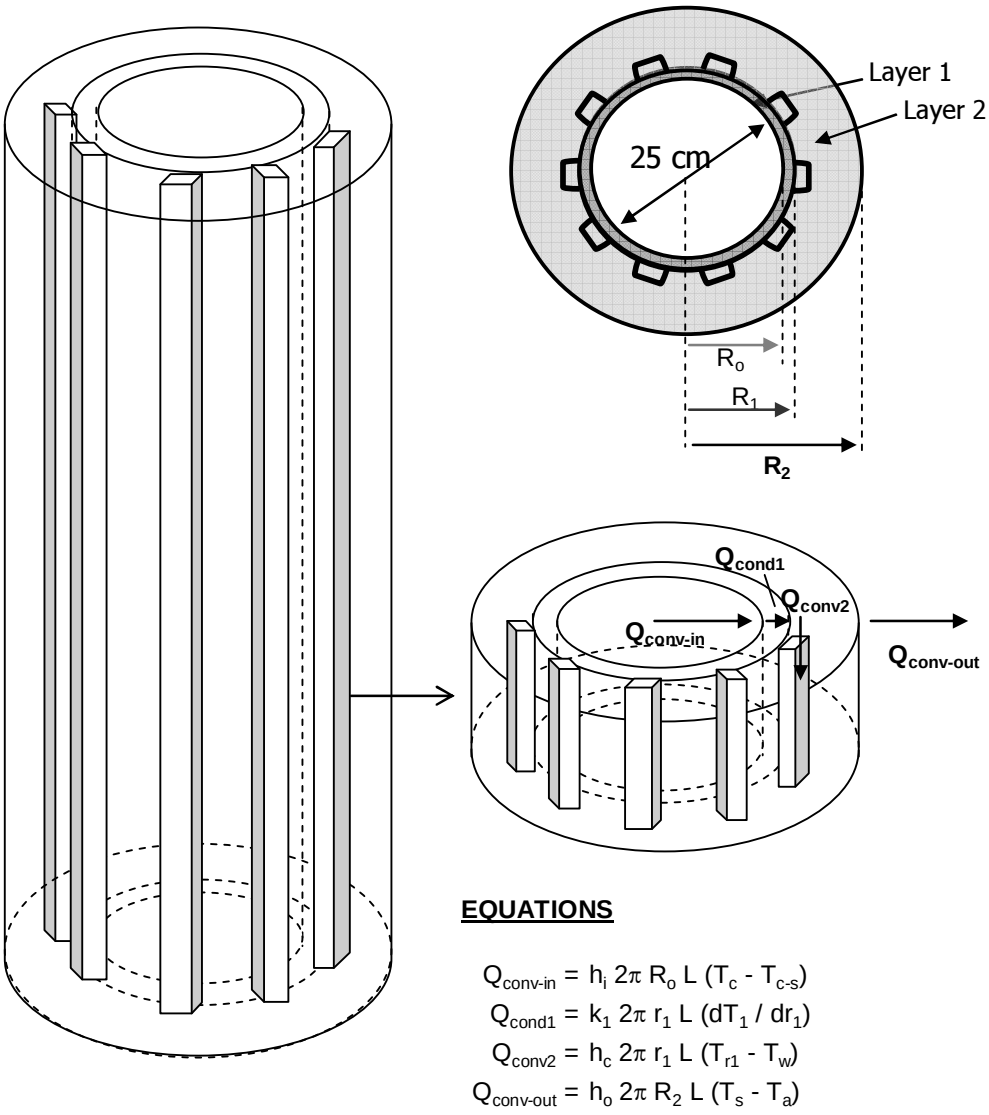

Figure 2.15 Schematic Diagram for Cooled Second and Third Modules

Heat balance over the system leads to the second equation for module surface temperature:

$$T_{r1} = T_w + \frac{h_i\, R_o\, (T_c - T_{c-s}) - h_o\, R_2\, (T_s - T_a)}{h_w\, R_1} \qquad (2.43)$$

Employing (2.42) and (2.43), temperature of outer surface of refractory is iterated until the results from these equations are equal to each other. For the application

of this procedure, some of the input data in Table 2.11 and the equivalent heat transfer coefficients of 125 W/m²K and 80 W/m²K obtained from the correlation for flow in cooling tubes [40], for cooling water channels of module-2 and module-3, respectively, are used.

According to these analysis, cooling water flow rates at module-2 and module-3 are predicted to be 890 kg/h and 420 kg/h, respectively, and the number of cooling water channels on the modules are ten (10) pieces for module-1, and six (6) pieces for module-3.

2.2.6 Detailed Design of Combustor

As an outcome of the basic design studies, the height of the combustor (riser) was chosen to be 8 m where as the cross sectional area was calculated to be 0.25 m to have a superficial velocity of 5 m/s within the riser.

As there is no waterwall within the furnace, the inner surface of modules is directly exposed to combustion and erosion effects. Then, no common pipe material, carbon steel or stainless/alloy steel is resistant to these conditions. Although the unit will not operate frequently, pipe material may be incandescent, deformed and eroded during operation, if there is no refractory layer inside the inner surface of the steel pipe. Then there need to be a refractory layer inside, resistant to erosion. However, refractory is not a good insulator, so that it is not required to have a thick refractory layer. As a result, the thickness is determined by the manufacturing limitations as 4.75 cm.

The combustor is required to be manufactured as smaller modules to be integrated. The reason for this design is as follows: Refractory layer is 4.75 cm thick and there are a number of ports along the combustor for instruments, solids feeding, circulation leg etc. Therefore, if refractory is casted into 8 m long pipe, the refractory layer may not be homogeneous while there are so many obstacles (ports). In addition, regarding the modularity of the system in terms of flexibility

for modifications in the future and ease of installation and dismantling, 8 m combustor as a single piece would not be effective.

Based on the explanations given above, the combustor riser is decided to be composed of 6 pieces given below. Air box module is not referred as combustor module within the text, so that numbering starts from dense zone module as module-1 and ends up with exit module as fifth module, where from module – 2 to exit module are totally referred as dilute zone modules:

1. air box module (height : 400 mm)
2. module – 1 (dense zone module) (height : 1500 mm)
3. module – 2 (cooled module-1) (height : 2000 mm)
4. module – 3 (cooled module-2) (height : 2000 mm)
5. module – 4 (height : 2000 mm)
6. exit module (height : 500 mm)

The detailed design drawing of the combustor is given in Figure 2.16.

2.2.6.1 Windbox module

The height of this module is 400 mm and the outer diameter of the pipe used for manufacturing is 273 mm. As there is only the start-up burner in this module, not to be operated continuously through the test runs, no refractory layer is casted. Primary air enters the air box from the side through a pipe with a size of DN 100. On the other side, there is a port for pressure (PT) and delta pressure transmitters (DPT). Instrument ports of windbox and other modules are given in Appendix C.

2.2.6.2 Distributor

Distributor plate is manufactured from a 5 mm thick plate of AISI 304 material and it is integrated to a flange to be installed between windbox and dense zone module. Distributor plate has 645 holes of 2 mm size to have an orifice velocity of 33.6 m/s and creating a pressure drop of 99 mmWC that is approximately 21% of

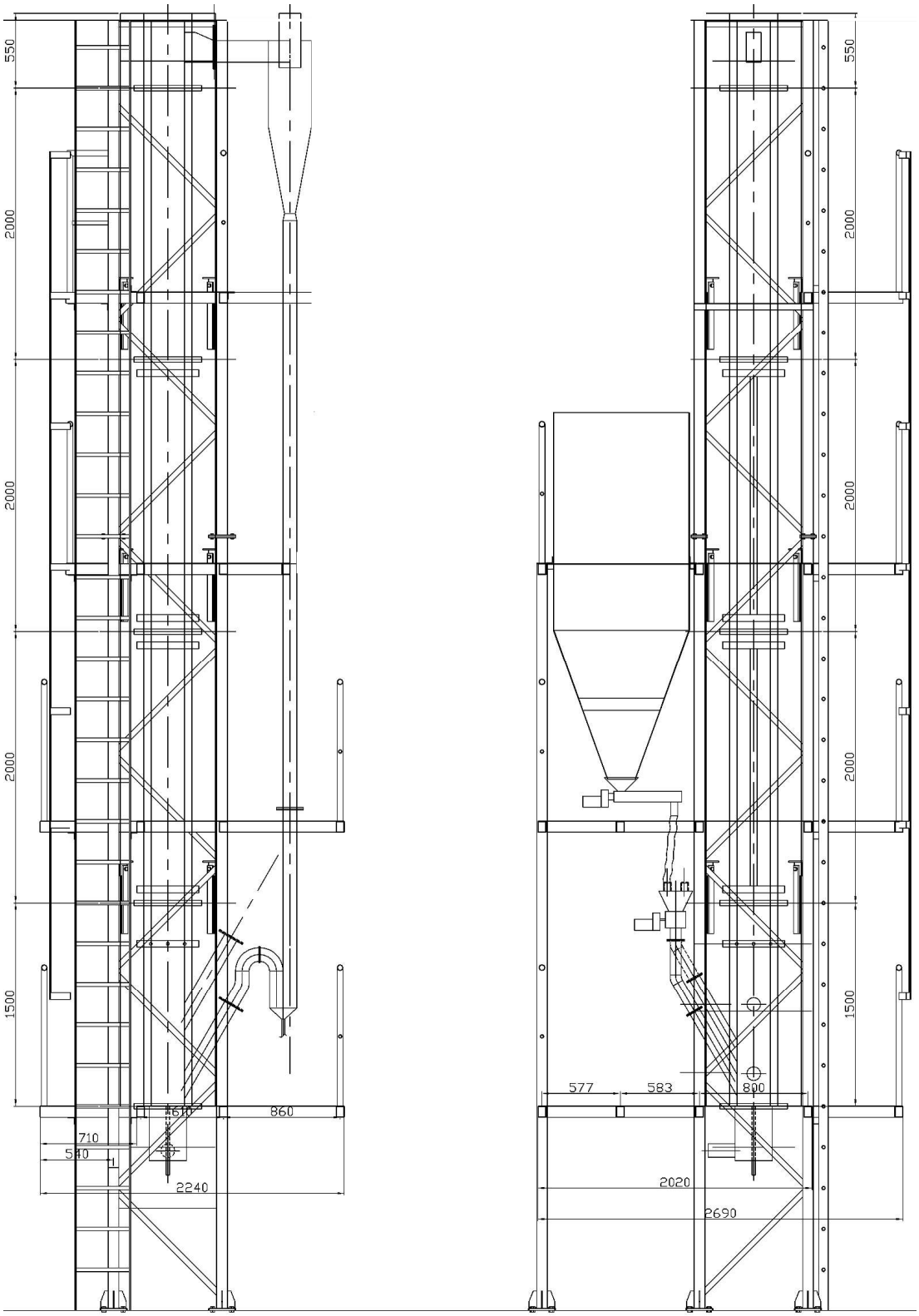

Figure 2.16 Detailed design drawing for the CFBC

dense zone pressure drop. At the center of the distributor plate, there is an opening for a 1” size pipe to discharge the bed material to control the pressure drop within dense zone during operation and to empty the riser after shut down

2.2.6.3 Module-1

The height of module-1 is 1500 mm and pipe diameter is 355 mm as there is a refractory layer of 47.5 mm thick at the inner surface of pipe, resulting in a riser diameter of 250 mm. Bottom of the module is connected to distributor and windbox module. Solid feed enters from 250 and 500 mm height through DN 80 pipes from the eastern side with an angle of 60°. On the western and northern sides, there are ports for transmitters and gas probes. The circulating particles coming from loop seal enters the combustor at 250 and 750 mm height through DN100 pipes with an angle of 60°. At 1200 mm, secondary air enters the combustor through a collector surrounding the combustor that feeds symmetrically located 8 pieces of ½” pipes having an angle of 60° with the horizontal axis. There are no cooling water pipes at this module. There are ports for transmitters and a gas probe along the height. (Appendix C)

2.2.6.4 Module-2

The height of module-2 is 2000 mm and pipe diameter is 355 mm. Bottom of the module is connected to module-1. There is a refractory layer of 47.5 mm inside the pipe. At the outside wall of the pipe, 10 pieces of vertical cooling water channels with 50 mm width are almost symmetrically welded, and there are collectors at the top and bottom that are connected to cooling water pipes. There are also ports for transmitters and gas probes along the height. (Appendix C)

2.2.6.5 Module-3

The height of module-3 is 2000 mm and pipe diameter is 355 mm. Bottom of the module is connected to module-2. There is a refractory layer of 47.5 mm inside the pipe. At the outside wall of the pipe, 6 pieces of 50 mm vertical cooling water

channels are symmetrically welded, and there are collectors at the top and bottom that are connected to cooling water pipes. As explained before, cooling requirement is expected to differ along the combustor, as combustion takes place all over the height. This brings different cooling duties with respect to height and different number of cooling channels. There are also ports for transmitters and gas probes along the height of this module, too. (Appendix C)

2.2.6.6 Module-4

The height of this module is also 2000 mm and pipe diameter is 355 mm. Bottom of the module is connected to module-3. There is a refractory layer of 47.5 mm inside the pipe. There are also ports for transmitters and gas probes (Appendix C). There are no cooling water pipes at this module as the cooling duty is at the second and third modules.

2.2.6.7 Exit module

The height of exit module is 500 mm and pipe diameter is 355 mm. Bottom of the module is connected to module-4. Top of the module is covered and the cyclone exit is at the southern side. There is a refractory layer of 47.5 mm inside the side walls and top cover of the module. There are also ports for transmitters and a gas probe (Appendix C). There is no cooling at this module.

2.2.6.8 Instrument Ports

In order to summarize the distribution of each type of port, height and distance with previous instrument along the combustor for pressure, differential pressure, temperature and gas probes are tabulated, and the layout of instruments and gas probe ports with respect to their axis are given in Appendix C.

CHAPTER 3

PROCUREMENT and INSTALLATION

3.1 Procurement Activities

The procurement activities include detailed design and manufacture of components and purchase of some of the equipment.

3.1.1 Steel Structure

Based on the loads of riser, silos and other auxiliary equipment, the steel structure was designed. The structure was manufactured of 80mmx80mm profiles as main column and beams, and 40mmx40mm profiles as transversal components. The structure was designed to be composed of two parts; main body as the structure up to 5500 mm elevation, and the upper element to be connected to main body going up to 9500 mm elevation. 3-D view of structural design and picture of main body before installation are given in Figure 3.1.

3.1.2 Circulating Fluidized Bed Combustor Riser

As previously given in 'Detailed Design' section of Chapter 2, the insertion ports at appropriate size and for functions given below were welded to each module.

- Temperature, pressure, delta pressure and gas probe ports
- Solids feeding pipes (Fuel, limestone, bed material)
- Solids recycle pipes (Fly ash)
- Secondary air ports
- Riser-cyclone connection

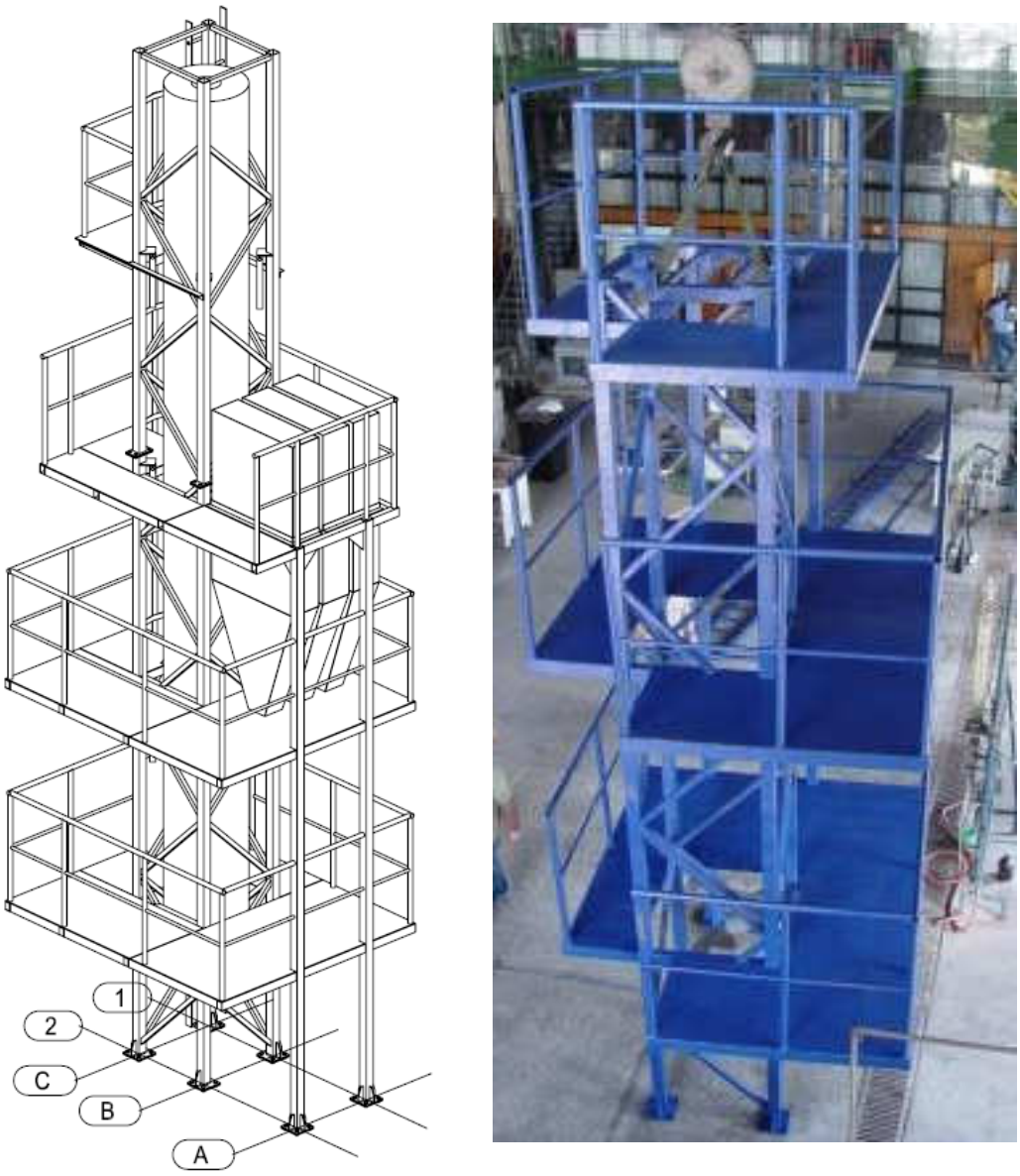

Figure 3.1 Main Steel Structure of the Test Unit

Details of the components like distributor and bearing plates, combustor modules, cyclone and loop seal are given in the following sections.

3.1.2.1 Distributor and Bearing Plates

Distributor plate, which is a key component for the fluidization of the bed, is a perforated plate composed of 645 orifices with 2 mm diameter. It was designed to

fit on a bearing plate that also takes on all the load of combustor modules. This design gives the capability to dismantle the windbox module from the bottom without disturbing the bearing system of combustor modules at the upper levels. The pictures of distributor and bearing plates, and combustor modules are given in Appendix D.

3.1.2.2 Module – 1

This first module of the combustor, standing on the distributor plate, bearing plate and windbox module is the dense zone module within which the dense bed will be formed. This module is separated from other modules because of the number of insertion ports.

There are two alternative feed points for fuel and limestone at eastern axis, two alternative feed points made of stainless steel for circulating fly ash at southern axis, eight ports symmetrically distributed to the axis covered with a collector for secondary air injection, and various temperature, pressure and gas probe ports distributed along the height of module at other axes. The ports described above are stainless steel pipes for which the 47.5 mm of their length was inserted into the module to be embedded in the refractory layer, and the outer part to be embedded in the insulation that is 50 mm thick. After welding the pipes, a template with a diameter of 250 mm was coaxially fixed to the module, and the refractory was casted under vibration in between the module and the template. After the template was removed, a refractory layer having a smooth surface with an inner diameter of 250 mm was obtained as shown at Figure 3.2 (a) and (b).

3.1.2.3 Module – 2

Module-2, standing on the dense zone module (module-1) has instrument ports and it is the first module with cooling system. There are ten (10) vertical water channels with 5 cm width, welded almost symmetrically to the outer surface of the module. The top and bottom of the cooling water pipes are connected to feed and discharge collectors of cooling water, that surrounds the module.

(a)

(b)

(c)

Figure 3.2 Inner views of Modules 1 and 2

Similar to the other combustor modules, pipes for instruments are welded to this module prior to refractory casting. The picture showing the inner view of this module is also given at the bottom of Figure 3.2 (c).

3.1.2.4 Module – 3

Module-3 is the third module along the combustor, has instrument ports and it is the second and the last module with cooling system. As a result of the cooling duty assumed to vary along the height of combustor, there are six (6) vertical water channels and two collectors at the outer surface of this module for feeding and discharge. The instrument pipes and water channels were welded, then the refractory was casted, same as the application in previous module.

3.1.2.5 Module – 4

Module-4, being the fourth module along the combustor and the last one before the short exit module, has instrument ports but there is no cooling system, as the unit was designed for absorbing the heat of whole system in the previous two modules. The instrument pipes were welded and the refractory was casted, same as the other modules.

3.1.2.6 Exit Module

Exit module, having the connection to the cyclone is the fifth and the last module along the combustor. There are three ports in total; one for temperature transmitter, one for pressure impulse line and one for gas probe. After welding the cyclone duct to the southern axis with a cross section of 220 x 110 mm, and welding the instrument ports, refractory was also casted to this short module having a height of 500 mm.

3.1.3 Cyclone

Detailed design of cyclone, which has a total height of 1,270 mm was presented in the previous chapter. Based on this design, cyclone was manufactured of stainless

steel to resist the high temperature and abrasive fly ash particles. The connecting duct between riser and cyclone was designed to have 10 m/s gas velocity at riser exit and get narrower to reach 20 m/s at the cyclone inlet within a small distance. The picture of cyclone prior to installation is given in Appendix D.

3.1.4 Start-Up Burner

The start-up burner was not only required for heating up the combustor before feeding coal to the system, but also for supplying the necessary heat during the refractory drying operation. As the heat loads required for drying and start-ups are lower and the design of the combustor is not similar to conventional boilers, industrial start-up burners can not be used in this test unit. Therefore, a start-up burner to fire natural gas and LPG was designed to be integrated to the wind box of the combustor having a similar function to a duct burner in a conventional boiler. This start-up burner heats up the combustion air before entering the furnace through the distributor. The schematic diagram of the burner is given below in Figure 3.3.

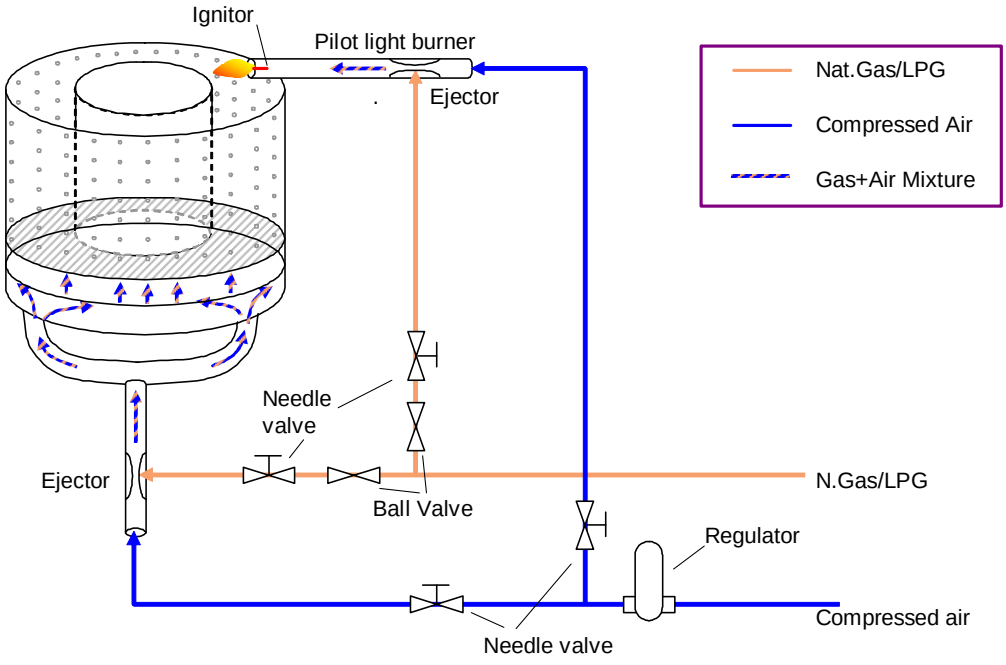

Figure 3.3 Schematic Diagram of Start-up Burner System

As can be seen from the figure, compressed air and fuel are mixed at the ejectors and fed to the burner from the bottom for main flame and to the pilot light burner that is for ignition and flame continuity.

Start-up burner was designed for firing pressurized natural gas and liquified petroleum gas (LPG) with compressed air to prevent breaking off the flame by the flow of fresh air coming from the blower at a pressure slightly higher than atmospheric. However, unless necessary measures are taken, compressed air limits the gas flow at the mixing point because of pressure dominancy of compressed air over fuel. Therefore, the ejectors also given in Figure 3.3 were manufactured to generate a suction of fuel by using pressure of compressed air.

In order to achieve efficient reaction, a reservoir is located at the bottom of burner, where compressed air and gas is mixed prior to combustion. As the temperature at the core of flame is expected to be over 1000°C at the burner, alloy steel material of AISI 310 standard was used for main body.

As the burner was integrated to the windbox, and the distributor is located at the top of burner at an elevation of 25 cm from the burner throat, it was required to limit the expansion of flame to minimize direct exposion of distributor plate to the flame. For this purpose, top of the burner was covered with a stainless steel sieve as seen from the picture given in Figure 3.4. During operation of burner, steel sieve becomes incandescent and it enhances the combustion while unburnt fuel passes through it.

Pilot flame is ignited with an electrical lighter, continuously generating an arc at a high frequency to guarantee the flame, not only for the initial ignition of burner but also for system safety. An observation window is located at windbox for watching both flame contact with distributor plate and flame break off during combustion test start-ups.

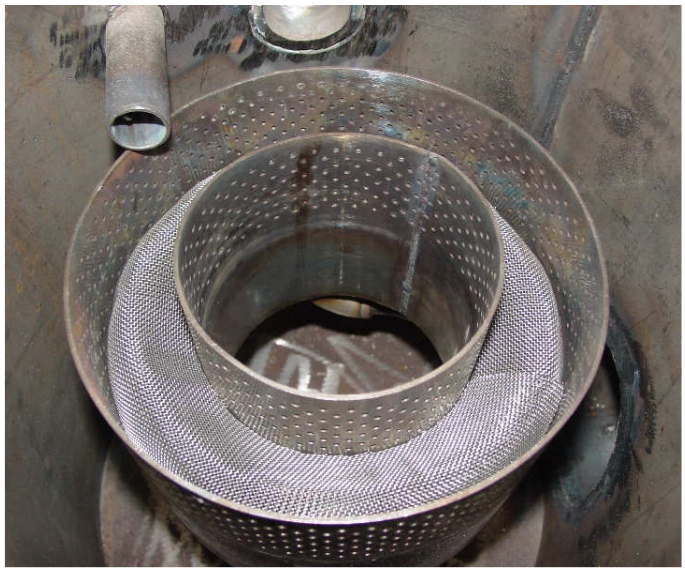

Figure 3.4 Start-up Natural Gas/LPG Burner

As can be seen from the top in Figure 3.4, start-up burner was integrated to the windbox from inside, primary air inlet is at the right below the burner, observation window is in the middle at the top, and the pilot light burner is at the left which is located at the exit of burner.

The regulators, connections, ejectors and ball and needle valves for compressed air and gas that are shown in schematic diagram were installed outside the windbox.

After the gas and compressed air valve train were integrated with the burner, ignition tests were carried out before the windbox was connected to the bearing plate at the bottom of combustor. As the tests were successfully completed, the windbox was installed. The final picture of windbox is given in Appendix D.

3.1.5 Piping

The piping system for air, gas and water connections including pipes, elbows, Te's, flanges and other elements, are composed of the following lines with given materials:

- Primary and secondary air lines for combustion air (carbon steel)
- Flue gas line (carbon steel)
- Cooling water lines for cooled combustor modules (standard water piping and flexible hydraulic hoses)
- Cooling water lines for gas sampling probes (standard water piping)
- Process connections for differential pressure transmitters (stainless steel)
- Compressed air lines (carbon steel)
- Purge tubing (stainless steel)
- Gas lines for start-up burner (standard natural gas pipes and stainless steel tubes)

3.1.6 Combustion Air Fan

Combustion air flow rate requirement was presented in the basic design section. The relevant data from that section for combustion air fan selection is given below.

The maximum dry air flow rate based on an excess air ratio of 20% is 210.66 Nm^3/h. For experimental purposes, excess air ratio may be increased up to 60% temporarily. Therefore, maximum air flow rate based on 60% excess air was calculated as 280 Nm^3/h.

The other important parameter for fan design is the discharge pressure. Although the exact pressure drop of the combustor will be observed during the operation, modeling studies predicts the maximum pressure requirement to be in the range of 1800 – 2000 mmWC. Then the main operating conditions for the fan are; air flow rate: 280 Nm^3/h, and discharge pressure: 2000 mmWG.

For the conditions given above, conventional centrifugal fan designs are not suitable. Conventional fans for the discharge pressure given above need to have a design capacity of almost 2000 Nm^3/h. Using that kind of a fan, it is required to control the flow with a damper, which would be working at 10% open position that would be creating a pressure drop exceeding the operation pressure limits of the fan, and there would be no flexibility for controlling the flow rate. Therefore, it was required to install an equipment that gives higher pressure at lower flow rates, and has an identical characteristic to that of a centrifugal fan. The best solution was found to be the equipment defined as 'Side Channel Blower'.

There need to be a butterfly valve installed at the discharge of the blower to control the flow of the combustion air by creating an additional pressure to that of the system. Thus, at normal operating conditions (200 Nm^3/h = 3.33 Nm^3/min), the blower discharge pressure will be increased to almost 300 mbar by the help of this valve. The driver of the blower was selected to be CT VFD – Constant torque, variable frequency driver, to control the speed of motor for better tuning of the air flow in addition to air flow control valve.

3.1.7 Solids Handling and Feeding

3.1.7.1 Solids Handling

Fuel and limestone handling system is composed of three (3) identical silos, each with a capacity of 0.65 m^3. As given in detailed design section, rectangular part of the silos have a cross section of 300mm x 1000 mm and a height of 1600 mm. Bottom part of the silos has a slope of 70° with the normal and the discharge cross section of the silos has the dimension of 200mm x 200mm. The silos were manufactured from carbon steel sheet with a thickness of 3 mm. The picture of the silos before installation are given in Appendix D.

3.1.7.2 Solids Feeding

Fuel and limestone stored in the silos are discharged by screw conveyors having frequency invertor drivers. The flow rate of the solids are determined by the variation of weight of the silo, then the frequency of the electric motor is to be varied to reach the target flow rate.

The screw conveyors at the bottom of each silo are connected to an intermediate bunker of an air lock that will feed the solids and isolate the combustor from the solids feeding system. Otherwise, the pressure at the dense zone of combustor results in backflow of solids and combustion gas out of the system. Solids feeding system is composed of 2 (two) screw conveyors of 50 kg/h capacity for fuel, 1 (one) of 10 kg/h capacity for limestone, 1 (one) for bed material silo with 150 kg/h capacity, and 1 (one) air lock as main feeder with 150 kg/h capacity. Details and pictures can be found in Appendix D.

3.1.8 Instrumentation

Process instruments for which the specifications were presented in the previous chapter were purchased and the details are presented in this section. The specifications of all instruments are given in Appendix D.

3.1.8.1 Pressure transmitters (PT)

Gage pressure transmitters for absolute pressure determination were supplied from Dwyer Instruments Inc. These transmitters are for measuring combustion air pressure at primary and secondary air lines to correct air flow rate calculations and for pressure at the windbox.

3.1.8.2 Delta Pressure transmitters (DPT)

Delta pressure transmitters for measuring the pressure drop at various points within the system were supplied from Dwyer Instruments Inc. These transmitters are required for the measurements along the riser and downcomer and at the riser exit, cyclone exit and distributor plate.

3.1.8.3 Air flow rate transmitters (FT)

Air flow rate is determined by the combination of flow sensors and delta pressure transmitters supplied from Dwyer Instruments Inc. Two flow sensors and their differential pressure transmitters are required for determining the air flow rate through primary and secondary air lines.

3.1.8.4 Air rotameters (RM)

Fluidizing and conveying air required for J-valve is measured and manually controlled by rotameters supplied from Dwyer Instruments Inc.

3.1.8.5 Water flowmeters (FT)

Cooling water flow rates at the cooled modules of the combustor (module-2 and module-3) are determined by the flow sensors supplied from Teksan.

3.1.8.6 Temperature transmitters (TT)

Temperature of air, cooling water, flue gas, combustion chamber and circulation system are measured by temperature transmitters of K type T/C and Pt100 temperature elements supplied by EPA Ltd.

3.1.8.7 Air flow control valves (FCV)

Air flow rates are controlled by the pneumatically actuated control valves supplied from MCS Ltd. The butterfly valves, actuated by double effect pneumatic piston actuators with analog I/P positioners are located on primary and secondary air pipes right after the lines are separated at blower exit.

3.1.8.8 Load Cells (WT)

Solid flow rates are determined by continuously measuring the weight of silos by the load cells supplied from ZEMIC Inc. The weight of each silo is measured by two off model L6G load cells with a capacity of 600 kg and C3 accuracy level.

3.1.8.9 Load Cell Current Transformers

As the load cells generate electrical signals (mVolts/Volt) directly proportional to the load that it is weighing, it is required to add up the signals from two load cells of each silo, and to convert that electrical signal to an analog signal with the range of 4-20 mA that is convenient for the DCS. For this purpose, three (3) separate current transformers, model ST-50811, manufactured by Sistek Electronic Systems are purchased for each silo, and the signals coming from load cells of each silo were connected in parallel to a single transformer that generates 4-20 mA analog signal against silo weight within the range of 0 – 1200 kg.

3.1.8.10 Oxygen Analyzer

The aim of combustion control in a furnace is mainly maximizing the combustion efficiency. One of the most important indicators for efficient combustion is the oxygen concentration within flue gas leaving the furnace. Professional experience on industrial boilers resulted in oxygen concentration ranges for efficient combustion of different type of fuels ranging from coal to natural gas and fuel oil. For a circulating fluidized bed boiler operation, it is recommended that flue gas oxygen concentration on wet basis should be kept in the range of 3.5 – 4% to achieve maximum combustion efficiency. It has been experienced that, below this range, oxygen concentration within the furnace is not sufficient to complete the combustion reactions, and on the contrary, over the range, excessive amount of air enters the system, and some amount of combustion energy generation is consumed for heating up this excess air. In order to attain oxygen concentration for most efficient combustion, fuel and combustion air flow rates are adjusted. For this combustion control, common application is to employ an on-line oxygen analyzer with ZrO_2 (zirconium oxide) cell at the exit of furnace.

Oxygen concentration of flue gas entering the zirconia cell affects the conductivity of the cell, and this change in the conductivity is transformed into an analog signal by a transmitter standing for the oxygen concentration within the range of 0 – 21%.

Figure 3.5 Trimox ZrO_2 Oxygen Analyzer

As there is not a long gas sampling system including gas sampling probes, suction lines, gas conditioning system and analyzers, this type of online analyzers simultaneously transmits the oxygen concentration on wet basis to the control system without any lag in measurements.

For this purpose, TRIMOX ZrO_2 Oxygen/Temperature Analyzer Model YTK-400 was purchased to be integrated to the Test Unit, for which the picture is given in Figure 3.5. As the temperature limit for the analyzer is 400°C, it was installed on the flue gas line at a point that the cooling analysis for flue gas gives a temperature lower than this limit.

In addition, as the zirconia cell of the analyzer operates at 600°C, the cell is heated up with a resistance fed by a 10VDC power supply. Besides, the transmitter of the analyzer for generating analog signal for oxygen concentration

requires 24VDC power supply. Both of these external power supply systems were manufactured and installed within the control system panel.

3.1.8.11 Purge System

Process connections of gage and differential pressure transmitters that were installed on systems containing particles have a considerable potential to be blocked by the solids within the stream. Accumulation of these particles in the process impulse lines results in unreliable measurements. Therefore, process connections of pressure transmitters in any industrial application having the risk of blockage, are installed together with a purge system. Therefore, a purge system for which the schematic diagram is given in Figure 3.6 was designed for the riser and downcomer of the Test Unit.

As can be seen from the diagram, solenoid valves of type 3/2 (2 of 3 channels open) were located between the combustor and the transmitters. Each stainless steel impulse line inserted to a pressure port along the combustor, enters solenoid

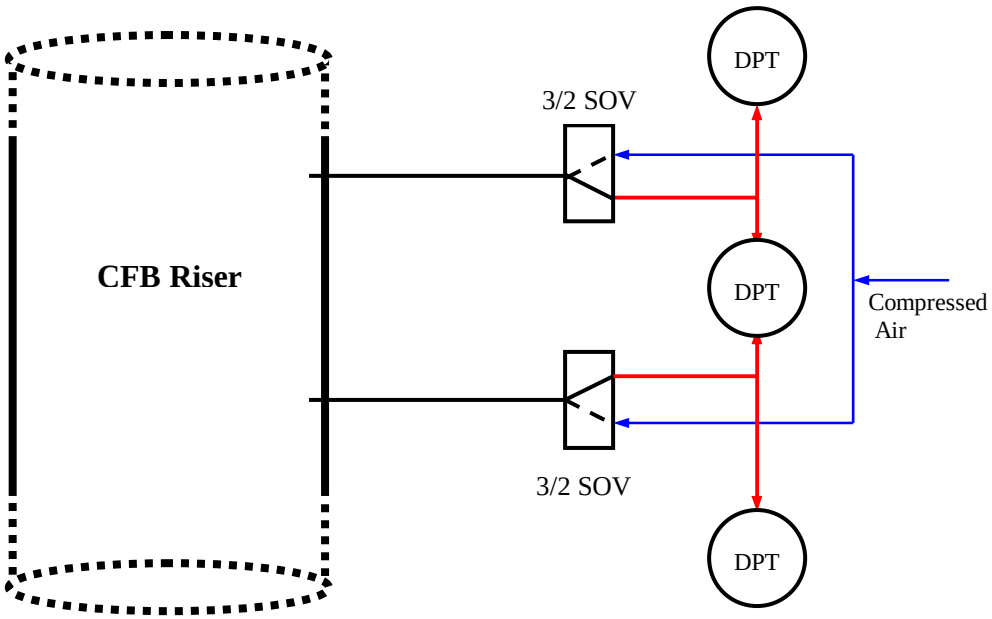

Figure 3.6 Sample Diagram for Purge System

valve, and in normal position of valve, the piston in the valve is in the position to keep the line to the transmitter open. When the valve is energized, piston within the valve switches to the other line, which is connected to compressed air piping. By this way, compressed air purges the impulse line up to the combustor to avoid any accumulation within the tubing for pressure measurement.

3.1.9 Electrical System

3.1.9.1 Motor Control Hardware

The requirement for fine tuning of combustion air blower, solids feeders and bed drain necessitates utilizing frequency invertor drivers (FID) for the motor control of these equipment. The FIDs and other auxiliary contactors and hardware were donated by Schneider Electric company for the Test Unit Project. In the scope of donation, Telemecanique products of main thermic magnetic switch, 1 off 7.5 kW, 2 off 0.55 kW and 3 off 0.37 kW FIDs, magnetic circuit breakers of these drivers, contactors, relays, selector switchs and other accessories were supplied by the company.

3.1.9.2 Motor Control and Auxiliary Loads Panel

In addition to the motor control hardware, there are auxiliary loads within the system, like lighting, field energized tranmitters, purge system and local electrical network. For feeding all of these loads and for installing the motor control hardware, a motor control and auxiliary panel was designed and manufactured by Eptim Electric Ltd. Company.

The panel has selector switches at the front panel for the control of motors either from the panel (local) or directly from DCS computer (remote). By this function, the start/stop commands and motor frequencies can be dictated from the DCS computer in the control room.

3.1.9.3 Motor Protection and Isolation Reactors

During commissioning tests of the Test Unit, it was realized that there appears a typical problem that is experienced in facilities using frequency invertors (FID). The harmonic signals generated as a result of electrical load accumulated on the FIDs are reported to affect the transmitters within any system, unless necessary measures are taken. Although compensation panels for electrical side and isolation filters for instrumentation side are typical precautions for industrial applications, these methods are not convenient for this simple design of electrical system of the Test Unit. Moreover, after diagnostic tests, it was concluded that only the temperature transmitters in contact with the metal body of combustor modules are affected from the harmonic signals generated by FIDs. After this conclusion was reached, first of all, earthing application for these thermocouple transmitters was improved, then a research was carried out on the methods of reducing harmonic signals. As a result, it was decided to use motor protection reactors before feeding, and isolation reactors at the outlet of FIDs. By this way, it was aimed at absorbing the harmonic signals generated by the noisy voltage output of FIDs.

The reactors were supplied from ERGUN Electric Ltd. and installed in the motor control panel. Reactors were connected to input and output of all motor feeders having FID. During the tests and combustion runs, it was observed that the error of temperature readings (8-10°C), was at least 95% reduced for each transmitter.

3.1.9.4 Cabling

The application details for the cabling were determined based on the requirement for the separation of the routes of electrical cables and signal cables not to have any impact of AC current on the 24VDC analog signals. Based on these details, necessary cables, cable trays, covers, conduits and other cable laying accessories were supplied.

For electrical cabling works, cross section of each cable was chosen to be appropriate for the power of the motor. Then, cable trays between motor control

panel and the consumers, hangers, cables for lighting and 220 V distribution, distribution boxes, lighting elements, sockets with suitable protection class, spiral conduits for connection to every consumer, cabling for low load field energized instruments like solenoid valves, load cell current transformers and oxygen analyzer, and glands and connection elements for all these cabling works were supplied and installed due to the application plan.

For control cabling works, multi channel cables were used for reducing the number of cables. Then, for collecting and distributing these multi channel cables, a central junction box was installed. From the central junction box, 6-channel cables were laid to local junction boxes, that are connected to the nearby transmitters by one-channel control cables. Moreover, a switch box was designed for selecting the control system of the instruments commonly used with the 0,3 MWt BFBC Unit. Similar to electrical cabling, cable trays, hangers, spiral connections and other accessories for signal cable laying were used.

3.1.10 Insulation

In order to insulate the combustor, the material should be resistant to the high temperature at the outer surface of combustor, minimum 900°C, and should have superior thermal insulation characteristics to result in minimum thickness. The research for the commercial product to fit this requirement was found to be the ceramic based blankets which belongs to the class of refractory fiber blankets. Ceramic fiber blanket that has a classification temperature of 1260°C, also has excellent insulating performance and thermal stability. For this application, ceramic blankets with 96 kg/m³ density, 7320 mm long with 25 mm thickness and 3660 mm long for 50 mm thickness, both having 61 cm width were supplied. For covering the insulation material, aluminum sheets of 1000 mm x 2000 mm having 0.8 mm thickness were used.

3.2 Installation Activities

3.2.1 Combustıon Air System

The combustion air system starts from the blower, and ends with the windbox and secondary air collecter inlets. Within the scope of this system, following equipment were installed and tested:

- Side Channel Blower
- Primary and Secondary Air Control Valves
- Instrumentation – Temperature, Pressure and Flow Rate Measurements

As the noise level was lower than expected, side channel blower was installed indoors, and the piping at the outlet of blower was divided into two for feeding primary and secondary air lines having diameters of 4 inches and 3 inches, respectively. In order to control the flow through these pipes, pneumatically operated butterfly valves with I/P positioners were installed on each line.

Both valves were set to operate linearly in between 0% - 100% opening range according to the analog output signal generated by the DCS depending on the command given by the operator. However, as the valves are butterfly type, the flow passing through the valve is not linearly proportional with percent opening.
For this reason, it is not reliable to depend on the position of valves to predict flow rates. Then, it was required to have continuous measurements on primary and secondary air lines and to control the valve position manually or automatically from the DCS to attain the set point of air flow.

For air flow rate measurement, flow sensors at appropriate size were installed on both pipes. Impulse lines coming from two flow sensors at different locations along the pipe cross section were connected to the low and high pressure sockets of Magnesense differential pressure transmitter manufactured by Dwyer. Moreover, gage pressure transmitters and a temperature transmitter is located on

the lines for the correction of flow rate calculation. The analog signals generated by these transmitters are logged by the DCS, and are employed in the flow rate expression. Based on air flow rates calculated from this expression, control valves are adjusted for supplying required amount of primary and secondary air.

3.2.2 Instrumentation

The instruments for which the details were given in previous sections were installed, and cabling works and signal tests were completed. The integration activities are presented in this section for the following instrument groups:

- Temperature Transmitters
- Pressure Transmitters
- Differential Pressure Transmitters
- Load Cells
- Cooling Water Flowmeters

3.2.2.1 Temperature Transmitters

Temperature transmitters (TT) with K type thermocouple were installed into stainless steel insertion tubes for TTs along the combustor. The transmitters were inserted into the combustor through tubings such that the the tip of stainless steel thermowell is at the center line. Then, the threaded fitting on each transmitter was screwed tightly to its counterpart at the insertion tube providing sealing of insertion port against gas leakage to the outside of combustor.

Similarly, transmitters of Pt100 type resistance thermometers were installed tightly to inlet and outlet collectors of water cooled combustor modules, and to primary air pipe.

3.2.2.2 Differential Pressure Transmitters

As it is described within purge system section, differential pressure transmitters were installed along the combustor to measure the pressure drop. In addition identical transmitters were connected to the impulse lines along the downcomer to determine the height of particles accumulated within the pipe. For this purpose, one of the ports of the transmitter was connected to the process (downcomer pipe), and the other is left open to the atmosphere. By this way, the transmitter connected to the level higher than particle bed in the downcomer senses the vacuum created by induced draft fan, as the downcomer is directly connected to the cyclone. Then it can be realized that the particle level within the downcomer is at an elevation in between two differential pressure transmitters; one measuring vacuum pressure and the other measuring atmospheric pressure. Three differential pressure transmitters were connected to three different levels along the downcomer. Similar to combustor riser, the process connections of these transmitters also pass through solenoid valves, as there are only particles within downcomer pipe expected to block the impulse lines unless purged.

3.2.2.3 Load Cells

Installation of load cells were done after the mechanical installation works of the test unit were completed. The reason for this is that it is not allowed to carry out any welding work at anywhere of the system, as the load cells can be damaged by welding. This is because load cells are made of metal, directly in contact with the carbon steel silos touching the steel structure, and they are generating mV signals.

For the mounting of load cells, steel profiles were located at both sides of three silos for fuel and limestone. On this structure, base plates were welded for each load cell. At the front side of the load cell, the silo is hanged to the load cell by a chain as seen in Figure 3.7. The design of this hanging system prevents the silo from transferring any portion of its load to the steel structure of test unit, and it provides bearing of the silos only by the load cells. However, it is required to absorb the side loads on the silos that can be generated by any external effect, and

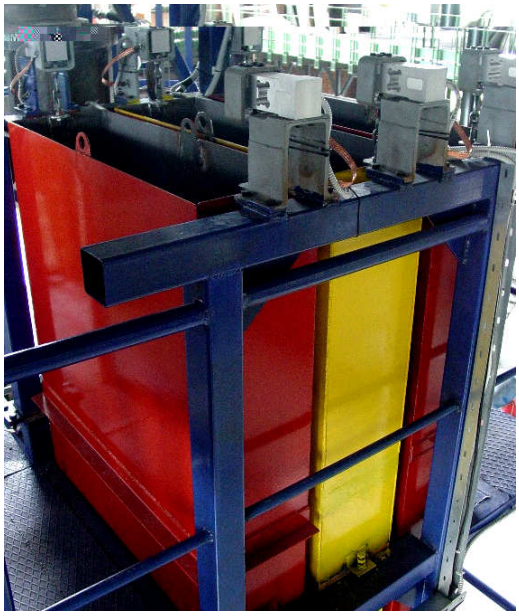

Figure 3.7 Load Cell Installation

can result in weighing failure. In order to prevent this failure, special components were manufactured and the silos were fixed to one of the main columns of test unit. It is worth noting that these connection parts do not take any vertical load on themselves or transfer it to the column, which can otherwise result in measurement error.

On the other side, in order to weigh the silo accurately, the feeder located at the bottom of each silo for discharging the solids should not contact with the platform under it. Otherwise, some of the load of solid material is transferred to the feeder via the outlet of silo, then to the platform, which will result in lower reading of silo weight.

This deviation from the real load can not be expected to be constant that the error varies with the total amount of solids in the silo and prevents a reliable correction of the measurement. Therefore, as it was decided during detailed design studies, the feeders were integrated to the silos via flange connections, thus the weights of motor, gearbox and the screw feeder are transferred to the load cells. The

installation works for the solids handling system were completed in accordance with this design approach, and the picture of the feeders are given in Figure 3.8.

In addition to these three (3) silos designed for handling fuel and limestone, a smaller silo was manufactured for bed material. As the bed material consumption was not required to be logged, it was not required to have a load cell system for this silo to measure its weight continuously. Instead, bed material flow is determined by weighing the solids before loading into the silo.

After the installation works were completed, the feeder rotation speeds were tested for variable solid flow rate for fuel and limestone silos, and the silo weights were followed from the DCS computer. All motors including bed material feeder that only has start/stop control, were also tested for remote control from DCS.

The outlet of these four (4) screw feeders integrated to the silos were directly connected to the bunker of main feeder by flexible pipes. As described previously, main feeder, which extracts the solid mixture in its bunker and feeds into the combustor, is air lock type, and it prevents leakage of combustion gases through

Figure 3.8 Screw Feeders of Fuel and Limestone Silos

the solid feeding leg. Even there is a trace amount of clearance within the main feeder for leakage, the screw feeders under the silos were designed to operate fully charged by particles, which seals the solids feeding system. Although there are two solid feeding points with different elevations at the first module of combustor for experimental testing purposes, there is only one main feeder for solids feeding. As the main feeder was fixed in position to the steel structure, two different connection parts were designed and manufactured. Each one of these parts is suitable for connecting one of the feeding points to main feeder. This design gives the flexibility for switching between solid feeding heights.

3.2.2.4 Water Flowmeters

Cooling requirement for the combustor is met by the cooling water channels vertically placed on the external surface of modules 2 and 3. In order to determine the water flow rate through each moule, water flowmeters were installed upstream the inlet collector of each module. Based on the analog signals generated by these flowmeters and by Pt100 transmitters at hot water outlet collector of each module, heat transfer analysis for cooling was carried out. Water flow rate to the modules were manually controlled by ball valves at the drainage pipe of each module, based on the temperature readings within the combustor and within hot water collectors displayed on computer screen.

3.2.3 Control System

The signal cables coming from each instrument of the test unit were collected in local junction boxes, each grouping six (6) signals. The group of signals from each local box were carried by a single cable having six channels, to the central junction box installed at 5.0 m elevation nearby the test unit. From the central box, the signals were carried to the control room via identical multi-channel cables and each channel was terminated at the DCS panel. Each signal cable coming from a local junction box was labeled with a unique cable number at the instrument connection, and this label was kept unchanged at local boxes, central junction box, and upto the termination modules at DCS panel. By this approach,

input of the instruments at the DCS panel were easily tracked by following the cable number of any device. During the progress of cabling works for control signals, DCS cabinet of DeltaV control system and its desktop PC donated by Emerson Process Management Ltd. were also installed in the control room.

DCS hardware including controller, analog input, analog output, digital input and digital output cards were installed on the card carrier by following the instructions supplied with the hardware. Following that, the PC, by which control programming and system operation is executed, was installed, and the communication functions between PC and DCS were tested. After the diagnostic tests of control cards were completed, the input location of each signal coming from the test unit was verified by cross check of cable number and performing loop-check tests. Following verification, signals were entered to the control software installed in the computer to define their tag names, signal types and physical ranges. The picture of controller and I/O cards installed on DCS panel is given in Figure 3.9.

The next step for control system set up was to program the DeltaV controller to perform the following functions for process control, data acquisition and logging:

Figure 3.9 DeltaV Controller and I/O Cards

- It is provided that all the instrument signals due to I/O lists based on process and instrumentation diagrams of test unit, and the data to be calculated by the control system are logged within control computer.

- A representative diagram of the test unit and other pages were prepared for displaying on-line data coming from the instruments and calculated parameters, and also for input data entry, start/stop functions and set point definition of motors, control valves, solenoid valves etc. The list of display screens are as follows:

    - Main page representing the general view of the test unit (Figure 3.10), displaying online data necessary for operator.
    - Solids handling and feeding system page, displaying the weight of silos and allowing start/stop commands and frequency entry for screw feeders and main feeder.
    - Analysis entry page for entering ultimate analysis of fuel(s) and limestone handled in each of three (3) silos.

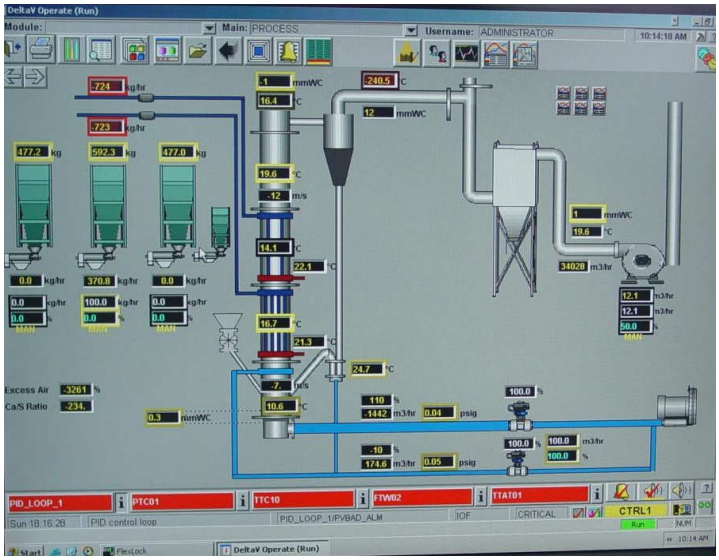

Figure 3.10 Main Display Page of Control Computer

- Graphical displays for process history view, and instantaneous data of main parameters were prepared for the following data allowing the operator to follow the trends even months old:

    - Temperature history for each transmitter at dense zone (first module of combustor)
    - Temperature history for each transmitter at lean zone (rest of the modules of combustor)
    - Differential pressure history for each transmitter at dense zone (first module of combustor)
    - Differential pressure history for each transmitter at lean zone (rest of the modules of combustor)
    - Weight history for each silo
    - Solid flow rate history for each silo

  In addition to these graphical displays prepared for following a group of data from instruments/equipment simultaneously, historical view for any other data that is logged by the PC can be displayed on the screen.

- For output signals, modules for set point and status entry were located on the screens. The set point entries that can be made via the control computer are as follows:

    - Solids feeding and discharge system: Start/stop commands and frequency set points for screw feeders and main feeder.
    - Combustion air and flue gas systems: Start/stop commands and frequency set point for blower, and set point for percent opening of air and flue gas flow control valves.
    - Purge system: Start/stop commands for energizing each group of solenoid valves connected to differential pressure transmitters.

- Control system was programmed to calculate some parameters, display them on the screen, and log to the control computer to help operation by employing measurements and input data entered by the operator. These calculated parameters and how they are obtained are as follows:

    - Primary and secondary air and flue gas flow rates: Differential pressure through the flow elements and static line pressure and temperature of these streams, are employed in the equations of the flow elements to reach volumetric flow rate in terms of m^3/h unit.
    - Average temperatures of dense and lean zone: Temperature data from transmitters within both zones are separately sent to averaging modules to obtain a average temperature for each zone.
    - Superficial velocity: Based on primary and secondary air flow rates and average temperatures for each zone, superficial velocity within the zones are calculated to help the operator keep the velocity within design conditions for a circulating fluidized bed combustor.
    - Solids flow rates: The decrease in the weight of each silo in a specified time is converted to flow rate of each solid stream extracted by its screw feeder. As the sensitivity of silo weighing is not appropriate for short term differentials, this calculation is done by long term averaging of silo weight signals going up to 1 min.
    - Excess air: Based on coal flow rate, theoretical air demand for the combustor is calculated. Then, dividing actual total air flow rate by the air demand, actual excess air entering the system is determined.
    - Ca/S ratio: For each fuel, the flow rate and combustible sulphur content is multiplied and total sulphur is converted to molar basis. Then, amount of calcium entering the system is calculated from its flow rate and analysis, followed by conversion to molar basis. Division of calcium by sulphur amount in molar basis gives instantaneous Ca/S ratio of the solid feed. This parameter helps the operator to get an idea about actual sulphur capture efficiency.

- For a stable operation, automatic control loops were programmed for some of the main output parameters as given below:

    - ID Fan damper control: One PID loop was programmed to control existing ID fan damper to be automatically commanded by the DCS to keep the pressure in balance at a defined location like furnace exit or cyclone exit.
    - Solids flow rates: Three PID loops were programmed to control the frequencies of screw feeders for each solid stream to be automatically commanded by the DCS to keep the flow rate at the set point entered by the operator to the control module on the screen.
    - Secondary air ratio: One PID loop was programmed to control the opening of secondary air flow control valve to be automatically commanded by the DCS to keep the ratio of secondary air to total air flow rate, when the frequency of blower or primary air valve position is changed.

In addition to the functions summarized above, minor improvements were done on the control system based on the operational experiences gathered during refractory drying and coal combustion test runs.

3.2.4 Summary of Installation and Commissioning Works

Installation of 150 kWt Circulating Fluidized Bed Combustor Test Unit was completed with small deviations from detailed design. Then, the auxiliary equipment and instruments were tested for operation.

The pictures of the facility after installation are given in Figures 3.11 to 3.15. Figure 3.11 is the picture taken from ground floor. The next picture given as Figure 3.12, is taken from 5.5 m elevation (1st floor) of Unit Operations Laboratory. This elevation is the level where the silos were installed. The picture

of CFBC together with existing BFBC Test Units can be seen in Figure 3.13, which was taken from 9.5 m elevation (2nd floor). Another picture taken from the same level but from a different angle is in Figure 3.14. The final picture of the test unit is also given from 9.5m level, from an opposite angle of the previous one.

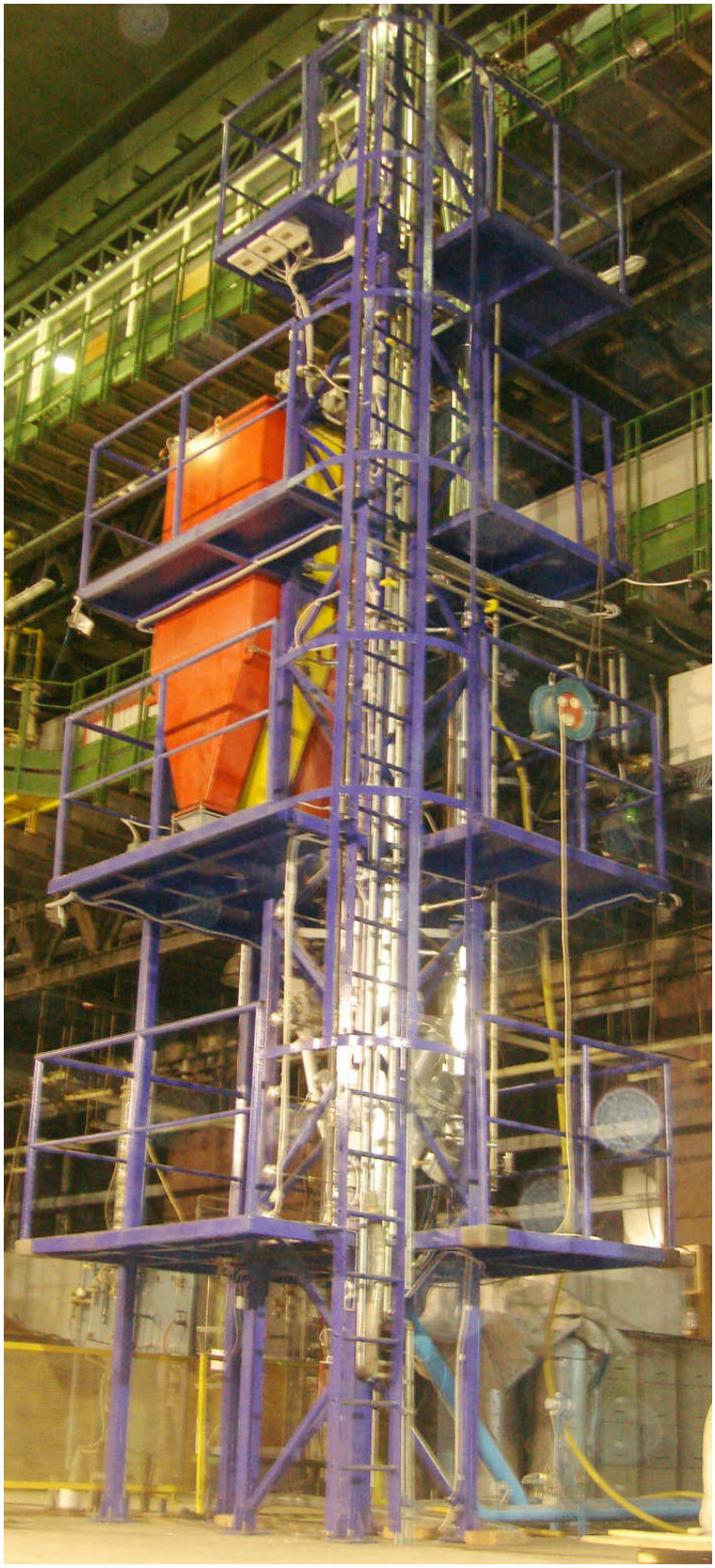

Figure 3.11 Test Unit - Elevation: 0 m

Figure 3.12 Test Unit - Elevation: 5.5 m

Figure 3.13 CFBC and BFBC Test Units

Figure 3.14 Test Unit – Elevation 9.5 m (1)

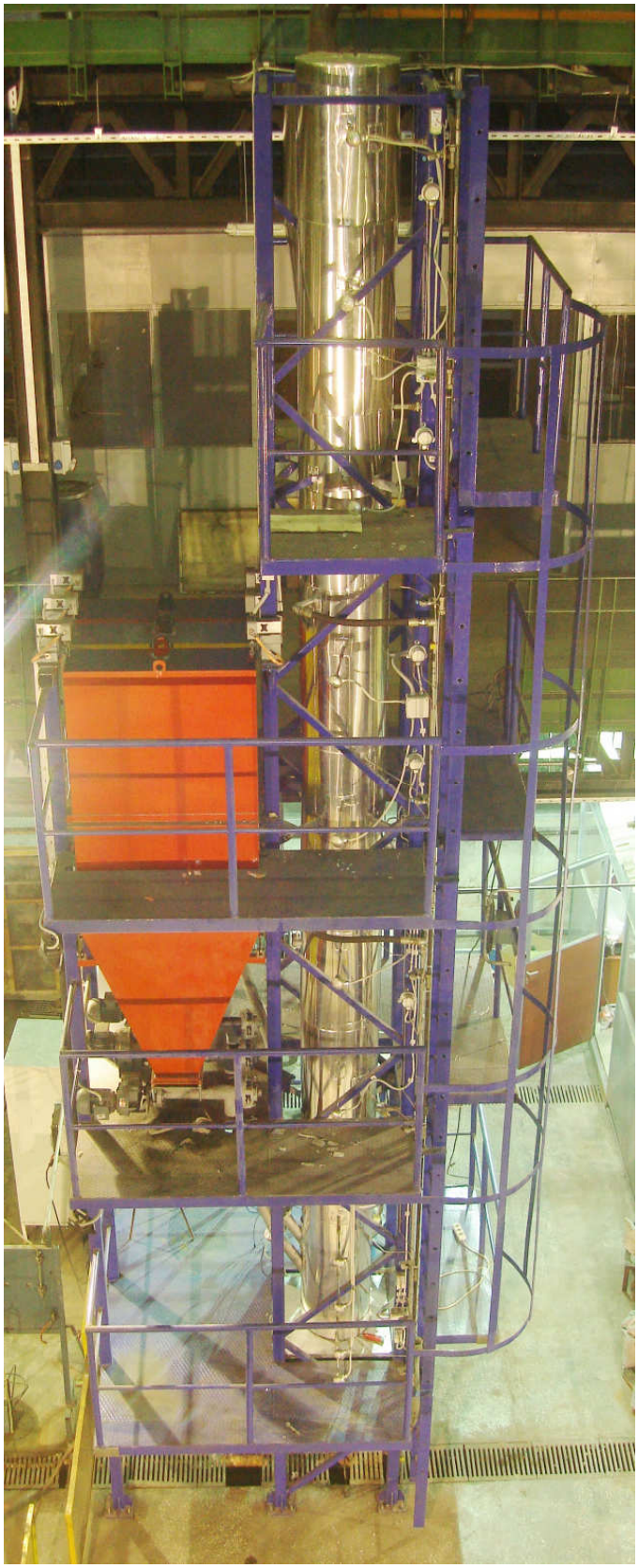

Figure 3.15 Test Unit – Elevation 9.5 m (2)

CHAPTER 4

OPERATION

The operation of the Test Unit is executed in two steps. The first step is refractory drying done by firing LPG at the start-up burner for 39 hours, and second step is the commissioning and combustion tests firing Çan lignite for design assesment of Test Unit and for investigating combustion characteristics of this lignite.

4.1 Refractory Dryıng

4.1.1 Procedure

As given in detailed design section, inner surface of the combustor is lined with castable refractory with a thickness of 4.75 cm, from dense zone module up to the exit module. The refractory material with high coldcrushing strength and resistance to erosion effects caused by high temperature and high particle concentration, is supplied from KIL&TAS company. The brand name of refractory is HyCast NG which is characterized by high alumina and moderate silica content.

After the refractory powder is mixed with 10% water by weight, casting process is applied to each module separately. Each module is installed in its place after the template is dismantled and setting time of at least 24 hours have passed. Setting time is defined as the time required for the refractory to become physically stable.

After casting, the refractory contains very fine pores filled with water. Therefore, it needs to be carefully dried to remove the contained moisture to avoid cracking and explosive spalling when exposed to a rapidly elevated temperature during

operation. Initial heating of the refractory causes the contained moisture to evaporate in the pores and produces pore steam pressure. When the temperature of the refractory is raised too fast, the contained moisture does not have enough time to dissipate to the outer surface. This can result in excessive pore steam pressure buildup causing cracking and explosive spalling. To avoid these problems and to have a good quality refractory, a carefully planned drying procedure suggested by refractory manufacturer must be followed. A typical drying schedule for castable refractories is illustrated in Figure 4.1.

Refractory drying procedure supplied by refractory manufacturer suggests three holding periods. First one is around 150°C which is slightly higher than the boiling point of water. The second one is around 300°C, which is the expansion temperature that is critical for alumina rich refractories. The third one is around 800°C.

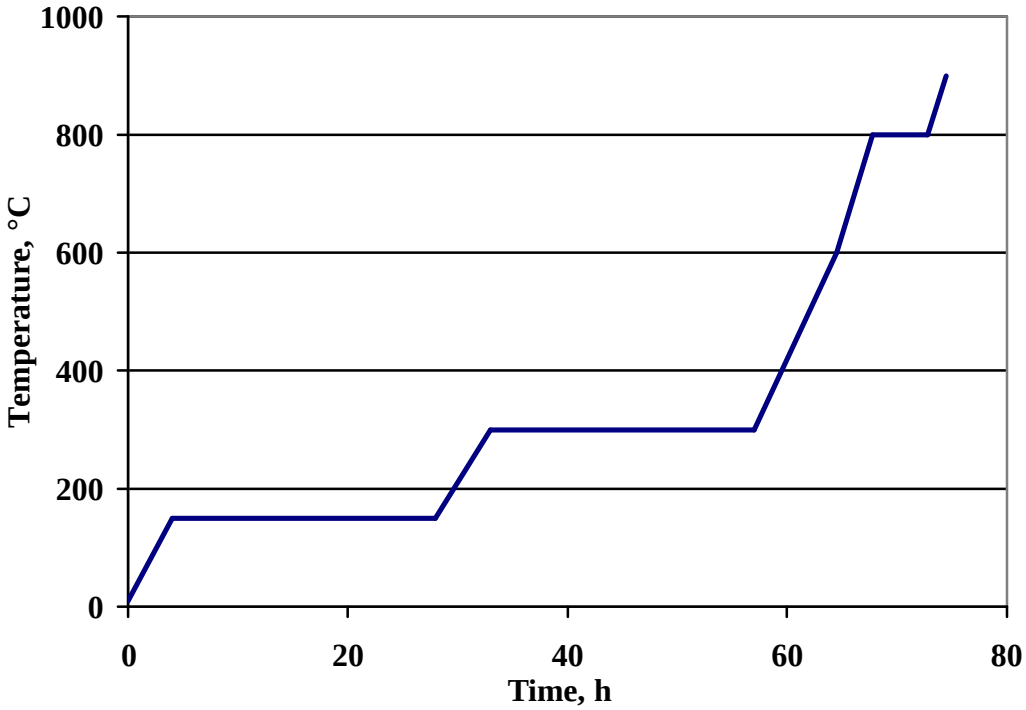

Figure 4.1 Typical Drying Schedule for Castable Refractories

According to refractory supplier, the durations for constant temperature drying change depending on the amount of refractory, heat dissipation and steam release rates from the surface. Based on these criteria, a detailed refractory drying procedure given in Table 4.1 was prepared for 150kWt CFBC Test Unit, where the holding times at critical temperatures are revised.

The fuel for drying operation was chosen as LPG, as it is not prefered to fire the combustor with coal because of two main reasons: (i) coal can not be fired stably at temperatures lower than 600°C; (ii) even at higher temperatures, it is not recommended to use coal because of its physical interactions with the porous surface of refractory. However, it could not have been estimated whether the combustor can reach 850°C from the bottom to the module at the top while firing LPG at the start-up burner located in the windbox. In addition to this, another unknown was that at what extent the uniformity of temperature could be achieved along the combustor throughout the phases of drying run. Both questions found their answers during the drying operation that lasted 39 hours long, covering all the phases of the schedule.

Table 4.1 Ideal Time Schedule for Drying Operation

Phase	**Temperature (°C)**	**Heating rate (°C / min)**	**Duration (hours)**
Heating No.1	20 – 150	0.6	3.5
Constant T - 1	150	-	12
Heating No.2	150 – 300	0.5	5
Constant T – 2	300	-	12
Heating No.3	300 – 600	0.7	7
Heating No.4	600 – 800	1	3.5
Constant T – 3	800	-	5
Heating No.5	800 – 900	1	1.5
Cooling	900 – 150	–1	12.5

4.1.2 Drying Operation

The stages of drying operation are summarized in this section. In order to display the progress of temperature values along the combustor throughout the operation, average temperatures of dense zone (module-1) and dilute zone modules (modules-2 to 5) are illustrated in Figure 4.2. Although the drying operation was intended to be executed according to the schedule, the operating conditions, especially the significant variation of temperature along the height made some modifications inevitable during operation.

Initially, ID fan and FD blower were started up to sweep away the unburnt gas in case complete combustion can not be achieved at the burner. However, both ID fan damper and primary air control valves were adjusted for low flow rate to prevent burner flame from blowing off. Then the pilot light was ignited by supplying LPG and compressed air at low flow rates. Following the pilot light, gas and air valves for main flame were gradually opened to achieve minimum heat input with stable combustion.

Heating Phase No.1 (30 – 150°C)

Ignition of pilot light and main flame both resulted in a sudden increase in the temperature with a higher slope than the rate defined for the first heating phase. In order to compensate this, air flow rate was increased to cool down the combustion gas generated at the burner. As a result of this, the proposed rate, 35°C/h, was achieved as an overall average throughout the phase. From start-up of the system, first heating stage was completed by reaching 150°C at dense zone module in 210 minutes. However, average temperature of the dilute zone modules was 132°C and it was intended to be increased to the target value during the next phase.

Constant Temperature Phase - 1 (150°C)

This phase of drying was especially for vaporizing the water within the refractory. Holding time for this phase was determined by the progress of steam release. The system was kept at constant temperature for 4 hours. Then the burner load was

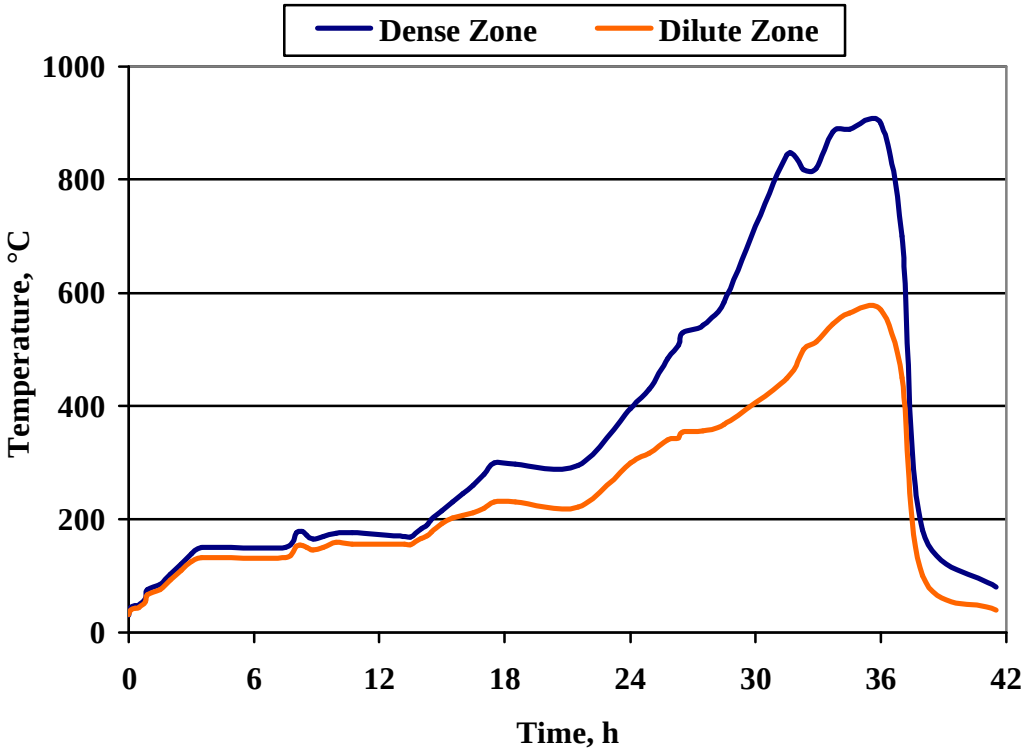

Figure 4.2 Average Temperature Profiles during Drying Process

increased to reach the average temperature of 150°C along the dilute zone modules. In response to the temperature increase at the bottom of the combustor, air flow rate was increased to have better heat dissipation from bottom to top. This action helped preserving the slight variation of temperature along the riser. After 10 hours of total duration, next phase was started.

Heating Phase No.2 (150 – 300°C)

After the completion of Constant Temperature Phase-1, the system was heated with a rate of 30°C/h to reach 300°C at the dense zone module in 4 hours. However, the gap between the average temperatures increased to 70°C. Although the air flow rate was increased, average temperature of the dilute zone modules only reached to 230°C by the end of heating. Similar to the previous heating phase, it was intended to reach the target value for dilute zone during the next constant temperature phase.

Constant Temperature Phase - 2 (300°C)

This phase of drying is for controlled expansion of the refractory and also for vaporizing the remaining water. From the end of previous stage, the system was kept at constant temperature for 4 hours, and then the temperature was increased for 150 minutes to reach an average of 300°C at the dilute zone modules. Although the average temperature reached 300°C, the measurement at the exit module was 267.4°C. Therefore, it was continued to heat up the system for another 150 minutes to have the exit module reach target temperature for this phase. However, the gap between bottom and top of the combustor increased significantly after this heating operation. Total duration for this phase was 10 hours.

Heating Phases No.3 and No.4 (300 – 600°C and 600 – 800°C)

As the dense zone module reached 542°C while bringing exit module to 300°C during the previous phase, consequent heating phases were merged. After the previous phase was completed, the system was heated with an average rate of 60°C/h for reaching 800°C at the dense zone by the end of 4 hours. Although the temperatures at the dense zone module were increased within the limits of recommended heating rate, upper modules could not reach the temperatures required by the procedure. As a result of this, following heating and constant temperature phases were also merged.

Constant Temperature Phase No.3 (800°C) and Heating Phase No.5 (800-900°C)

As the increase in the average temperature of dilute zone was experienced to be half of the rate of dense zone module, it was required to close the gap between the temperatures along the combustor. For this purpose, burner load and air flow rate were increased to their maximum levels which helped better heat dissipation provided by high velocity within combustor. Temperature within first three modules reached values over 600°C. However, the target temperature could not be attained by dilute zone average, as it was reduced by the lower values at the last three meters of combustor.

As the temperature of the upper modules could not reach 850°C, it was decided to end the drying operation and cool down the combustor. The cooling process was executed by reducing the burner load initially, then by shutting down the burner, blower and ID fan for free cooling. Although it was intended to carry out the cooling phase at the proposed rate, a higher cooling rate reaching up to more than 3°C/min was experienced.

For the uppermost two modules, the drying process had to be finalized during commissioning tests with coal firing, as the operating temperature of FBCs could not be attained even at maximum capacity of start-up burner. By firing coal, it was aimed to take advantage of dispersion of heat generation through the riser, as the combustion of coal particles takes place along the height rather than gas combustion at the bottom of riser. In addition to combusting coal particles, circulating solids originating from inert material and coal ash, help enhanced heat transfer throughout the combustor, also at the uppermost modules.

4.2 Coal Fired Combustion Tests

4.2.1 Commissioning Tests

As the refractory drying process did not go to completion by firing LPG at the start-up burner, coal fired commissioning tests were planned to include finalization of drying procedure for modules 4 and 5. For this purpose, two separate commisioning test runs were carried out by firing Çan lignite that had recently been fired in METU 0.3 MWt Bubbling AFBC Test Rig as a part of an extensive research study on cofiring biomass with this lignite [41].

During the commissioning runs, not only the drying process was completed, but also the performance of combustor, auxiliary equipment, instrumentation and control system were tested for combustion test operations.

4.2.1.1 Procedure

As the phases of refractory drying procedure up to 600°C was finished at all the modules of combustor, initial heating of the unit before feeding the coal was not required to be at slow rates. Therefore, the procedure for these complementary coal fired drying operations was prepared accordingly. The main phases of operation are given in Table 4.2. As can be seen from the table, it was planned to start-up the system by firing gas at the burner, followed by feeding bed material to be heated up prior to coal feed to combustor. After reaching 600°C while the bed material was fluidizing, coal feeding was started while the combustion was still supported by firing LPG until the temperature reached 800°C. The final step was constant temperature operation at 850°C for finalizing refractory drying and also for observing coal fired operation performance of the system with respect to design outputs. After this phase was finalized, the system was shut down.

4.2.1.2 Operation

The profiles of average temperatures within dense and dilute zones, and solids temperature at loop seal during commissioning run-1 are given in Figure 4.3 from which the phases of operation can be followed from start-up to shut down.

The system was started up by igniting the gas burner and the temperatures started to increase along the height of the combustor. After the temperature within dense zone module exceeded 300°C, bed material was started to be fed into the combustor.

Table 4.2 Phases of Coal Fired Complementary Operation for Drying

Phase	**Temperature**	**Fuel**
Heating	30 – 300 °C	Nat. Gas / LPG
Bed Material Feeding	300 – 600 °C	Nat. Gas / LPG
Coal Feeding	600 – 850 °C	LPG + Coal
Drying and Operation	850 °C	Coal

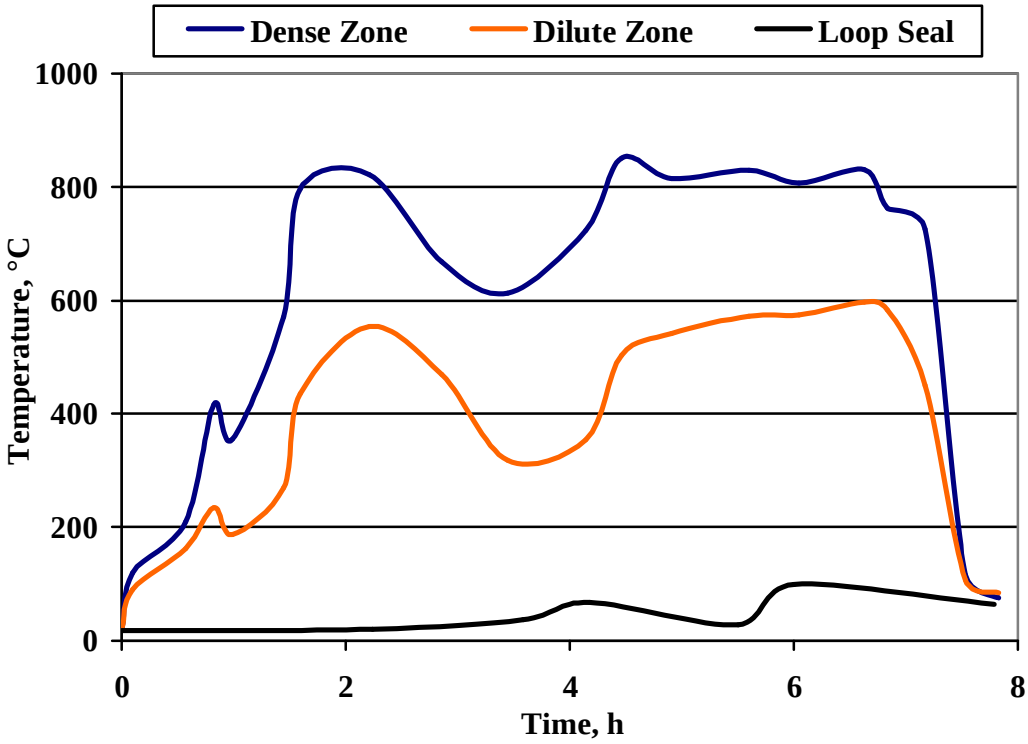

Figure 4.3 Average Temperature Profiles for Commissioning Run-1

Resulting in the first peak at dense and dilute zone profiles, cold bed material absorbed the heat accumulated within the system and reduced the temperature. In order to balance this decrease and to cover additional heat capacity arised from bed material, heat input supplied via the burner was increased. Reaching 600°C at the dense zone module, small amount of coal was fed to the system to observe whether the conditions within dense zone was appropriate for coal combustion or not. As the temperatures increased rapidly to 750°C at the dense zone and the flue gas oxygen concentration decreased simultaneously, it was realized that the conditions within the system was appropriate for continuous coal feeding. After the coal feeding was started, the temperature increased to 850°C within the dense zone. However, as the circulation was started by feeding fluidization air to loop seal, cold particles in the loop seal destroyed the conditions within the dense zone. This resulted in sharp decrease of temperature along the riser forming the second peak after two hours from start-up as shown in Figure 4.3.

The reason for the circulated particles not being at high temperature is as follows: Fine particles filled in the downcomer leg and loop seal before start-up were initially not recycled until the system was heated up. Then, the circulation of these cold particles was started at a low rate, such that the particles collected by the cyclone spent too much time to cool down within the downcomer leg which was not insulated during these trial operations.

As a result of cold inert material flow into the dense bed, interruptions of coal combustion was experienced and start-up burner was taken into operation for number of times. At the same time, by increasing coal flow rate, it took more than two hours for the whole system to recover from this temperature drop, of which the minimum value can be seen from the figure at a point before the fourth hour of operation. After 800°C was reached at the dense zone again, heat input support by start-up burner was ended, then the combustor was operated by firing coal only. By the end of almost 7 hours of total operation time, it was realized that the loop seal and dilute zone temperatures would not increase to required values at this heating rate within a short period of time. Due to this reason and requirements of some minor revisions on the test unit, the system was shut down to finalize drying procedure at the next run.

Based on the experiences gathered from the first coal fired run, another commissioning run was carried out by revising the procedure to start solid circulation at a higher rate than the first run once dense zone temperature reaches 600°C. Except this revision, the same procedure was followed for this run too.

Average temperature profile of dense and dilute zones and loop seal during commissioning run-2 are given in Figure 4.4. As can be seen from the figure, temperature dropped after bed material feeding, forming the first peak. Then the second peak was observed after circulation was started. Then, the temperatures at loop seal and dilute zone rapidly increased and got closer to dense zone values compared to previous drying and coal fired runs.

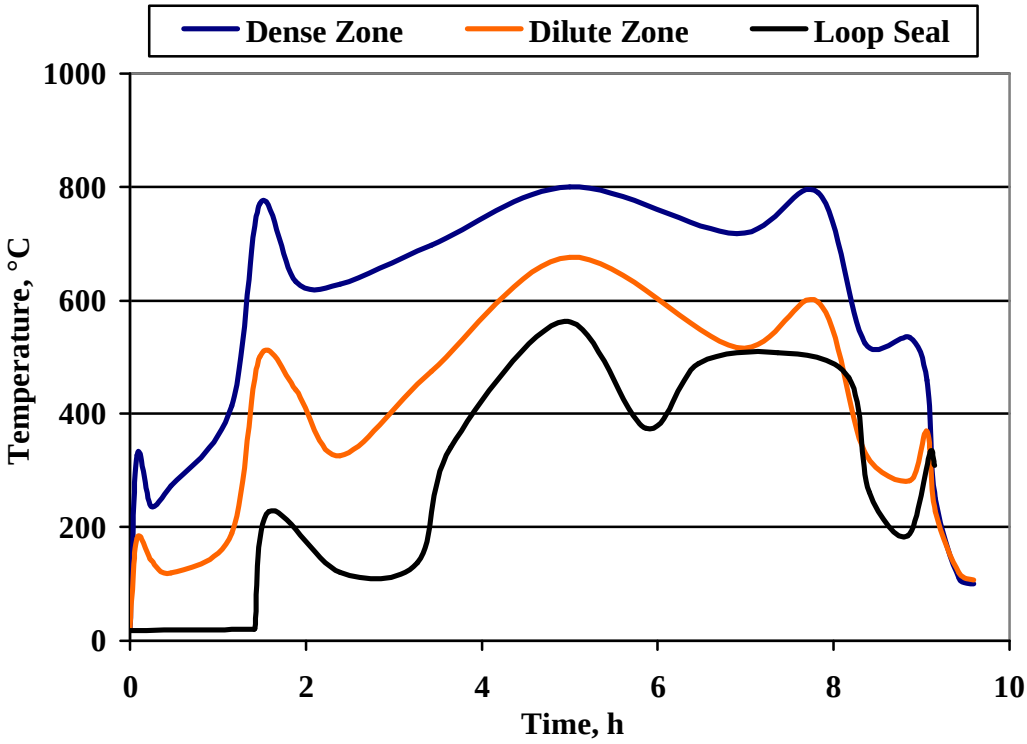

Figure 4.4 Average Temperature Profiles for Commissioning Run-2

The next temperature drop at loop seal profile was caused by the decrease of circulation rate which was readily lowered to observe its effect when the particle temperature at the loop-seal was increased. As can be seen from the figure, decreasing the solid circulation rate resulted in a similar trend in solids temperature in the loop seal due to increase of residence time of particles to cool down. Then, the rate was increased again by increasing the loop seal air flow rate.

Finally, coal flow rate was increased to reach higher temperatures, forming a new peak value at almost eighth hour of the test. However, a blockage within solids feeding system occured, suddenly decreasing the temperatures. After this disturbance, combustor was shut down. One of the main differences of this run from the previous one was that the higher temperature of loop seal was attained by earlier start of circulation at higher rates, which was done by increased fluidization air flow rate within the loop-seal.

The other achievement of this run was the higher dilute zone temperatures, where every measurement point within the dilute zone including the riser exit exceeded 680°C. This improvement can be explained with the circulation of hot particles through loop seal that reached 600°C, which did not cool down the dense bed, and resulted in more heat generation by increased combustion of circulating fine particles at hotter upper modules. In order to investigate this effect, maximum temperature profiles along the combustor during drying and commissioning runs are given in Figure 4.5. As can be seen from the figure, the profile for maximum temperatures at each measurement point attained during commissioning run-2 had the smallest slope compared to the previous runs, as a result of solid circulation rate at high temperature. In light of this investigation, it was determined that the temperatures at the dilute zone are higher for both coal fired commissioning runs compared to drying process.

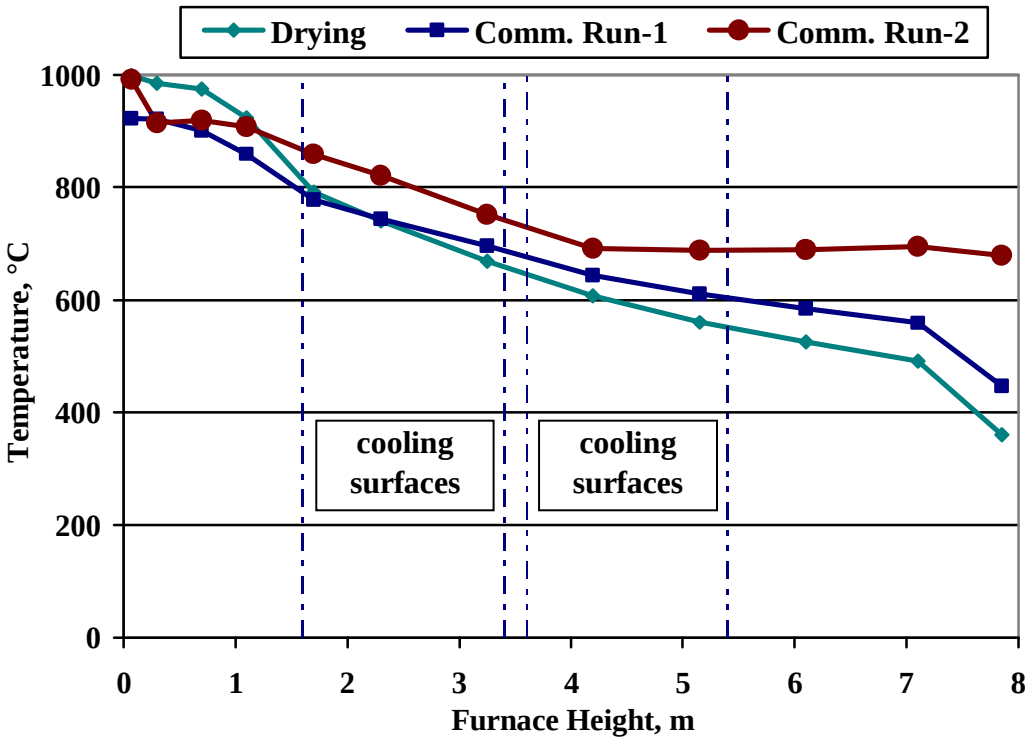

Figure 4.5 Maximum Temperature Profiles - Drying and Commissioning Runs

It can be seen that from first coal fired run to second one, maximum temperature profile was improved to be closer to a uniform trend as in ideal CFB combustors. On the other hand, these temperature profiles of coal fired runs are not acceptable for a combustion test in a CFB. The reason is that the temperature drop going up the riser was mostly caused by the lack of insulation. Insulation was not completed at this stage, as the drying process at upper modules were not finalized. Since there were many small holes drilled to the external surface of combustor for helping the refractory loose its water, it was required to keep the combustor uncovered from outside. As a result of the significant heat loss from external surface, typical operation temperature (850°C) for a CFBC could not be reached at the top modules, but considerably higher values could be attained by coal firing compared to gas fired run and coal fired run with limited solids circulation.

Examining the operating data of these three runs, it is concluded that refractory drying was completed, drying holes can be sealed and insulation application can be done. Furthermore, the system proved its performance for a complete coal fired combustion test with minor revision requirements.

Before the coal fired combustion test, all of the drying holes were welded and the system was inspected for any leakage prior to wrapping the ceramic fiber insulation blanket around the combustor. After insulation works were finished, the system was prepared for the operation. Regarding the revision requirements, the following works were carried out:

- A venturi was manufactured and installed in the solids feeding leg as shown in Figure 4.6. The leg was drilled to insert a stainless steel tube for feeding air to the venturi. The venturi was manufactured by welding two reduction elements to eachother from the narrow sides. One reduction had the dimensions of Ø76mm x Ø48mm with a length of 90 mm. The dimensions of the short reduction was Ø60mm x Ø48mm with a length of 75 mm. Total length of the venturi is 165 mm.

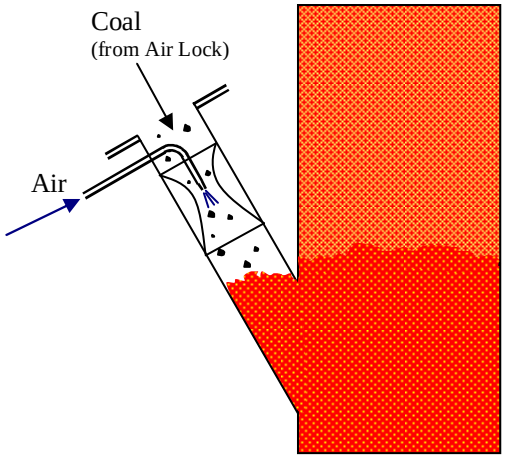

Figure 4.6 Schematic Diagram for Vacuum System in Solids Feeding Leg

This system was designed to generate vacuum at the outlet of main feeder to prevent combustion gases from reaching the feeding system, which was experienced during commissioning runs. For this sealing purpose, air was supplied from secondary air line through a flexible tubing.

- In order to see the dense bed during test runs, an observation window was installed on the top of upper loop-seal connection leg. Cooling air for the glass was also supplied from the secondary air line.

- As the support air for solids feeding and cooling air for observation window are supplied from the same point connected to secondary air line, diameter of flexible tubings for loop-seal fluidization air were increased to lower the resistance of the lines feeding the windbox of loop seal.

4.2.2 Combustion Tests

After the commissioning tests were completed satisfactorily, the next and the main step of operation phase was the combustion tests firing a typical Turkish

lignite for design assessment of the Test Unit and for investigation of the combustion characteristics of this lignite at CFBC conditions.

The design fuel for the test unit was selected to be Çayırhan lignite, as its analysis can be accepted as an average for the main lignite reserves within Turkey. However, another lignite reserve from Çan town of Çanakkale province in northwestern Turkey, which is also within the design range of the unit was prefered for these coal fired combustion tests. There were two main motivations underlying this decision:

- The lignite under consideration in this study was recently fired in bubbling mode in METU 0.3 MWt AFBC Test Rig as a part of an extensive research study including biomass cofiring tests [41]. As an outcome of this study, comprehensive sets of data and results about this lignite and its combustion characteristics within BFBC conditions were generated. Therefore, it is considered advantageous to fire Çan lignite in the METU 150 kWt CFBC Test Unit based on these extensive experiences. In addition, it is considerably valuable to have combustion test results for the same coal, at bubbling and circulating FBCs for comparison studies.

- Çan lignite is already being fired at 2 x 160 MWe Çan Power Plant that is located at the town of Çan, which is the first large scale utility power plant in Turkey that is based on CFBC technology. The boilers with a steam capacity of 490 t/h each are under operation since 2003 [13]. Therefore, data generated from combustion tests with this lignite may be of future use in the mentioned power plant.

After the lignite to be fired was determined, preperation works before the tests were started: Test procedure was formed, coal was analysed for ultimate and

approximate analysis, mass and heat balances were carried out resulting in the predictions for steady state operating conditions.

4.2.2.1 Procedure

The procedure for the coal combustion test is mainly the same as the one given in Table 4.2 for commissioning runs. The only difference is that there is no drying phase but only the steady state operation at 850°C. This procedure includes burner ignition, heating up of the combustor, feeding bed material followed by coal, reaching 850°C and examining the operating data for the steady state.

4.2.2.2 Operation

In the scope of this study, two combustions tests were carried out. Average temperature profiles for dense and dilute zones and loop seal are given in Figure 4.7 and Figure 4.8 for combustion test-1 and combustion test-2, respectively.

The first stage of the test runs; heating up the combustor to 300°C, was carried out by firing LPG at the start-up burner, following a procedure similar to the one given before, but with a higher heating rate.

After the target temperature was reached, mixture of the bed material generated during the previous test runs with Çan lignite at bubbling test rig and during commissioning runs at CFBC were fed to the combustor. The amount of material in the dense bed was followed from the pressure drop through dense zone. As the bed material absorbs the heat within the system, energy input through the start-up burner was increased to continue with the same heating rate. During this stage, bed material, of which the fine particles started circulation via the cyclone and loop seal, was heated up and the average temperature along the riser was brought to 600°C to start feeding coal.

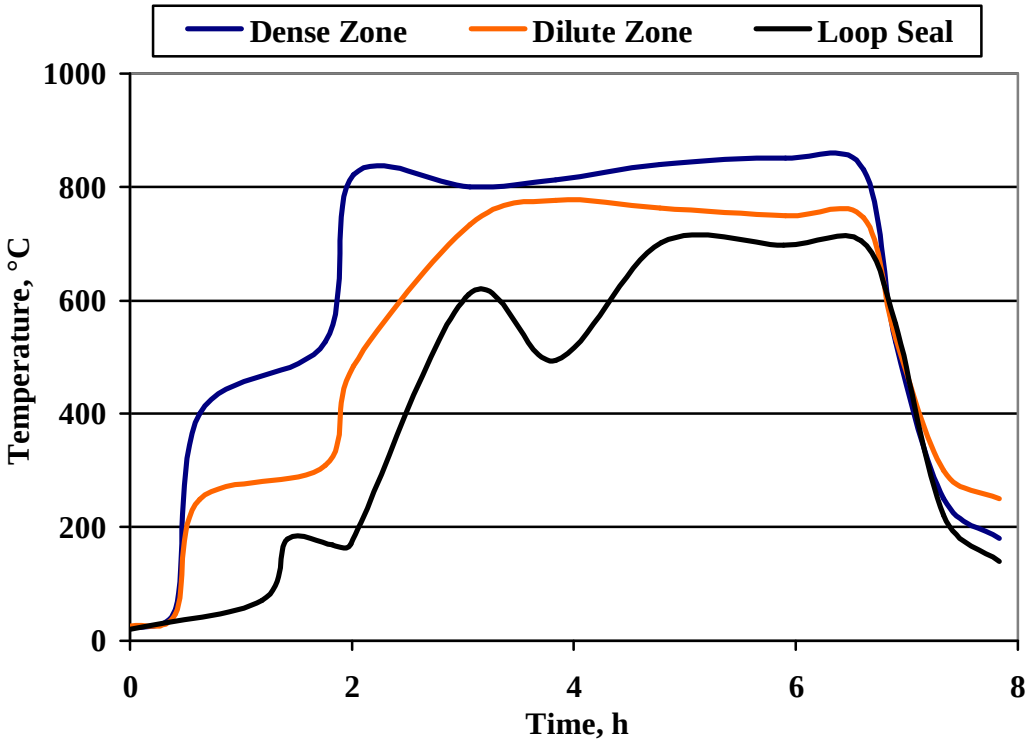

Figure 4.7 Average Temperature Profiles for Combustion Test-1

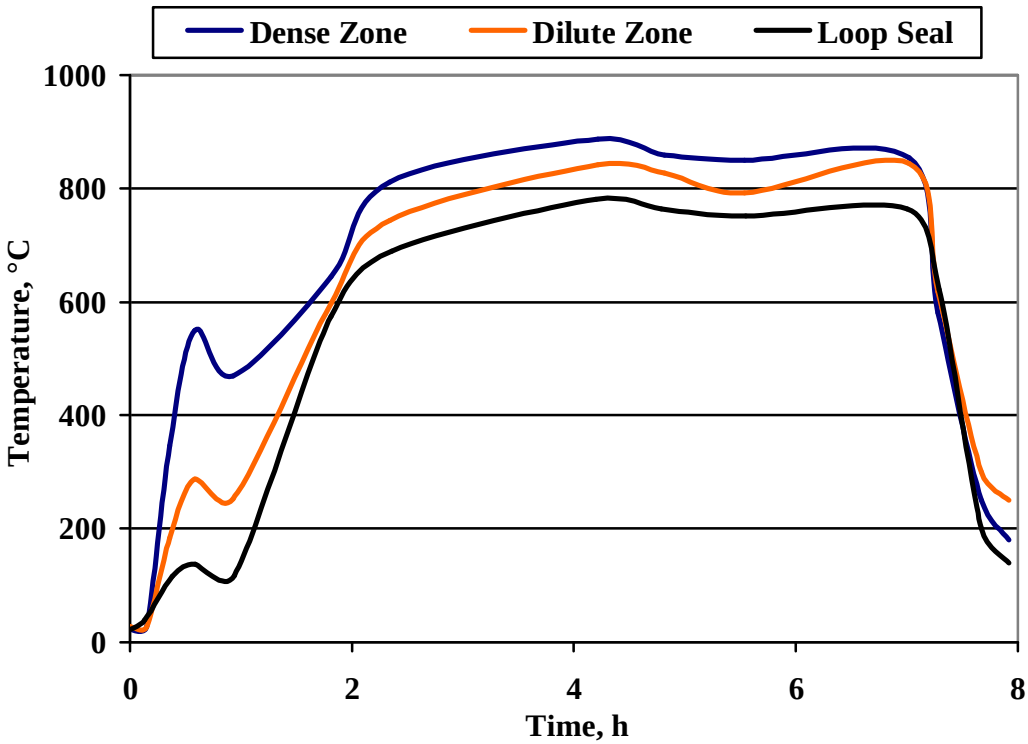

Figure 4.8 Average Temperature Profiles for Combustion Test-2

Coal was fed to the combustor with bed material as transient injections to keep coal particle concentration within the limits, to make sure combustion was complete, and to control temperature rise. At the same time, the heat input from the start-up burner was decreased and finally it was shut down for coal combustion to take over all the heat input requirement. As a result, temperature along the combustor was increased and kept at 850°C. The trends of online data logged by control system was checked to see whether steady state conditions were achieved.

During steady state, operational data was followed carefully not to have significant fluctuations at the conditions throughout the system. After the collection of data for a certain time and investigating the operation of combustor and its auxiliaries in terms of achieving their design functions, the system was shut down and cooled.

The physical condition within dense zone module was continuously followed from the observation window installed on the top of upper circulation leg. The pictures of red-hot fluidized bed taken from this window are given in Figure 4.9.

During both test runs, especially in run-2, all the temperatures rapidly converged to each other after feeding coal, as the particles provided dispersion of heat to whole system. Since a time lag for the increase in loop seal temperature was experienced during Test-1, amount of inert material initially fed to loop seal was increased in Test-2 . The source of this material was the particles extracted from the bottom of loop seal at previous runs. As a result of this increased amount fed to the loop seal, temperature of circulating particles in Test-2 had a more similar trend to riser temperatures. However, the main reason for having higher temperatures at dilute zone and loop seal, closer to dense zone values compared to commissioning runs was the presence of insulation during these combustion tests. By the help of insulation, heat loss to the surroundings were kept within design limits, forming almost uniform temperature profiles along the height of riser.

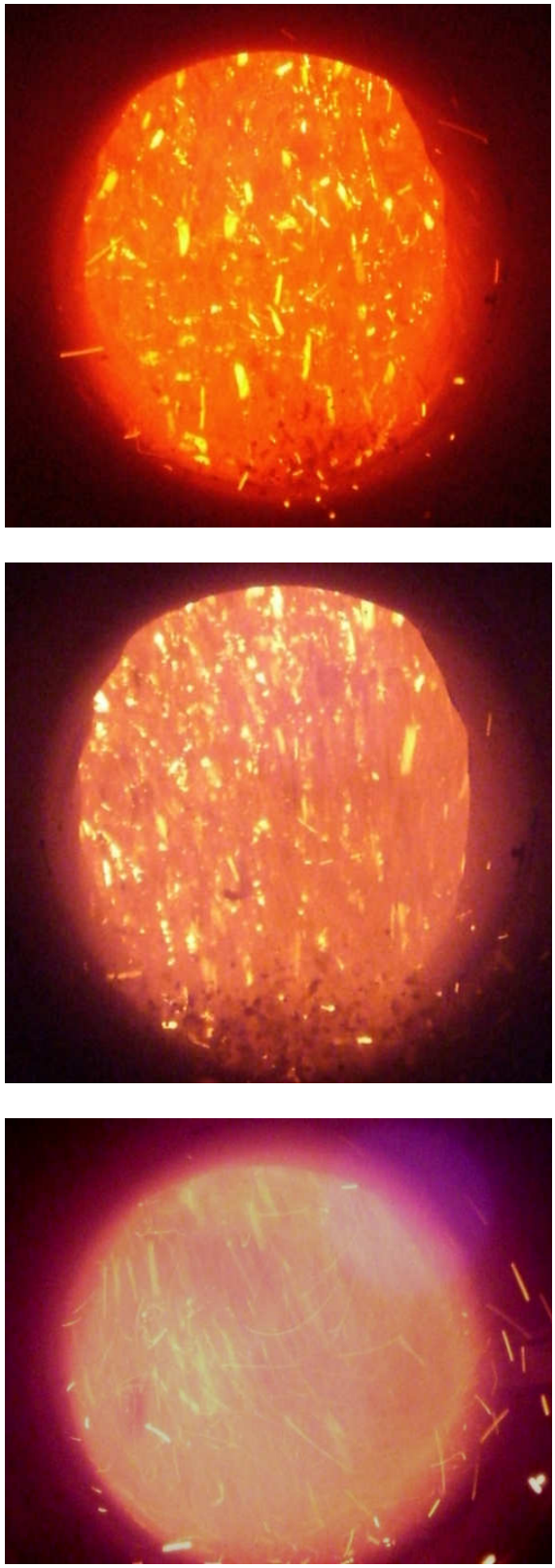

Figure 4.9 Dense Bed Pictures During Operation

In order to work on design assessment, steady state intervals of the logged data and solid stream analysis were isolated and processed for generating significant data sets to obtain steady state operating conditions.

4.2.2.3 Coal Properties

In order to collect operating data for design assessment and investigation of combustion in CFB conditions, a typical low quality Turkish lignite with high ash and sulphur content from Çan city of Çanakkale was burned during combustion tests. Characteristics of Çan lignite fired at each test, including sieve, proximate and ultimate analyses are summarized in Tables 4.3 and 4.4 for Test-1 and Test-2, respectively.

As can be seen from the tables, Çan lignite burned at the tests are characterized by high ash and sulfur contents. These are main indications for an indigenous coal reserve to be defined as a typical Turkish lignite.

Table 4.3 Coal Analysis for Combustion Test-1

Sieve Analysis		**Proximate Analysis (as fired)**		**Ultimate Analysis (dry)**	
D_p (mm)	**Weight (%)**		**Weight (%)**		**Weight (%)**
6.30-4.75	8.13	Moist.	15.03	C	44.23
4.75-3.35	35.93	Ash	24.69	H	3.58
3.35-2.00	20.00	VM	31.95	O	19.13
2.00-1.00	25.45	FC	28.33	N	1.10
1.00-0.60	8.47	LHV:3615kcal/kg d_{50}: 2.95mm ρ_{bulk}: 784 kg/m³		S_{comb}	2.91
0.60-0.43	1.50			S_{tot}	3.13
0.43-0.18	0.11			Ash	29.05
0.18-0.11	0.06				
0.11-0.00	0.35				

Table 4.4 Coal Analysis for Combustion Test-2

Sieve Analysis		**Proximate Analysis (as fired)**		**Ultimate Analysis (dry)**	
D_p (mm)	**Weight (%)**		**Weight (%)**		**Weight (%)**
6.30-4.75	5.88	Moist.	16.24	C	41.05
4.75-3.35	15.64	Ash	32.72	H	3.31
3.35-2.00	12.65	VM	29.20	O	12.18
2.00-1.00	22.27	FC	21.44	N	1.10
1.00-0.60	11.02			S_{comb}	3.30
0.60-0.43	6.68	LHV:3085kcal/kg		S_{tot}	4.59
0.43-0.18	10.72	d_{50}: 1.29mm		Ash	39.06
0.18-0.11	5.11	ρ_{bulk}: 932 kg/m³			
0.11-0.00	10.02				

The discrepancies between the analyses can not be explained only by the heterogeneous characteristic of coal resources, but also by the distinction between particle size distributions. For experimental purposes, the lignite was resized to have different particle size distributions by using different sieve combinations for each test. Although the lignite fired at both tests was from the same origin, there occured different coal analysis in each run. As the contents of each size range of coal may differ from eachother, the resizing process resulted in distinct coal analysis.

The reason for resizing raw lignite was the high d_{50} value of the fuel as received, reaching up to 3.60 mm. For the commissioning runs, enough amount of raw lignite stock which was delivered in 1 m³ capacity big bags was sieved to eliminate coarse particles larger than 5.6 mm. This screening operation resulted in a d_{50} of 1.06 mm that was lower than expected. However, as it was required to have increased heat generation by finer particles at the upper modules for completion of drying process, this lower average size was acceptable. In addition,

those runs were done for investigating the performance of the whole system, so that it was not required to have well defined coal PSD. However, average size of coal should be higher than that value for a real combustion test.

Based on the experience at commissioning runs, coal was sieved to get rid of coarse particles with a size higher than 6.3mm and fine particles smaller than 0.5 mm for the first combustion test. This resulted in a size distribution to be mainly within 1.00 – 4.75 mm range with a d_{50} of 2.95mm that is higher than typical value for commercial units. Then, for the next test run, only the coarse fraction with a size larger than 6.3 mm was eliminated and a d_{50} value of 1.29 mm was obtained.

4.2.2.4 Initial Bed Material

Commissioning and combustion test runs were performed by burning the lignite in its own ash. As mentioned before, bed material was initially supplied from the bottom ash generated while firing Çan lignite at the 0.3 MWt AFBC test rig.

Similar to coal, there exist large particles within this bottom ash compared to the requirements of the CFBC test unit. Therefore, the bottom ash was also sieved to obtain initial bed material with appropriate size distribution and average size. Based on the experience from commissioning runs, sizing of the bed material was changed for combustion tests. The sieve analysis of the initial bed material for commissioning runs and combustion test runs are given in Table 4.5.

Regarding the commissioning runs, d_{50} of the initial bed material prepared by sieving the bottom ash of bubbling test unit was 1.157 mm. After these runs, it is observed that it takes more than the duration of one test run for the required amount of circulating fine particles to accumulate in the loop seal. Although 5-6 kg of fly ash was filled into the loop seal at each run, the particle size of fly ash was small to stay within the system until the end of the operation without escaping from the cyclone.

Table 4.5 Particle Size Distribution of Bed Material

Sieve Analysis	**Weight (%)**	
D_p (mm)	**Commissiong Runs**	**Combustion Tests**
6.30 – 4.75	2.41	1.21
4.75 – 3.35	15.14	8.22
3.35 – 2.00	12.67	8.07
2.00 – 1.00	23.46	25.96
1.00 – 0.60	16.80	19.46
0.60 – 0.43	10.19	18.68
0.43 – 0.18	9.47	10.73
0.18 – 0.11	5.03	4.41
0.11 – 0.00	4.81	3.28
d_{50}, mm	1.16	0.87

Therefore, it was decided to increase the fraction of fine particles within the initial bed material to increase the amount of ash to be circulated through loop seal. In light of these discussions, bed material for combustion test runs was prepared to have particles with a d_{50} of 0.87 mm. By this resizing process performed before combustion tests, the portion of particles under 1 mm size was increased. The bottom ash generated during commissioning runs of CFBC was mixed with the sieved material that was generated in the bubbling unit. The sieve analysis of bed material given in Table 4.5 for the combustion tests belong to this mixture.

4.2.2.5 Operating Conditions

During the steady state operation of the unit, operating parameters including temperature and pressure drop along the combustor; coal, fresh air, flue gas and cooling water flow rates were logged continuously. Steady state operating conditions for both combustion tests are presented in Table 4.6.

Table 4.6 Operating Conditions of the Combustion Tests

Parameter	**Test-1**	**Test-2**
Thermal fuel input, kW	157.5	174.1
Coal flow rate, kg/h	37.45	48.55
Fly ash flow rate, kg/h	not available	7.04
Primary air flow rate, kmol/h	7.21	7.95
Secondary air flow rate, kmol/h	1.12	1.01
Total air flow rate, kmol/h	8.33	8.96
Excess air, %	20.9	16.5
Primary air : Secondary air, % in total	86.6 : 13.4	88.7 : 11.3
Superficial Velocity at dense zone, m/s	4.07	4.63
Superficial Velocity at dilute zone, m/s	4.33	5.07
Flue gas oxygen concentration, % (in wet basis)	5.27	3.25
Average dense zone temperature, °C	834.7	861.5
Average dilute zone temperature, °C	747.1	828.7
Average Loop seal temperature, °C	700.9	762.7
Cooling water flow rate at module-2, L/h	805.6	695.4
Cooling water flow rate at module-3, L/h	746.2	570.8
Cooling water inlet temperature, °C	13.8	16.7
Cooling water exit temperature at module-2, °C	53.5	64.8
Cooling water exit temperature at module-3, °C	47.2	64.9

Thermal Fuel Input

As can be seen from the table, each operating condition of Test-1 differ from those of Test-2. One of the determining parameters of this discrepancy is the thermal fuel input which was significantly increased in the second test to reach higher temperatures throughout the system; not only in the dense and dilute zones, but also in the loop seal.

Coal Flow Rate

It should be noted that almost 30% increase in the coal flow rate resulted in only 10% increase in thermal input because of the decrease in lower heating value, approximately by 17%, from Test-1 to Test-2 as given in Table 4.3 and Table 4.4.

Fly Ash Flow Rate

Regarding the fly ash flow rate at Test-1, the data is reported as not available, as the fly ash accumulation under the bag filter during steady state operation could not be determined exactly. The procedure was modified for the next test run, and the flow rate shown in the table was determined.

Combustion Air

As a requirement for the change in fuel input, combustion air flow rate was increased, but this increase was limited by the decrease in excess air ratio. The difference between the superficial velocities attained at the tests was not only because of this increase in total air flow rates, but also was a result of the difference between average temperatures within dense and dilute zones.

Primary : Secondary Air Ratio

Examining the ratio of primary and secondary air flow rates to total flow rate, it is obvious that the secondary air ratios at both runs are too small compared to the design value of test unit, 40%, which is a typical operating parameter for CFB boilers. Although the Test Unit was operated at 11.3% and 13.4% of secondary air ratio, this low ratios were inevitable for uninterrupted flow of air to loop seal to provide continuous particle circulation. In order to discuss the relationship between circulation and secondary air system, it is required to explain the interaction of these systems of the Test Unit. All the auxiliary air including loop seal air is supplied from the secondary air line as the air flow rate entering the combustor through this line is continuously measured. The impact of auxiliary air on secondary air flow rate is as follows:

Auxiliary air is fed to: (i) loop seal for fluidization; (ii) solids feeding leg for sealing; (iii) observation window for cooling, via small diameter (8 mm) lines. In addition to line resistance, most significant pressure drop within these consumers is at the loop seal that contains a solid bed with high pressure drop. However, as the secondary air piping up to the combustor has significantly lower pressure drop compared to auxiliary air, the efforts to increase secondary air flow rate prevented auxiliary air from flowing to loop-seal and to the other points mentioned above. Therefore, high secondary air ratio was sacrificed for stable circulation of particles, which is prior in terms of achieving CFB combustion conditions. On the other hand, as a future work, the design of auxiliary air supply system should be modified, either by isolating it from secondary air system or improving the pressure control of secondary air line.

Flue Gas Oxygen Concentration

Another parameter that requires detailed discussion is the deviation of oxygen concentration within the flue gas given on wet basis. Refering to the mass balance results, 5.27% of oxygen concentration measured during Test-1 can not be attained with 20% excess air, so that it was required to investigate the reasons underlying this measurement. Finally, it was found that the gasket in between the connection flanges at the exit of combustor was slightly damaged during the test. This resulted in dilution of flue gas by fresh air suction from the surroundings. It was concluded that this failure had an effect only on oxygen measurement in the positive direction, and this deviation was taken into account in the mass balance studies within design assessment. Before the second test run, damaged gasket was replaced with a new one, and necessary measures were taken to prevent the same failure. The flange was checked during Test-2, and no more problem is observed at that point.

Cooling Water

In addition to increased heat input, decreasing the cooling water flow rates also helped reaching increased temperatures, but not that much significant as heat

input. Decreasing the cooling load at second and third modules, significantly reduced the temperature difference between dense and dilute zones. As expected, this reduction increased exit temperatures of cooling water streams of both modules as given at the bottom of table.

Coal Feeding Point

An important distinction between the tests that is not displayed in Table 4.6 was the coal feeding point. As given in the design chapter, there are two solids feeding ports entering the dilute zone module from the same axis, at the heights of 25 cm and 50 cm from the distributor plate. Lower feeding port was employed for the first combustion test. However, it was observed that high pressure of combustion gases prevent the solids from flowing through feeding leg after some hours of operation, even the feeder is an air lock type. In order to reduce this effect, the feeding point was switched to the upper port before the second test. By this modification, solids feeding system was connected to the combustor at a level where pressure is lower than the previous setup.

Based on the discussions given above, it was concluded that Test-2 was more satisfactory than Test-1, as an outcome of the experiences gathered during the first test. However, this conclusion did not prevent Test-1 from being presented as a part of this study, despite the fact that fly ash flow rate could not be determined and there has been a dilution at the flue gas line.

In conclusion, after refractory drying operation and coal fired commissioning tests, two combustion tests were carried out to generate the extensive set of data given above. Based on this experimental data, further results were generated and utilized in the analysis for design assessment and for investigating combustion characteristics of the lignite.

CHAPTER 5

RESULTS AND DISCUSSION

Following satisfactory combustion tests executed at the METU 150 kWt CFBC Test Unit, the experimental data was not only rearranged for generating extensive results, but also utilized as input data for design assessment. In the extent of these studies, performance of the combustor was analyzed with respect to temperature profiles, pressure profiles, flue gas emissions, ash compositions and particle size distributions. In addition, operation performance was compared with the design data by reperforming heat and mass balances and pressure balance model.

5.1 Temperature Profiles

Temperature measurements were carried out on a discrete grid of points along the combustor. The temperature profiles at steady state operation along the riser are given in Figures 5.1 and 5.2 for each combustion test. Tabulated data for the temperature profiles are given in Appendix E.

As discussed and shown in the relevant figures in Chapter 4, steady state temperatures along the combustor are lower for Test-1 compared to Test-2. Examination of Figure 5.1 reveals that dense zone temperatures are slightly lower than the operating temperature of 850°C typical for CFBCs. In addition, the inflection of the profile at the entrance of first cooled module determines the profile within dilute zone. The effect of cooling at these modules clearly shows that a uniform profile with a lower temperature compared to the bottom section of the riser was obtained at the upper half of riser.

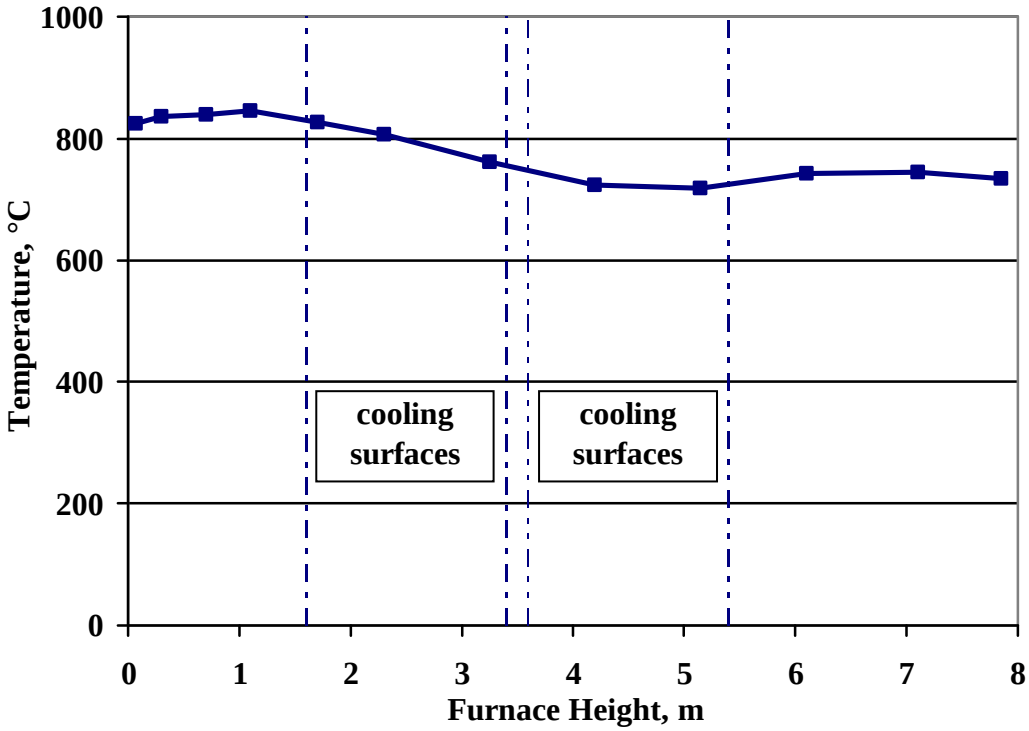

Figure 5.1 Steady State Temperature Profile for Combustion Test-1

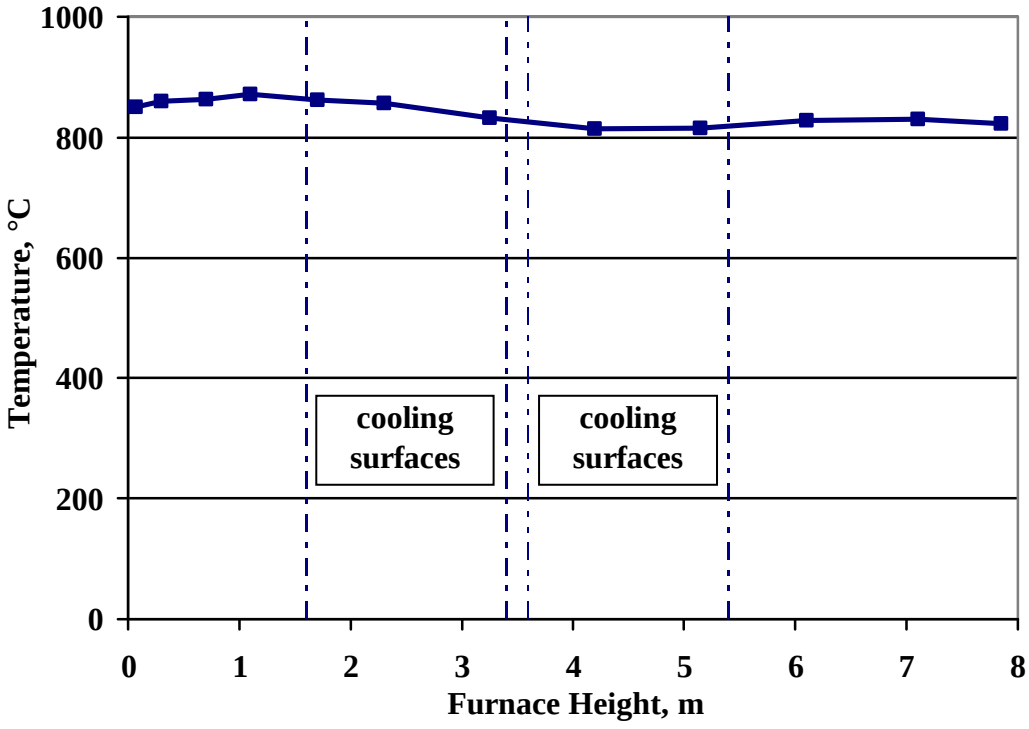

Figure 5.2 Steady State Temperature Profile for Combustion Test-2

Although coal flow rate could have been increased and cooling load could have been lowered to reach higher temperatures with a more uniform profile, they were not performed not to destroy the steady state. The conditions of this steady state were found to be acceptable in terms of experimental purposes.

Temperature profile for Test-2 given in Figure 5.2 shows that the temperatures were higher than 815°C throughout the riser as a result of increased fuel input and reduced cooling. This profile is an indication that ideal CFB combustor conditions were attained in terms of temperature in the test unit.

5.2 Pressure Profiles

Differential pressure measurements were also carried out on a discrete grid of points through pressure impulse lines along the combustor. Steady state measurements logged during both runs were carefully averaged over the time as the values fluctuate especially within dense bed, because of particle movement along the riser. The average of measurements for distributor plate, dense zone, dilute zone, cyclone, downcomer and loop seal are given in Table 5.1.

As the distributor plate was designed to have a pressure drop of 99 mmH_2O, the values given in the table can be accepted to be within the limits of design. One of the most important assumptions made in distributor design was the temperature of air flowing through the orifices which directly affects the orifice velocity. Temperature of air flowing through distributor plate is affected by the metal temperature of the distributor plate which is a function of dense bed temperature and heat transfer from the bed to the plate. Comparison of the temperatures measured at 7 cm above the distributor plate in both tests shows that this temperature is approximately 26°C higher in Test-2 than Test-1. This difference was assumed to be approximately valid for distributor plate temperature too. Therefore, it is believed that the difference between pressure drops through the distributor plate in two tests was due to the difference in the temperature of air flowing through the orifices.

Table 5.1 Overall Pressure Drop Values through Main Parts

Pressure drop through (mmH_2O)	**Design**	**Test-1**	**Test-2**
Distributor Plate	99.0	84.6	113.2
Dense Zone	471.8	413.4	367.2
Dilute Zone	740.4	38.4	27.2
Cyclone	59.6	17.4	22.0
Downcomer	1565.8	889.7	684.5
Loop Seal	508.4	623.4	445.9

The differential pressure measured between the ports at the bottom of riser and at 50 cm height is reported as dense bed pressure drop in Table 5.1. The difference in the pressure drop between the two tests was mainly due to difference in bed inventory. The total amount of bed material discharged from the unit at the end of Test-1 and Test-2 were 23.3 kg and 19.8 kg, respectively. This difference was most probably caused by the amount of initial bed material and increased fine fractions within the bed material in Test-2, which resulted in decreased amount of coarse particles staying in dense zone, and increased amount of fine particles circulating within the system.

Regarding the pressure drop through the dilute zone, there is not a significant pressure difference between the exit of dense zone and top of the riser at both tests. This data indicates that the solid hold up within dilute zone is negligible compared to dense zone.

The pressure drop through the cyclone, measured to be around 20 mmH_2O, is significantly lower than the design prediction: (59.6 mmH_2O). Main reason for this discrepancy is suspected to be the flue gas temperature at one of the measurement points. Examining the temperature near the impulse line of differential pressure transmitter at the outlet of the cyclone is found to be lower within a range of 250 – 300°C than the temperature at the inlet for both test runs.

This temperature drop is considered to be due to uninsulated flue gas line at the exit, and it was believed to be responsible for the reduced measurement of cyclone pressure drop.

Pressure drop through loop seal and downcomer were not directly measured values. They were calculated from the pressure measured at the air piping that feeds the loop seal. By subtracting predicted values of resistances within the pipes and pressure drop through loop seal distributor plate from line pressure, gage pressure at the bottom of downcomer was obtained. Then the pressure drop for the loop seal was calculated from the difference between downcomer pressure and dense zone pressure at the level of circulation leg entrance to riser. This method was same as the approach of pressure balance model for calculating ΔP through loop seal. In conclusion, these calculated data given in the table is in line with the requirement for balancing the pressure at the bottom of riser. As the ΔP through riser was higher for Test-1, the values for downcomer and loop seal were also higher compared to Test-2. These higher values of ΔP were also the indications of the presence of increased amount of solids within downcomer, and higher solid bed height as a result of that.

Regarding the pressure balance, it is more expressive to present overall pressure profile within the system than giving each differential pressure value one by one. Starting from the side channel blower and including the loop comprised of riser, cyclone, downcomer and loop seal, pressure values are calculated and these data are used as input data for the pressure and solid mass balance analysis. Pressure profile of each run at steady state operation are given in Figures 5.3 and 5.4. Steady state average values for the gage and differential pressure measurements within the system are given in Appendix E.

As can be seen from both figures, the profile starts from the pressure at the exit of the blower for which the value is displayed at the right bottom. As there is no pressure transmitter right at the discharge of the blower, pressure at that point was

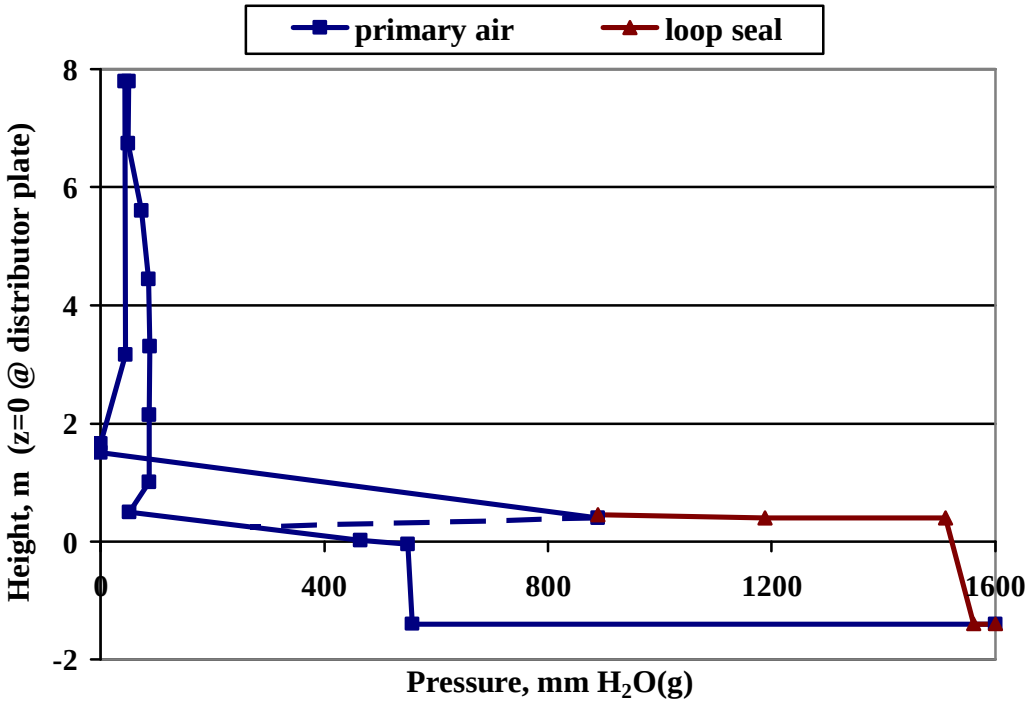

Figure 5.3 Steady State Pressure Profile for Combustion Test-1

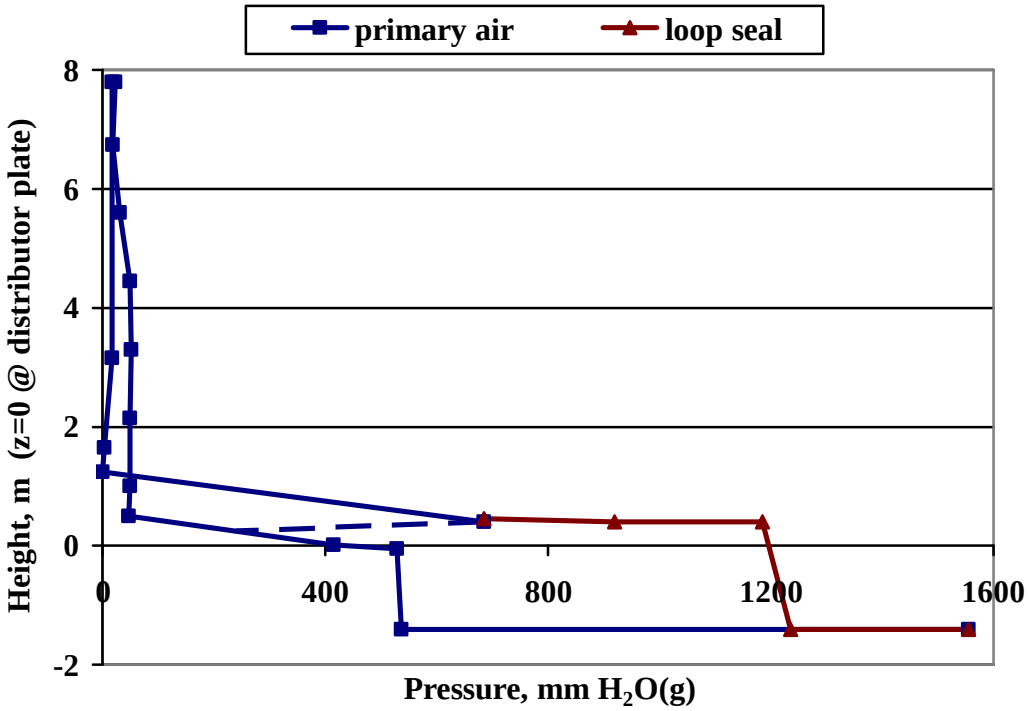

Figure 5.4 Steady State Pressure Profile for Combustion Test-2

calculated from the operation curve, which displays the design performance of the equipment. Knowing the blower motor frequency (around 40 Hz.) and total air flow rate data logged during the tests, the pressure at the discharge line of the blower was determined to be 1607 and 1555 mmH_2O (g) for Test-1 and Test-2, respectively. As the equipment was not operated for a long period of time since its start-up, factory performance was accepted to be reliable for obtaining these data.

Following the blower, there comes the primary air flow control valve that was operated around 30% open position during both runs. The significant resistance created at this position of the valve was calculated from the difference between the blower outlet pressure and the gage pressure transmitter downstream the valve. Pressure drop arised through this valve was found to be 1050 mmH_2O and 1019 mmH_2O for Test-1 and Test-2, respectively.

Instead of operating the blower at high frequency and the valve at a position creating higher resistance, motor speed could be decreased resulting in a reduction in discharge pressure for the same air flow, and as a result of this the opening of the valve could be increased. However, this change in the primary air valve position prevents air flow via secondary air line to loop seal windbox that has a high pressure solid bed over it and to highly resistant small diameter (8 mm) lines for solids feeding support and observation window cooling. Therefore, primary air control valve was operated at 30% open position, while the position of secondary air valve is kept at 100% open to help the best distribution of air in both lines.

After the primary air valve, the pressure decreases to almost 540 mmH_2O (g) at both tests and flows to the riser through windbox and distributor plate whose pressure drop was measured as 84.6 and 113.2 mmH_2O in Test-1 and Test-2, respectively.

Passing through the dense bed after the distributor plate, pressure reduces to almost 40 mmH_2O (g), and no significant change within dilute zone is observed.

This trend is an indication of low variation of particle load towards the riser exit and negligible pressure drop values are explained by low solid hold-up within dilute zone. However, this finding is in contradiction with the considerable amount of solid hold-up predicted by the pressure balance model. Possible reasons of this significant discrepancy are discussed in detail at section 5.8.

After leaving the riser there comes the measurements at the cyclone and the downcomer leg. At this point the profile named as primary air is merged with the loop seal air profile at the point corresponding to the bottom of downcomer.

Regarding the profile for loop seal air given in Figures 5.3 and 5.4, data points start from the exit of blower at the right bottom of figures and is followed by the gage pressure measurement at the exit of secondary air control valve. The rest of the data points are; calculated data for auxiliary air coonection point on the secondary air line, inlet of loop seal windbox and the bottom of downcomer, in the order from right to left of profile. The origin of pressure drops resulting in these data points are the resistances through secondary air piping and through air supply tubing and distributor plate of loop seal. Finally, the loop seal pressure profile is intersected with the dense bed at the point corresponding to the level of circulation leg entrance to the riser. By this line closing the profile, pressure loop is completed. However, this final line is displayed as dashed line, as there is not any direct or indirect data for the pressure at the level of circulation leg entrance.

5.3 Flue Gas Emissions

The concentrations of O_2, CO, CO_2, SO_2, NO and N_2O within the flue gas were measured at a point downstream the connection of CFBC flue gas line with the existing flue gas system of Bubbling AFBC Test Rig. As this is an existing sampling point of bubbling unit for emissions monitoring, gas conditioning and analysis system of the existing unit were employed. In this system, combustion gas is sampled from the flue gas line via a heated stainless steel tubing and transferred to gas conditioning system to be filtered, dried and cooled. Sampled

gas then passes through two analyzers in series, ABB Advanced Optima 2000 including Magnos 106 analyzer module for O_2 and Uras 104 analyzer module for CO, CO_2, NO and N_2O, and Siemens Ultramat 6 for SO_2. Output signals from analyzers are logged to the PC of the existing data acquisition and control system of the Bubbling AFBC test rig. Details of sampling, gas conditioning and analysis system can be found elsewhere [41].

Gas analysis system was only used during Test-2. The steady state emission data on dry basis is given in Table 5.2.

As explained before in Chapter 3, oxygen concentration was continuously monitored on wet basis for combustion control by a zirconia cell oxygen analyzer installed on the flue gas line. The locations of this analyzer and the sampling point for the gas analysis system are separated by less than 4 meters, so that it is expected to have similar results from zirconia analyzer and Magnos 106 analyzer module of existing analysis system. As Zirconia analyzer measures O_2 concentration in wet basis and Magnos analyzer measures it in dry basis, it was required to convert one of the data to the basis of the other to check the reliability of both analysis. For this conversion, water vapor concentration within the flue gas was required. As there is no measurement for water vapor concentration, this data was predicted from the mass balance model as 12.6%. In conclusion, it was

Table 5.2 Flue Gas Emissions for Test-2 (dry basis)

	Concentration
O_2	3.63 %
CO, ppm	108.0
CO_2	15.87 %
SO_2, ppm	4946.0
NO, ppm	29.8
N_2O, ppm	57.0

found that the equivalent of zirconia output on dry basis is 3.71% and there is an acceptable error of 2.35% between two measurements converted to same basis.

Regarding the other gaseous content of flue gas given in the table, CO and NO emissions are fairly lower and N_2O emission is higher compared to past experiences when AFBC Test Rig firing Çan lignite was operated in bubbling mode [41]. As there is no limestone addition, there is no SO_2 capture so that the emission is very high.

5.4 Ash Compositions

During the combustion tests, ash generated within the system is found in the form of:

- dense bed ash: to be drained from the bottom of riser,
- circulating ash: to be drained from the bottom of loop seal,
- fly ash: to be collected at the bottom of bag filter.

Within these three forms, dense bed ash and circulating ash can be defined as coarse and fine particle size fractions, respectively, originating from the mixture of initial bed material and ash generated by the combustion of coal. First group of this ash mixture, mostly composed of coarser particles within a certain size range, stays in dense bed or moves between dilute and dense zones. This group of particles are drained via the bottom ash removal system for balancing the excess pressure drop within dense zone or for taking samples during steady state operation to determine size distribution and chemical composition. The second group is composed of finer particles that travel through dilute zone and leave the riser but is captured by the cyclone to be recycled to the riser via the loop-seal. Finest ash particles escape from the cyclone and this group of particles are defined as fly ash. Considerable portion of these particles is captured by the bag filter located upstream the ID fan and stack, and is collected in the bin at the bottom of the filter. However, there is still a small portion of fly ash within the gas stream,

composed of finest particles that can not be captured by the bag filter. Other than fine ash particles originating from bed material and coal ash, fine particles of unburned carbon is also present in small amounts within the fly ash.

The chemical analyses of the samples taken during both tests from the dense bed as defined as bottom ash and from the bag filter defined as fly ash were carried out in the laboratories of Chemical Engineering Department and the results for both runs are given in Table 5.3.

Examining the compositions given in the table, it can be seen that the concentrations of compounds within bottom and fly ash streams of each test are similar to each other. The deviation between the tests is attributed to the heterogeneous characteristic of the lignite.

One of the most significant difference of composition between two ash streams of each test is the higher Fe_2O_3 content in the bag filter ash. This difference, which is

Table 5.3 Chemical Analysis of Bottom Ash and Bag Filter Ash

	Weight (%)			
	Test-1		Test-2	
	Bottom Ash	Bag Filter Ash	Bottom Ash	Bag Filter Ash
SiO_2	56.37	48.94	58.09	56.51
Al_2O_3	18.44	16.22	19.48	20.25
Fe_2O_3	6.71	12.10	7.10	12.27
CaO	2.11	2.32	1.84	0.41
MgO	1.21	1.08	1.34	0.64
SO_3	9.76	11.39	7.29	5.24
Na_2O	2.22	3.96	1.46	2.31
K_2O	1.59	1.97	1.48	0.42
TiO_2	1.59	2.02	1.93	1.97

typically due to higher concentration of this compund in fine particles, was also observed in the previous research studies with the same and other lignites [41, 42]. Based on the experiences reported in these studies, another deviation between the ash streams is expected to be in CaO concentrations during the combustion tests with limestone addition that will be carried out in the future.

5.5 Ash Split

Ash generated during combustion splits to coarse and fine ash particles. As discussed above, most of the coarse particles stays within the riser and are discharged as bottom ash, whereas fine particles with appropriate size that are captured by the cyclone are circulated within the system and most of fines that escape from the cyclone are collected at the bag filter. Ash split is the percent distribution of total ash between bottom and fly ash streams leaving the combustor. Size distribution, grindability and nature of coal and its ash determines the ash split.

Bottom ash is discharged from the center of distributor plate via an extraction pipe. However, during the combustion tests, it was not required to discharge bottom ash, as there was no significant increase in the pressure drop through the dense zone. Therefore, the only solid output from the system was the fly ash stream, most of which was collected by the bag filter.

As mentioned before within the discussions of operating conditions, fly ash collection rate at the bag filter could only be determined during combustion Test-2. Fly ash flow rate at steady state operation during this test is 7.04 kg/h. As the ash input by coal was calculated to be 15.89 kg/h and no other ash stream was drained from the system during the combustion test, the difference between these values mostly stands for the accumulation rate of circulating particles but also includes a small fraction of finest particles of fly ash within flue gas discharged via the stack.

5.6 Particle Size Distributions

Particle size distribution (PSD) for the ash streams drained from the bottom of loop-seal and riser at the end of both tests were determined by sieve analysis and given in Tables 5.4 and 5.5, respectively. On the other hand, PSD of fly ash collected at the bottom of bag filter was measured by Malvern Mastersizer 2000 equipment at the METU Central Laboratory. Measurement principle of this equipment is based on Mie scattering theory, and the detectable particle size range is 0.02 to 2000μm. Results of particle size analysis of fly ash generated during both runs are given in Figure 5.5, which also displays the PSD of all other input and output solid streams. Tabulated data for differential size distributions of fly ash samples are given in Appendix E.

Table 5.4 Particle Size Distribution of Loop Seal Ash

Sieve Analysis	Weight (%)	
D_p, (mm)	Test-1	Test-2
> 6.3 mm	0.00	0.00
6.30 – 4.75	0.04	0.00
4.75 – 3.35	0.54	0.17
3.35 – 2.00	0.66	0.36
2.00 – 1.00	2.10	4.04
1.00 – 0.85	0.56	1.87
0.85 – 0.60	9.32	15.97
0.60 – 0.43	31.66	31.03
0.43 – 0.36	14.60	12.79
0.36 – 0.18	28.25	23.12
0.18 – 0.11	6.48	6.66
0.11 – 0.00	5.79	4.00
d_{50}, mm	0.40	0.44

Table 5.5 Particle Size Distribution of Bottom Ash

Sieve Analysis	Weight (%)	
D_p, (mm)	Test-1	Test-2
> 6.3 mm	0.05	0.25
6.30 – 4.75	0.79	3.19
4.75 – 3.35	10.23	17.55
3.35 – 2.00	12.81	14.47
2.00 – 1.00	35.58	32.35
1.00 – 0.60	24.27	16.22
0.60 – 0.43	11.84	8.74
0.43 – 0.18	3.56	5.46
0.18 – 0.11	0.27	0.81
0.11 – 0.00	0.60	0.97
d_{50}, mm	1.27	1.55

Examining the size distribution given in Table 5.4 for circulating ash drained from the bottom of loop seal in Test-1, it is seen that the particle size is smaller than 0.85 mm for more than 96% of the sample. In order to analyze the significance of this particle size, terminal velocity for each fraction of sieve analysis was calculated. It was found that the average superficial velocity within dilute zone, 4.3 m/s for Test-1, is larger than the terminal velocity of particles smaller than 0.61 mm, showing that the possibility for these particles to be elutriated from the riser is maximum. However, it was required to check the design efficiency of the cyclone to find the captured fraction of these elutriated particles. Capture efficiency, found to be higher than 99.9% for particles larger than 240µm and decreasing to 98% for 55µm size, shows that the probability of particles larger than 240µm for being captured by the cyclone was maximum. In conclusion, high fraction of particles within 0.18 – 0.60 mm range determined by the sieve analysis as 74.51%, is verified by the predictions for terminal velocity and cyclone efficiency.

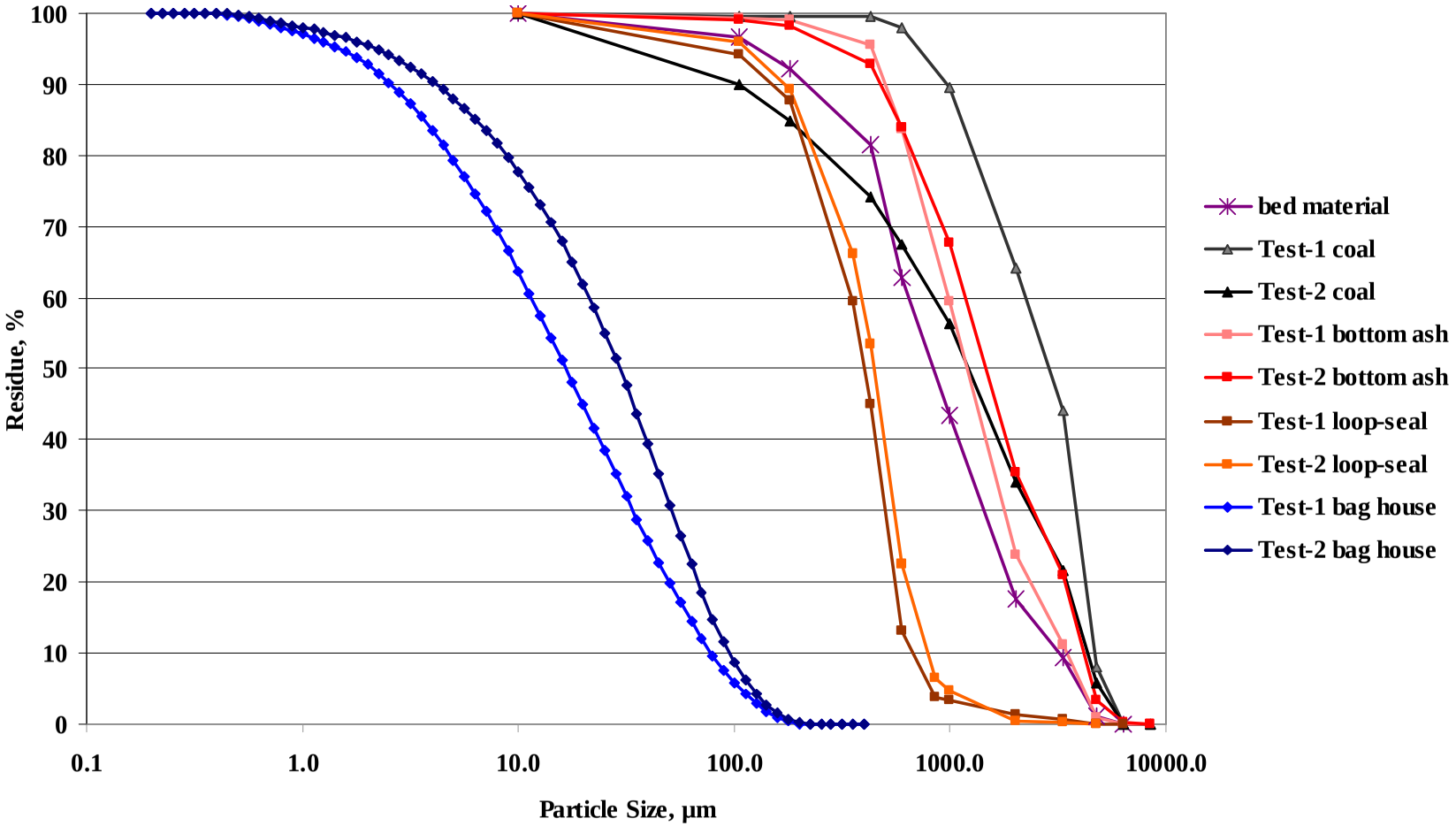

Figure 5.5 Particle Size Distributions of all Solid Streams

On the other hand, size distribution of the loop seal ash of Test-2 reveals that the fraction of particles in 0.18 – 0.60 mm range was lower (66.94%), but the fraction in 0.85 – 0.60 mm range was significantly higher than that of Test-1. This distinction resulted in a d_{50} value of 0.44 mm for the second test that is higher than 0.40 mm calculated for the first one. This finding is in line with the discussions given above for the elutriation effect of superficial velocity that is higher in Test-2.

Regarding the particle size distribution for bottom ash given in Table 5.5, weight fraction of particles within 0.425 – 3.35 mm size range is around 90% for both tests. As the average superficial velocity within dense zone; 4.07 m/s for test-1, was smaller than the terminal velocity of particles larger than 0.58 mm, the possibility of these particles to stay in the riser was maximum. Corresponding particle size for Test-2 is found to be 0.69 mm based on the higher superficial velocity of 4.66 m/s in the dense zone during this test. These findings can be observed from the sudden increase in weight fractions starting around 0.60 mm and increasing with size. The smaller fractions experienced in Test-2 up to 1 mm was an outcome of the increased superficial velocity at this run, resulting in increased elutriation of the mentioned range. This effect was also observed at d_{50} values of each run.

As can be seen from Figure 5.5, particle size decreases in the order of coal, bottom ash, loop seal ash and bag filter ash for each run, except the coal size in Test-2, that was resized to reach a lower d_{50} than Test-1. Regarding the fly ash size distribution, it is found to be increased from Test-1 to Test-2 for which the d_{50} values are 16.6 µ and 29.5 µ, respectively.

5.7 Heat Transfer Analysis

Heat transfer analysis is carried out in two parts: 1. Heat transfer in cooled modules. 2. Heat balance over combustor.

5.7.1 Heat Transfer In Cooled Modules

The second third modules of the combustor were designed to have cooling water channels at the external surface of module body. Based on the predictions for dispersion of heat generation along the riser, 10 water channels were installed on module-2, whereas 6 channels were installed on module-3. Cooling system was designed to have countercurrent flow with respect to the flow within the riser.

During the combustion tests, flow rates and temperatures of cooling water streams of both modules were logged by the control system. Based on these data, rate of heat removal at each module was determined. These results and further analyses are given in Table 5.6.

In order to obtain overall heat transfer coefficient from the inside of combustor to the cooling water, log mean temperature difference (LMTD) for each module is required. As furnace temperatures at the exact location of inlet and outlet of cooled zones were not available, these data are calculated by interpolating the temperature data measured by nearby transmitters.

Although total flow rate of water is decreased by 22.5% at Test-2, heat removal rate is increased by 6.5% as a result of the increase in outlet temperature of water, which also led to increased temperatures in dilute zone. On the other hand, heat transfer coefficient at each module remains almost constant at both tests within the range of 24.4 – 29.2 kcal/hm^{2}K, which are lower than the values predicted at the design phase. This may be due to the contribution of the heat loss to surroundings to overall cooling that is predicted to be lower than the actual case. Regarding the heat loss at cooled modules, it is calculated that approximately 42% of heat input by fuel is removed by cooling water. Rest of the heat generated by combustion leaves the system within solid and gas streams and as heat loss from external surfaces. The ratios of flow enthalpies of output streams and by heat transfer to surrroundings to total heat input were obtained from overall heat balance.

Table 5.6 Heat Transfer Data for Cooled Modules

Parameter	Test-1		Test-2	
	Module-2	Module-3	Module-2	Module-3
Cooling water flow rate, kg/h	805.6	746.2	695.4	570.8
Furnace temperature at module inlet, °C	830.7	748.3	863.9	826.3
Furnace temperature at module outlet, °C	754.7	725.0	829.2	819.1
Cooling water temperature at inlet collector, °C	13.8		16.7	
Cooling water temperature at outlet collector, °C	53.5	47.2	64.8	64.9
Log mean temperature difference, °C	758.89	706.14	805.76	781.71
Heat transfer area (internal surface of refractory), m^2	1.45			
Heat removal rate at each module, kcal/h	31977	24918	33430	27488
Total heat removed raate from cooled modules, kcal/h	56895		60918	
Overall heat transfer coefficient at each module, kcal/h m^2K	29.16	24.42	28.71	24.33

5.7.2 Overall Heat Balance

Overall heat balance analysis was carried out around the combustor and the heat balance terms are given in Table 5.7.

For the defined system of combustor, input terms are flow enthalpies of coal and air, whereas output terms are flue gas and the fly ash particles. As there was no reaction related with limestone in this study, only generation term was combustion. Putting these terms into steady state energy balance equation, rate of

Table 5.7 Heat Balance Analysis

	Test-1	Test-2
	kcal/h	
Input Terms		
Dry coal	197.3	252.1
Dry air	2728.9	2529.5
Water in coal	112.6	157.7
Water vapor in Air	65.9	61.1
Total Input	3104.7	3000.4
Output Terms		
Fly Ash	1410.6	1158.2
Dry Flue Gas	48002.3	57201.7
Water Vapor in Flue Gas	7357.9	11260.6
Total Output	56770.8	69620.5
Generation Terms		
Combustion	134333.8	148596.7
Total Generation	134333.8	148596.7
Balance: Heat Removed at Furnace	80667.7	81976.6
Heat Removal by cooling water	56894.2	60918.2
Remainder: Heat Loss to Surroundings	23773.5	21058.4

heat removal from the combustor is obtained. This heat removal is provided by cooling water and heat loss to the surroundings.

Energy supplied by coal combustion leaved the system within the flow enthalpies of cooling water and particle laden flue gas with a ratio of approximately 42% for each stream. The rest of heat input, almost 17%, was lost from the external surface of the insulation by natural heat transfer mechanisms. According to initial heat balance analysis at the design phase, heat loss by natural cooling mechanisms was predicted to be lower; around 6% of heat input. As a result of this, cooling requirement was predicted to be 47%, higher than experimental results. This deviation is attributed to low overall heat transfer coefficient predicted at the design phase for the heat loss to surroundings.

5.8 Combustion Efficiency

Combustion efficiency for both runs were calculated from the energy balance for combustion, for which the details are given in Table 5.8.

In order to calculate combustion efficiency, reaction enthalpies for the complete combustion of unburned carbon compunds within the output streams were added for total combustion loss, and this value was divided by the total energy input based on lower heating value of coal. Subtracting this percent loss from 100%, combustion efficiency was obtained as 98.90% and 99.37% for Test-1 and Test-2, respectively. However, although each terms for Test-2 given in the table was based on experimental findings, the efficiency value for Test-1 was based on some predictions as there was no experimental data for CO emissions and fly ash flow rate for this run.

Table 5.8 Combustion Efficiency Analysis

	Test-1	Test-2
Input Terms		
Coal consumption, kg/h	37.45	48.55
Lower heating value, kcal/kg	3618	3085
Total Energy Input, kcal/h	135499.0	149765.8
Output Terms		
CO, ppm	90.6	94.1
Combustion CO, kg/h	0.026	0.027
Incomplete combustion loss, kcal/h	62.3	65.6
Fly ash flow, kg/h	4.82	7.04
Unburnt carbon content, %	3.8	1.6
Carbon in fly ash, kg/h	0.183	0.111
Unburnt Carbon Loss, kcal/h	1434.0	871.8
Total Combustion Loss, kcal/h	1496.3	937.5
Combustion Efficiency, %	98.90	99.37

5.9 Pressure Balance Model

Based on the experimental data, pressure balance model is reapplied to the combustor. The results of the model are displayed with the pressure measurements for each test in the Figures 5.6 and 5.7.

Among the input data of pressure balance model, superficial velocity in the dense zone, gas velocity at loop seal and the bulk density and particle size of circulating ash were observed to deviate significantly from the design basis. In addition to these data, superficial velocity in the dilute zone, average particle size of dense bed, particle density of circulating ash and heights of dense and dilute zones were also found to deviate from the design basis within acceptable ranges. The deviated input parameters of pressure balance model are given in Table 5.9.

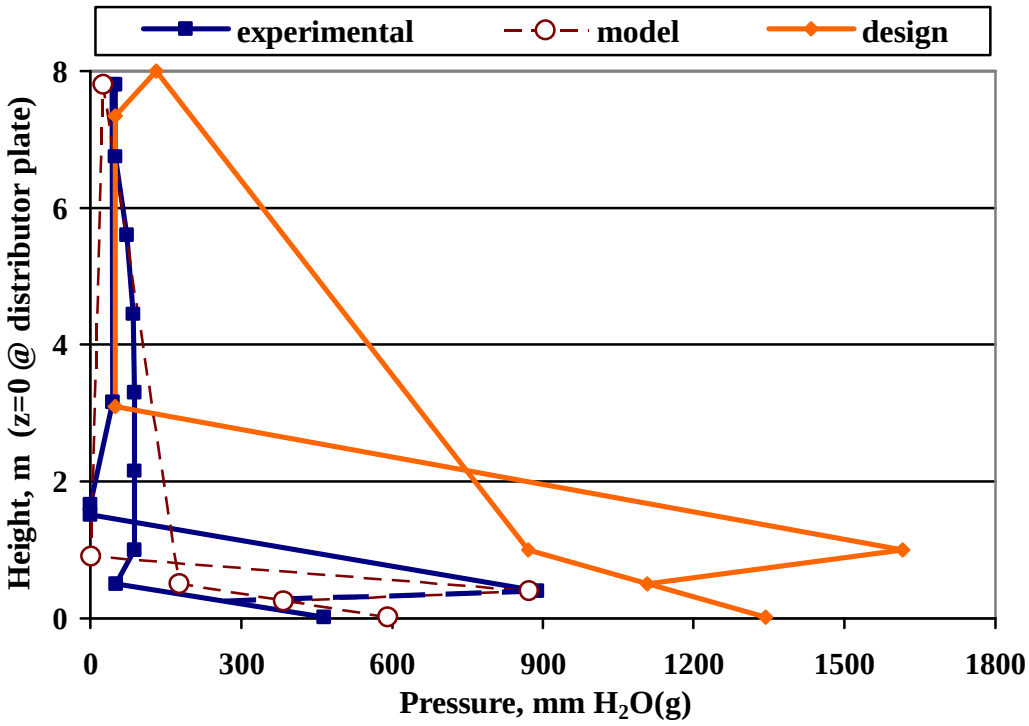

Figure 5.6 Predicted and Measured Pressure Profiles for Combustion Test-1

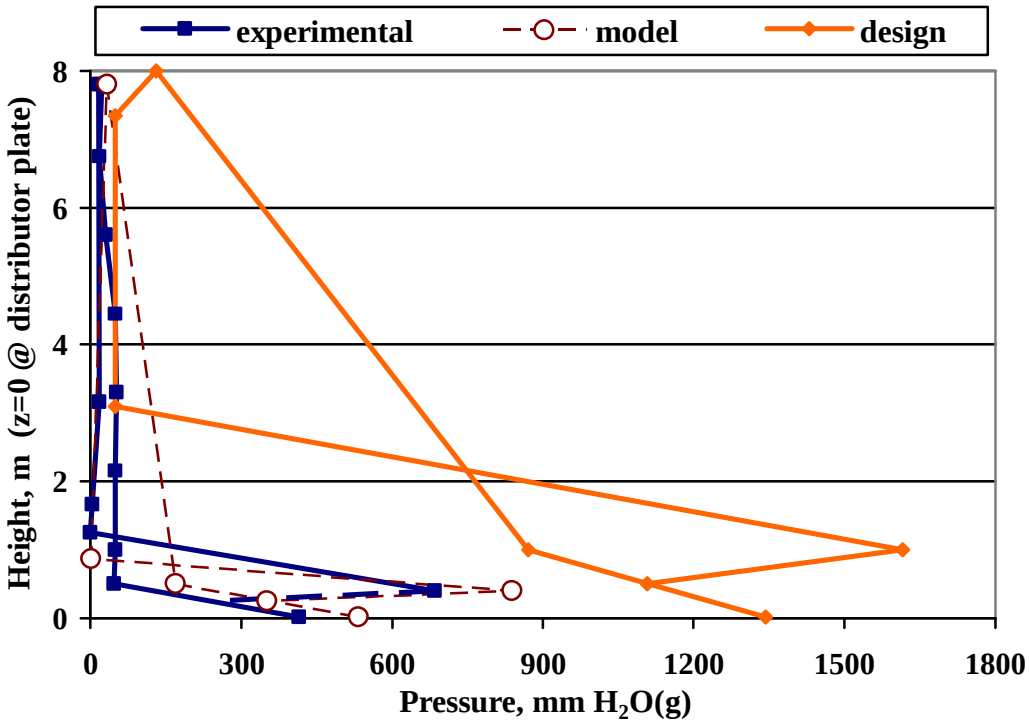

Figure 5.7 Predicted and Measured Pressure Profiles for Combustion Test-2

Table 5.9 Deviated Input Parameters of Pressure Balance Model

Parameter	**Design**	**Test-1**	**Test-2**
Superficial velocity in the dense zone, m/s	3.0	4.1	4.6
Superficial velocity in dilute zone, m/s	5.0	4.3	5.1
Gas velocity at loop seal, m/s	0.01	0.15	0.15
Height of the dense bed, m	1.0	0.7	0.7
Height of the dilute zone, m	7.0	7.3	7.3
Average particle size of dense bed, mm	1.16	1.27	1.55
Average particle size of circulating ash, mm	0.04	0.40	0.44
Bulk density circulating ash, kg/m³	536	1030	1010
Particle density of circulating ash, kg/m³	930	1200	1200

Average particle size of circulating ash is one of the most deviated parameters among these input parameters, and it is also very effective on number of parameters calculated within pressure balance model. This average particle size was based on the cyclone ash of previous experiments in 0.3 MWt AFBC test rig operated in recycling mode. The deviation is attributed to lower superficial velocity and the presence of a cooler module at the exit in AFBC test rig. Based on these, elutriation of coarser particles is reduced, resulting in significantly lower particle size for circulating ash compared to CFBC test unit.

As a result of the deviation from the design basis, the parameters calculated from these data also differed from each other. Consequently, the following parameters were found to differ from the pressure balance model at the design stage: Solid hold up in the dense bed (ε_{sd}); solid holdup at uniform flow with slip velocity (ε_s^*); average solid hold up at the dilute zone ($\varepsilon_{s\infty}$); decay (a, a_e) and reflux constants (C_e); solid hold up at the exit (ε_{se}); variation of solid holdup by exit effect ($\Delta\varepsilon_{sr}$). Among these parameters, the essential data are the solid holdup values, which affect the pressure profile. Solid holdup values predicted at the design stage and after combustion tests are given in Table 5.10

Table 5.10 Solid Holdup Values Predicted by Pressure Balance Model

Predicted Solid Holdup @	**Design**	**Test-1**	**Test-2**
The dense zone, ε_{sd}	0.25	0.26	0.28
The dilute zone (average), $\varepsilon_{s\infty}$	0.0041	0.0003	0.0003
The exit, ε_{se}	0.0048	0.0003	0.0003
The dilute zone (asymptotic), ε_s^*	0.0034	0.0004	0.0004

Comparing the predicted solid holdup values given in the table, it can be seen that the predictions for the solid holdup of dense zone is in good agreement with each other. However, solid holdup values for dilute zone predicted at the design stage were higher than the predictions after combustion tests. This result was attributed to the discrepancies between the input data and the parameters like decay and reflux constants calculated from these input data.

In order to illustrate the effect of the input data and the predictive accuracy of pressure balance model, measured and predicted pressure drop values are given in Table 5.11. As can be seen from the table, predicted pressure drop values for dense bed are in good agreement with measurements. However, there is a significant discrepancy between design data and measurements for dilute zone.

Table 5.11 Pressure Drops within the CFBC Loop

ΔP through (mmH_2O)	**Model (design)**	**Test-1**			**Test-2**		
		Exp.	**Model**	**Error**	**Exp.**	**Model**	**Error**
Dense zone	471.8	413.4	362.9	-12%	367.2	336.9	-8%
Dilute zone	740.4	38.4	152.5	297%	34.3	136.6	298%
Loop seal	508.4	623.4	487.6	83%	445.9	487.2	9%
Downcomer	1565.8	889.7	871.3	-2%	684.5	837.3	22%

This discrepancy was reduced for the predictions obtained after the revision of input data based on experimental results. The remaining errors of these recent predictions indicated that the solid hold up within dilute zone was still predicted to be higher than the actual value at the combustion tests.

Regarding the pressure drop through loop seal, the constant values predicted for all cases independent of input data, were attributed to the loop seal solid holdups that were calculated to be identical.

The predictions of the pressure drop through downcomer is dependent on the accuracy of other items, as the pressure balance model was set up based on the equality of pressure drop through downcomer to the total of other pressure drop items. This was the reason why the prediction of the model applied at the design phase was fairly inaccurate. As the other pressure drop items were predicted with poor accuracy, the errors of these predictions added up to result in a significant discrepancy in the predicted pressure drop for downcomer. On the contrary, the error for the downcomer in Test-1 was very low compared to the model predictions at design phase and for Test-2. This was attributed to the compensation of discrepancies in negative and positive directions for this test. Therefore, it is concluded that the error for the pressure drop prediction through downcomer may not be reliable for evaluating the accuracy of the model.

In conclusion, the predictions of the pressure balance model were improved to have more favourable agreement with the measurements, after the input data for the pressure balance model were revised based on the experimental results. However, pressure balance model can be improved for predicting the pressure profile througout the combustor with a better accuracy.

CHAPTER 6

CONCLUSIONS

6.1 General

In this study, a 150 kWt Circulating Fluidized Bed (CFB) Combustor Test Unit was designed and constructed in Chemical Engineering Department of Middle East Technical University, based on the extensive experience acquired at the existing 0.3 MWt Bubbling Atmospheric Fluidized Bed Combustor Test Rig. Following the commissioning tests, combustion tests were carried out for investigation of combustion characteristics of Çan lignite in CFB conditions and for comparison of the design of the test unit with experimental findings.

Based on the steady state results of the combustion tests and comparisons between these results and predictions of the design models, the following conclusions have been reached:

- Temperature profile was slightly far from being uniform in Test-1 due to the excess cooling rate, which resulted in a low average temperature along the riser (784°C). By better control of cooling water flow rate and the help of higher fuel input in Test-2, almost uniform temperature profile along the riser was achieved and the average temperature in the riser was increased to 842°C.
- Pressure drop through the dilute zone was observed to be negligible because of low solid hold up in the dilute zone.

- Based on the experimental results, the input data for the pressure balance model were revised and the predictions of the model were improved to have more favorable agreement with the measurements.
- The compositions of bottom and fly ash streams at each test were similar to each other, except the Fe_2O_3 content which was higher in the bag filter ash.
- Although the coal particle size was significantly differed between two combustion tests, particle size distributions of ash streams were not affected clearly from this deviation. On the other hand, the deviation observed at the size distributions of bottom ash and circulating ash among the tests were in line with the deviation of superficial velocity.
- Heat transfer coefficients observed at the cooled modules of the combustor were within the range of 24.4 – 29.2 kcal/h m² K.
- The heat losses from the external surface of insulation during the tests were observed to be higher than the values predicted during design studies.
- The combustion efficiencies of Test-1 and Test-2 were 98.90% and 99.37%, respectively.

In conclusion, the performance of 150 kW CFBC Test Unit was satisfactory to be utilized for the long term research studies on combustion and desulfurization characteristics of indigenous lignite reserves in circulating fluidized bed combustors.

5.2 Suggestions For Future Work

Based on the experience gained in the present study, the following recommendations for future extension of the work are suggested:

- Parametric studies can be carried out by firing Çan lignite and other Turkish lignite reserves with limestone addition.

- The mathematical model recently developed in METU Chemical Engineering Department for simulation of CFBCs can be applied to prediction of steady state behavior of the Test Unit.
- Pressure balance model can be improved for predicting the pressure profile throughout the combustor with a better accuracy.
- The design of downcomer leg can be modified for measuring solid circulation rate.
- A separate air supply system can be designed for loop-seal air to control the flow rates of secondary air and loop-seal independently. As a result of this, secondary air ratio can be increased to typical operating values of CFBCs.

REFERENCES

1. International Energy Outlook 2004, Energy Information Administration, Office of Integrated Analysis and Forecasting, U.S. Department of Energy, Washington, DC 20585, April 2004.

2. BP statistical review of world energy 2004, URL://*www.bp.com/ statisticalreview2004.*

3. Önal G., "Türkiye'nin Enerji Açığının Kapatılmasında Kömürün Önemi", TMMOB Elektrik Mühendisleri Odası Türkiye II. Enerji Sempozyumu, II. Baskı, s.131, Mayıs 2000.

4. Selçuk N., "Akışkan Yatakta Yakma Teknolojileri", TMMOB Kimya Mühendisleri Odası – TMMOB Maden Mühendisleri Odası, Türkiye'de Kömür Politikaları ve Temiz Kömür Teknolojileri Sempozyumu, Ankara, 21-22 Ekim 1999.

5. Annual Energy Outlook 2004 With Projections To 2025, Energy Information Administration, Office of Integrated Analysis and Forecasting, U.S. Department of Energy, Washington, DC 20585, January 2004.

6. Diversity of fuels used to generate electricity in the UK, EU and other major electricity producing countries, Energy Trends Special Features and Articles, The Department of Trade and Industry, U.K., December 2001 – URL://*www.dti.gov.uk/energy/inform/energy_trends/electricity_art_dec2001. pdf*

7. International Energy Outlook 2003, Energy Information Administration, Office of Integrated Analysis and Forecasting, U.S. Department of Energy, Washington, DC 20585, April 2003.

8. Selçuk N., Arabul H., "Elektrik Enerjisinde Ulusal Politika – 2000 Yılında Türkiye'de Elektrik Enerjisinde Mevcut Durum, Sorunlar ve Çözüm Önerileri", Ekim 2000.

9. Türkyılmaz O., “Türkiye’nin Doğal Gaz Temin ve Tüketim Politikalarının Değerlendirilmesi”, TMMOB Elektrik Mühendisleri Odası Türkiye II. Enerji Sempozyumu, II. Baskı, s.183, Mayıs 2000.

10. Ünver T., Ünal V., “Türkiye’nin Enerji Planlamasında Linyit Kaynaklarının Yeri”, TMMOB Elektrik Mühendisleri Odası Türkiye II.Enerji Sempozyumu, II. Baskı, p.137, Mayıs 2000.

11. 8. Beş Yıllık Kalkınma Planı, “Madencilik Özel İhtisas Komisyonu Enerji Hammaddeleri Alt Komisyonu Kömür Çalışma Grubu Raporu”, Ocak, 2000.

12. JEA Large-Scale CFB Combustion Demonstration Project, Advanced Electric Power Generation, Fluidized Bed Combustion, US Department of Energy, 1999.

13. Selçuk N., and Scheffknecht G., “Design of a 2 x 160 MWel CFB Boiler Utilizing High Sulfur Turkish Lignite”, 17th FBC Conference, Jacksonville, FL, 18-21 May 2003.

14. Selçuk N., “Practical Combustion Systems and Pollution Regulations”, Invited lecture of Nevin Selçuk for ICS Training Course on Laser Diagnostics of Combustion Processes NILES, Cairo, 18-22 November 2000.

15. Basu P. and Fraser S. A., “Circulating Fluidized Bed Boilers: Design and Operations”, Butterworth-Heinemann, 1991.

16. Selçuk N., “Fluidized bed combustion of coal”, Y.Yürüm (ed.), New Trends in Coal Science, 481-494, 1988.

17. Selçuk N., Atamer S., Eroğlu İ., Önal I., and Kırmızıgül Ü., "2 MWt Lignite Fired Atmospheric Fluidized Bed Boiler: Fundamental Process Design Philosophy", 12th FBC Conference (ed.Rubow, L.N.), ASME, 1, 303-308, 1993.

18. Park C. K., “Dynamic Behavior of Circulating Fluidized Bed Boiler Furnace”, Ph.D Thesis, Technical University of Nova Scotia, 1995.

19. Desai D. L., "Pilot Plant Investigation of N_2O Emissions Including the Effect of Long Term Operation in Circulating FBC", Proceedings of 13th FBC Conference, 1995.

20. Adanez J., Gayan P., Grasa G., de Diego L. F., Armesto L., and Cabanillas A., "Circulating Fluidized Bed Combustion in the Turbulent Regime: Modelling of Carbon Combustion Efficiency and Sulphur Retention", *Fuel*, Vol. 80, 1415 – 1414, 2001.

21. Alliston M. G., Probst S. G., Wu S., Edvardsson C. M., "Experience with the Combustion of Alternate Fuels in a CFB Pilot Plant", Proceedings of 13th FBC Conference, 1995.

22. Moe T. A., Mann M. D., Hajicek D. H., Weiss A. J., "Demonstration of Pelletized Fly Ash Reinjection for Reduction of Limestone Consumption and Ash Disposal", Proceedings of 13th FBC Conference, 1995.

23. Chemical and Technological Properties of Turkish Tertiary Coals, General Directorate of Mineral Research and Exploration, Ankara, 2002.

24. Endüstriyel Kaynaklı Hava Kirliliğinin Kontrolü Yönetmeliği, 2004.

25. Selçuk N., Değirmenci E., Oymak O., and Organ L., "Determination of NOx Emissions from a Lignite Fired Fluidized Bed Combustor," TUBITAK-MISAG Project No: 89, ODTÜ, Ankara, Turkey, January 1998.

26. Değirmenci E., "Dynamic Simulation of Fluidized Bed Combustors", Ph.D. Thesis, Department of Chemical Engineering, Middle East Technical University, Ankara, Turkey, 2000.

27. Göğebakan Y., and Selçuk N., "Assessment of a model with Char Attrition for a Bubbling Atmospheric Fluidized-Bed Combustor", *Combustion Science and Technology*, Vol. 176, 799 – 818, 2004.

28. Adanez J., De Diego L. F., Gayan F., Armesto L., and Cabanillas A., "A Model for Prediction of Carbon Combustion Effciency in Circulating Fluidized Bed Combustors", *Fuel*, Vol. 74, No. 7, 1049 – 1056, 1995.

29. Ducarne E. D., Dolignier J. C., Marty E., Martin G., and Delfosse L., "Modelling of Gaseous Pollutants Emissions in Circulating Fluidized Bed Combustion of Municipal Refuse", *Fuel*, Vol. 77, No. 13, 1399 – 1410, 1998.

30. Winaya N. S., Basu P., and Reddy B. V., "Experimental investigations on heat transfer from suspension to impact separators in the riser column of a circulating fluidized bed combustor", *Int. Journal of Heat and Mass Transfer*, Vol. 46, 71 – 75, 2003.

31. de Nevers N., "Air Pollution Control Engineering", McGraw Hill Inc., 1995.

32. Kim S. W., Kim S. D., and Lee D. H., "Pressure Balance Model for Circulating Fluidized Beds with a Loop-seal", *Ind. Eng. Chem. Res.*, Vol. 41, 4949-4956, 2002.

33. Bai D., and Kato K., "Quantitative Estimation of Solids Holdups at Dense and Dilute Regions of Circulating Fluidized Beds", *Powder Technology*, Vol. 101, 183 – 190, 1999.

34. Kunii D., and Levenspiel O., "Fluidization Engineering", Second Ed., Butterworth-Heinemann, 1991.

35. Harmandar H., "Effect of Recycling on the Performance of Bubbling Fluidized Bed Combustors", App. D, M. Sc. Thesis, Department of Chemical Engineering, METU, 2003.

36. Kozan M., Kırbaş G., Göğebakan Y., and Tarhan T., "Che.532 Fluidization Course Term Project", Chemical Engineering Department, METU, 1998.

37. Batu A., "Modeling of Radiative Heat Transfer in Freeboard of a 0.3 MW AFBC Test Rig Using Zone Method Of Analysis", M.Sc. Thesis, Middle East Technical University, 2001.

38. Perry R. H., and Green D. W., "Perry's Chemical Engineer's Handbook", Physical and Chemical Properties, Seventh Edition, McGraw-Hill, 1997.

39. Borman G. L., and Ragland K. W., “Combustion Engineering”, Appendix C, Mc-Graw-Hill, 1998.

40. Incropera F. P., and De Witt D. P., “Fundamentals of Heat and Mass Transfer”, Second Ed., p.397, John Wiley & Sons, 1985.

41. Göğebakan Z., “Cofiring Biomass with Coal in Bubbling Fluidized Bed Combustors”, Ph.D. Thesis, Middle East Technical University, 2007.

42. Altındağ H., “Mathematical Modeling of Sulfur Retention In Fluidized Bed Combustors”, M.Sc. Thesis, Middle East Technical University, 2003.

APPENDIX A

ENERGY FIGURES

Table A.1 World Total Energy Consumption by Fuel (2001 – 2025) [1]

	2001		2025	
	mill. toe	**%**	**mill. toe**	**%**
Petroleum	3943.5	38.7	6181.1	39.4
Natural Gas	2345.9	23.1	3943.5	25.1
Coal	2416.5	23.7	3532.8	22.5
Nuclear	665.2	6.5	1270.0	4.9
Others	811.4	8.0	19.8	8.1

Table A.2 World Energy Consumption for Electricity Generation by Fuel (2001 – 2025) [1]

	2001		2025	
	mill. toe	**%**	**mill. toe**	**%**
Petroleum	307.4	7.6	428.4	6.6
Natural Gas	745.9	18.4	1642.9	25.2
Coal	1539.6	38.1	2436.7	37.4
Nuclear	660.2	16.3	766.0	11.7
Others	793.7	19.6	1244.8	19.1

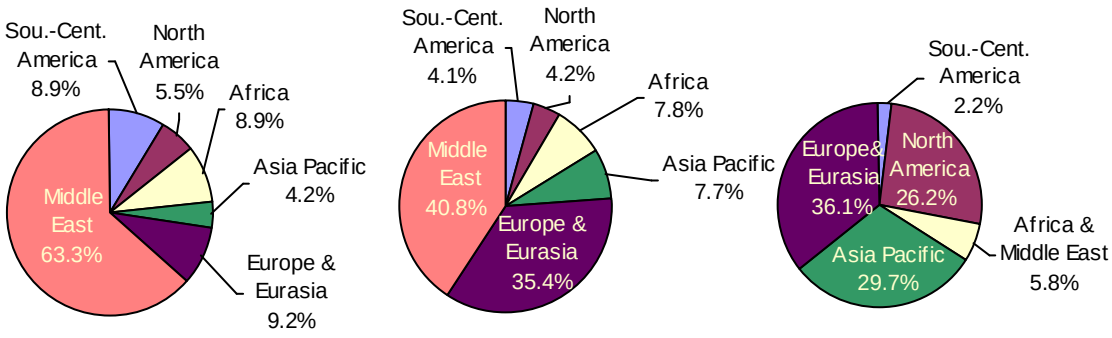

Petroleum **Natural Gas** **Coal**

Figure A.1 Distribution of world fossil fuel reserves [2]

APPENDIX B

BASIC DESIGN

Table B.1 Analysis of Beypazarı lignite

Coal Analysis (as fired)	**Design Coal (Beypazari)**
Carbon	31.68%
Hydrogen	2.58%
Oxygen	7.81%
Nitrogen	1.23%
Sulfur	2.49%
Ash	29.52%
Water	24.69%
LHV (kcal/kg)	2,669

Table B.2 Coal and limestone consumptions

Coal consumption, kg/h	48.36
Limestone consumption, kg/h	8.71

Table B.3 Oxygen demand and combustion air data

Oxygen demand, kg/h	52.68
Oxygen in coal, kg/h	3.78
Exact oxygen demand from air, kg/h	48.90
Theoretical air flow rate, kg/h	211.0
Total dry air flow rate, kg/h	253.2
Total dry air flow rate, Nm^3/h	196.32

Table B.4 Flue gas data

CO, kg/h	0.07
CO_2, kg/h	58.39
H_2O, kg/h	26.46
SO_2, kg/h	0.24
O_2, kg/h	10.77
NO, kg/h	0.19
N_2, kg/h	193.38
Flue gas flow rate, kg/h	289.51
Flue gas flow rate, dry, Nm^3/h	192.25
Flue gas flow rate, wet, m^3/h @ 850°C	909.92

Table B.5 Cross sectional area and dimensions

Cross sectional area, m^2	0.051
Diameter, cm	25.37
Side, cm	22.48

Table B.6 Flue gas composition

CO_2	13.2%
H_2O	14.6%
SO_2, ppm	374
O_2	3.3%
N_2	68.7%
CO, ppm	257.7
NO, ppm	633.9

Table B.7 Ash generation and contents

$CaSO_4$, kg/h	4.61
CaO, kg/h	2.70
Total ash generation, kg/h	22.27
Bottom ash, kg/h	8.90
Fly ash, kg/h	13.40
C in bottom ash, kg/h	0.09
C in fly ash, kg/h	0.27

APPENDIX C

DETAILED DESIGN

Table C.1 Cyclone Inlet Duct Data

Cyclone inlet velocity, m/s	20
Flue gas volumetric flow rate (@850°C, wet), m^3/h	910
Cyclone inlet cross section, m^2 (cm^2)	0.013 (126.4)
Cyclone inlet dimension (H x W_i), cm	7.95 x 15.90

Table C.2 Cyclone Dimensions (cm)

Cyclone diameter, D_o	31.80
Cyclone inlet width, W_i	7.95
Cyclone inlet height, H	15.90
Cylindrical part's height, H_1	63.60
Conical part's height, H_2	63.60
Gas outlet line's diameter, D_e	15.90
Gas outlet line's depth, S	19.87
Particle discharge line, D_d	7.95

Table C.3 Physical properties for pressure balance model

Combustion gas density [9]	ρ_g	0.31	kg/m^3
Combustion gas viscosity [8]	μ	4.5×10^{-5}	kg/ms
Dense zone particle density [5]	$\rho_{s\text{-dense}}$	1,850	kg/m^3
Dilute zone particle density [5]	$\rho_{s\text{-dilute}}$	930	kg/m^3
Fly ash particle bulk density [7]	ρ_{bulk}	536	kg/m^3
Particle size at dense zone [5]	$d_{p\text{-dense}}$	1.16	mm
Particle size at dilute zone [5]	$d_{p\text{-dilute}}$	0.042	mm

Sphericity of dense zone particles [6]	$\phi_{s\text{-dense}}$	0.939	
Sphericity of dilute zone particles [6]	$\phi_{s\text{-dilute}}$	1	

Table C.4 Calculated Parameters of Pressure Balance Model (G_s = 15 kg/m²s)

Superficial solid velocity	U_d	0.0081	m/s
Terminal velocity of fly ash particles	U_t	0.29	m/s
Solid holdup at uniform flow with the slip velocity = U_t	ε_s*	0.00342	
Decay constant in the riser	a	0.848	m^{-1}
Solid hold up at the exit	ε_{se}	0.004771	
Decay constant affected by the exit geometry of the riser	a_e	0.103	m^{-1}
Reflux constant	C_e	19.75	

Table C.5 Air box module ports

	Port Number	**Instr.**	**Hole size**	**Height* (mm)**
Pressure transmitter	PT – 1	PT	1/4"	-50
Delta Pressure transmitter		DPT		

**** distributor plate is the reference point (h = 0 m)***

Table C.6 Module-1 Ports

	Port Number	**Instr.**	**Hole size**	**Height (mm)**
Delta Pressure transmitter	DPT – 1	DPT	1/4"	20
Temperature transmitter	TT – 1	TT	1/2"	70
Temperature transmitter	TT – 2	TT	1/2"	300
Gas probe	G – 1	G	1"	400
Delta Pressure transmitter	DPT – 2	DPT	1/2"	500

	Port Number	Instr.	Hole size	Height (mm)
Temperature transmitter	TT – 3	TT	1/4"	700
Delta Pressure transmitter	DPT – 3	DPT	1/4"	1000
Temperature transmitter	TT – 4	TT	1/2"	1100

Table C.7 Module-2 Ports

	Port Number	Instr.	Hole size	Height (mm)
Temperature transmitter	TT – 5	DPT	1/2"	1700
Gas probe	G – 2	TT	1"	1800
Delta Pressure transmitter	DPT – 4	G	1/4"	2150
Temperature transmitter	TT – 6	TT	1/2"	2300
Temperature transmitter	TT – 7	DPT	1/2"	3250
Delta Pressure transmitter	DPT – 5	TT	1/4"	3300

Table C.8 Module-3 Ports

	Port Number	Instr.	Hole size	Height (mm)
Gas probe	G – 3	G	1"	3700
Temperature transmitter	TT – 8	TT	1/2"	4200
Delta Pressure transmitter	DPT – 6	DPT	1/4"	4450
Gas probe	G – 4	G	1"	5000
Temperature transmitter	TT – 9	TT	1/2"	5150

Table C.9 Module-4 Ports

	Port Number	Instr.	Hole size	Height (mm)
Delta Pressure transmitter	DPT – 7	DPT	1/4"	5600
Temperature transmitter	TT – 10	TT	1/2"	6100
Gas probe	G – 5	G	1"	6400

Delta Pressure transmitter	DPT – 8	DPT	1/4"	6750
Temperature transmitter	TT – 11	TT	1/2"	7100

Table C.10 Exit Module Ports

	Port Number	**Instr.**	**Hole size**	**Height (mm)**
Gas probe	G – 6	G	1"	7730
Pressure transmitter	PT – 2	PT	1/4"	7800
Delta Pressure transmitter		DPT		
Temperature transmitter	TT – 12	TT	1/2"	7850

Table C.11 Temperature Transmitters

Port Number	**Height (mm)**	**Distance from previous TT (mm)**
TT - 1	70	-
TT - 2	300	230
TT - 3	700	400
TT - 4	1100	400
TT - 5	1700	600
TT - 6	2300	600
TT - 7	3250	950
TT - 8	4200	950
TT - 9	5150	950
TT - 10	6100	950
TT - 11	7100	1000
TT - 12	7850	750

Table C.12 Pressure/Delta Pressure Transmitters

Port Number	Height (mm)	Distance from previous DP port (mm)
PT – 1	-50	-
DPT – 1	20	70
DPT – 2	500	480
DPT – 3	1000	500
DPT – 4	2150	1150
DPT – 5	3300	1150
DPT – 6	4450	1150
DPT – 7	5600	1150
DPT – 8	6750	1150
PT – 2	7800	1050

Table C.13 Gas Probes

Port Number	Height (mm)	Distance from previous gas probe (mm)
G – 1	400	-
G – 2	1800	1400
G – 3	3700	1900
G – 4	5000	1300
G – 5	6400	1400
G – 6	7730	1330

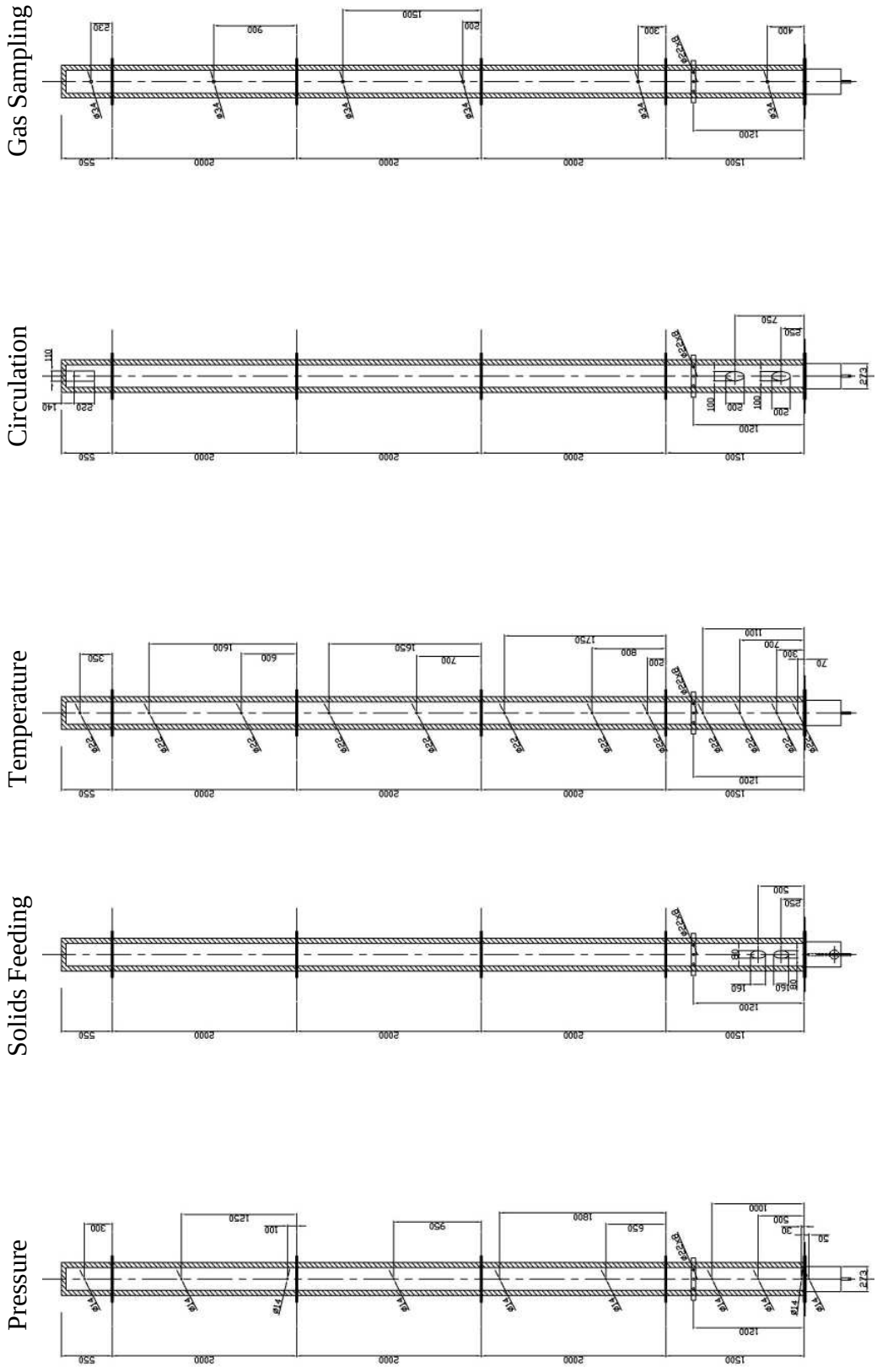

Figure C.1 Instrument Ports

APPENDIX D

PROCUREMENT and INSTALLATION

Figure D.1 Distributor Plate

Figure D.2 Bearing Plate

Figure D.3 Module – 1

Figure D.4 Module – 2

Figure D.5 Modules 3 and 4

Figure D.6 Cyclone

Figure D.7 Windbox after Burner Valve Train is Installed

Figure D.8 Solids Handling and Feesing

Table D.1 Specifications of Screw Conveyors and Air Lock

	Quantity	**Specifications**
Fuel silos discharge screw conveyors	2	Capacity: 50 kg/h (25 kg/h - 80 kg/h) Motor-Gearbox: 0.55kW 17 rpm
Limestone silo discharge screw conveyor	1	Capacity: 10 kg/h (2 kg/h - 20 kg/h) Motor-Gearbox: 0.37kW 11rpm
Bed material silo discharge screw conveyor	1	Capacity: 150 kg/h (constant speed) Motor-Gearbox: 0.75kW 25rpm
Solids feeding air lock	1	Capacity: 150 kg/h (constant speed) Motor-Gearbox: 0.37kW 11 rpm

Table D.2 Pressure Transmitters

Description	**Qty.**	**Model**	**Specifications**
Combustion air (fan exit)	1	Industrial Press. Transmitter Model: 626-08-CH-P1-E5-S1	(0 – 30 psi, 4-20 mA output)
Primary air (air box)	1		

Table D.3 Delta Pressure Transmitters

Description	**Qty.**	**Model**	**Specifications**
Riser exit	1	Bidirectional Range Diff. Press. Transmitter Model: 668C-16	-10”/+10” WC 4-20 mA output
Cyclone exit	1		
Distributor plate	1	Magnasense DP Transmitter Model: MS111	0 - 5" WC 4-20 mA output
Riser, downcomer	10		
Dense zone	2	Diff. Press. Transmitter Model: 668C-7	0 – 25" WC 4-20 mA output

Table D.4 Air Flow Rate Transmitters

Description	Qty.	Model	Specifications
Combustion air	1	In-Line Flow Sensor - DS300-4”	line size: 4”
	1	Magnasense DP Transmitter	0-5"WC / 4-20 mA
Secondary air	1	In-Line Flow Sensor - DS300-3”	line size: 3”
	1	Magnasense DP Transmitter	0-5"WC / 4-20 mA

Table D.5 Air Rotameters

Description	Qty.	Model	Specifications
J-valve fluidization	2	Rate Master Flowmeters Model: RMA-SSV-150	2” scale 10 – 100 cc/min
Solids feed conveying	2	Rate Master Flowmeters Model: RMA-SSV-11	2” scale 30 – 240 cc/min

Table D.6 Water Flowmeters

Description	Qty.	Model	Specifications
2nd module cooling water	1	Digisens Flow Sensor TRB DN20 brass 90°C	0 – 3 m³ / h 4 – 20 mA output
3rd module cooling water	1		

Table D.7 Temperature Transmitters

Description	Qty.	Model	Specifications
Combustion air Cooling water	6	Pt-100	0 – 100°C 4-20 mA output
Flue gas	5	T/C (K type)	0 – 1000°C 4-20 mA output
Combustor	14	T/C (K type)	

Table D.8 Air Flow Control Valves

Description	**Qty.**	**Model**	**Specifications**
Combustion air	1	ASTEKNIK butterfly valve Rilsan damper, Double effect pneumatic piston actuator, analog I/P positioner	DN 100 4 – 20 mA input
Secondary air	1		DN 80 4 – 20 mA input

APPENDIX E

RESULTS

Table E.1 Steady State Temperature Measurements along the Combustor

Tag	Height* (mm)	Test-1 °C	Test-2 °C
TTC01	70	824.6	850.8
TTC02	300	837.0	860.3
TTC03	700	839.4	862.9
TTC04	1100	845.5	871.4
TTC05	1700	827.0	862.1
TTC06	2300	806.8	856.7
TTC07	3250	761.5	832.3
TTC08	4200	723.5	815.0
TTC09	5150	718.3	815.5
TTC10	6100	742.0	828.4
TTC11	7100	744.1	830.3
TTC12	7850	733.8	822.6

* height above distributor plate

Table E.2 Steady State Pressure Measurements along the Combustor

Tag	Height* (mm)	Test-1 mmH2O	Test-2
PT – 1	-1400	557.1	1554.9
DPT – 1	20	464.4	527.8
DPT – 2	500	50.9	414.6
DPT – 3	1000	87.4	47.4
DPT – 4	2150	87.4	49.2
DPT – 5	3300	87.9	49.2
DPT – 6	4450	85.4	52.2
DPT – 7	5600	73.1	49.3
DPT – 8	6750	49.0	30.9
DPT – 9	7800	50.0	17.9
PT – 2	7800	43.7	22.7
DPT – 11	3160	45.1	16.9
DPT – 13	1660	0.0	17.5

* height above distributor plate

Table E.3 Particle Size Distributions of Bag Filter Ash

	Test – 1	**Test – 2**
Dp (µm)	**Cumulative %**	**Cumulative %**
< 0.356	0.00	0.00
0.399	0.04	0.00
0.448	0.15	0.07
0.502	0.39	0.23
0.564	0.71	0.47
0.632	1.10	0.74
0.710	1.54	1.05
0.796	2.00	1.36
0.893	2.48	1.69
1.002	2.97	2.01
1.125	3.48	2.33
1.262	4.03	2.67
1.416	4.66	3.03
1.589	5.38	3.40
1.783	6.23	3.94
2.000	7.23	4.50
2.244	8.39	5.14
2.518	9.71	5.87
2.825	11.18	6.68
3.170	12.80	7.57
3.557	14.55	8.54
3.991	16.43	9.60
4.477	18.45	10.75
5.024	20.61	12.01
5.637	22.91	13.37

	Test – 1	Test – 2
Dp (µm)	**Cumulative %**	**Cumulative %**
6.325	25.35	14.86
7.096	27.92	16.49
7.962	30.62	18.26
8.934	33.44	20.18
10.024	36.36	22.26
11.247	39.36	24.49
12.619	42.43	26.88
14.159	45.55	29.44
15.887	48.71	32.16
17.825	51.90	35.06
20.000	55.11	38.14
22.440	58.33	41.41
25.179	61.57	44.88
28.251	64.79	48.55
31.698	68.00	52.40
35.566	71.16	56.43
39.905	74.26	60.60
44.774	77.27	64.87
50.238	80.18	69.18
56.368	82.96	73.45
63.246	85.59	77.61
70.963	88.05	81.56
79.621	90.32	85.22
89.337	92.37	88.51
100.237	94.19	91.38
112.468	95.78	93.80
126.191	97.11	95.77
141.589	98.19	97.30

	Test – 1	Test – 2
Dp (µm)	**Cumulative %**	**Cumulative %**
158.866	99.02	98.45
178.250	99.60	99.24
200.000	99.94	99.69
224.404	100.00	99.89
251.785	100.00	99.96
> 282.508	100.00	100.00

VITA

PERSONAL INFORMATION

Surname, Name	: Batu, Aykan
Nationality	: Turkish (TC)
Date and Place of birth	: 7 March 1978
Marital status	: Married
E-mail	: aykanbatu@hotmail.com
Tel:	: +90 533 664 46 91

EDUCATION

Degree	Institution	Year of Graduation
M.Sc.	METU Chemical Engineering	2001
B.Sc.	METU Chemical Engineering	1999
High School	Atatürk Anadolu High School, Ankara	1995

WORK EXPERIENCE

Year	Place	Enrollment
2001 – present	MİMAG-SAMKO Enerji Teknolojileri A.Ş.	Business Development Manager

FOREIGN LANGUAGES

Advanced English

PUBLICATIONS

1. N. Selcuk, A. Batu and O. Oymak “NOx Emissions from Combustion of High Sulfur Lignite in an ABFBC Test Rig”, 17th International ASME Conference on Fluidized Bed Combustion, May 18 – 21, 2003, Jacksonville, FL.

2. A. Batu and N. Selçuk " Modeling of Radiative Heat Transfer in the Freeboard of a Fluidized Bed Combustor using the Zone Method of Analysis", Turk. J. Engin. Environ. Sci., 26, (2002), 49-58.

3. N. Selcuk, A. Batu and I. Ayrancı “Performance of Method of Lines Solution of Discrete Ordinates Method in the Freeboard of a Bubbling Fluidized Bed Combustor”, JQSRT, Vol. 73 (2-5), pp. 503-516, 2002.